Università degli Studi di Firenze
Dipartimento di Chimica
Scuola di Dottorato in Scienze
Dottorato di Ricerca in Scienze Chimiche
XXII Ciclo

CHIM/02 - Chimica Fisica

Synthesis and Characterization of Nanosystems for Polyfunctional Textiles

Sintesi e Caratterizzazione di Nanosistemi per Tessili Polifunzionali

Ph.D. Thesis by

Lorenzo Tattini

Tutor
Dr. Pierandrea Lo Nostro

Coordinator
Prof. Gianni Cardini

Contents

Introduction

The terms *nanotechnology* and *nanoscience* are concerned with the investigation and design of materials or devices at the atomic and molecular levels. The prefix *nano-* brings us down to a billionth of a meter length scale where only few atoms can find room. The promise and essence of the nanoscale science and technology is based on the demonstrated fact that materials at the nanoscale have properties (e.g. chemical, electrical, magnetic, mechanical and optical) quite different from the bulk materials. Some of these properties are, somehow, intermediate between the properties of the smallest building blocks they are made of, and those of the macroscopic materials.

Drawing up an exact definition of nanotechnology, however, is quite a difficult task. Even scientists working in the field believe that the answer strongly depends on whom you may ask. Some scientists use the term to describe almost any research where some critical size is less than a micron while others reserve the term for systems involving sizes between 1 and 100 nanometers. There is also debate over whether naturally occurring nanoparticles, e.g. carbon soot, fall under the nanotechnology area. Finally, some reserve the term nanotechnology exclusively for manufacturing with atomic precision whereas others employ the term to describe the use of nanomaterials to construct materials, devices, and systems. In this work we will refer to nanostructures as any material or device with submicron-sized characteristic length.

The dawning of the nanorevolution can be ascribed to the physicist Richard Feynman [1] (even though some criticism have been reported [2]). In a renowned talk titled "There's Plenty of Room at the Bottom" - it was

1959 - he hypothesized that atoms and molecules could be manipulated like building blocks. The first proof-of-principle that atoms could be exactly positioned by a man-made tool (living cells, of course, have been positioning atoms from time immemorial) took place in 1989 when scientists at IBM manipulated 35 xenon atoms to form the letters IBM. That was the very first example of the *bottom-up* strategy for producing nanosystems.

Several fields have been already involved in the nanorevolution: medicine and pharmacology (from drug delivery [3] to stem cell manipulation [4]), electronics and communication (e.g. for memory storage and semiconductor devices [5]), consumer goods (like textiles and household products), catalysis [6], energy storage, conversion and saving - and renewable energy sources too [7]- and many others. It must be stressed that chemistry is from this point of view a basic nanoscience since it provides - with both synthetic and self-assembly approaches - the tools for the production of nanosized materials.

In the world of nanotechnology the boundaries between chemistry, molecular biology, materials science and condensed matter physics dissolve as scientists struggle to understand new — and sometimes even unexpected — properties. Even though these professionals are only on the first leg of the journey, they have made significant progresses in synthesizing and understanding the building blocks of nanotechnology. In the following years, the ability to employ these building blocks for the construction of nanodevices of practical purposes will greatly increase. As a consequence the nanoworld will get in everyday life.

Nanotechnology is currently — and partially it's already happened — moving into into so many aspects of science and technology including, among the others, aerospace industry, bioengineering and biology, energy, environment and agricultural sciences, materials, manufacturing, medicine, military science and technology. It is truly an atomic and molecular manufacturing approach for building chemically and physically stable structures one atom or one molecule at a time. Presently some of the active nanotechnology research areas include nanolithography, nanodevices, nanorobotics, nanocomputers, nanopowders, nanostructured catalysts and nanoporous materials, molecular manufacturing, diamondoids, carbon nan-

otube and fullerene products, nanolayers, molecular nanotechnology, nanomedicine, nanobiology, nanoparticles and nanocomposites to name a few.

This volume is structured as follows: **Chapter 1** deals with nanosystems in general and will present the main concepts of nanosciences with particular emphasis on the properties and the applications of nanostructures. In **Chapter 2** we will explore piezoelectric materials, focusing on PZT materials and their properties. **Chapter 3** is devoted to textiles and geotextiles composites. The original contents are discussed in **Chapters 4** and **Chapters 5**. The first deals with PZT nanoparticles, their synthesis and their characterization. A smart synthesis for PZT nanosystem will be considered. The latter is concerned with PZT-based nanocomposites. A method for the electro-mechanical characterization of these nanocomposites will be detailed, and the results obtained will be discussed.

Chapter 1

Nanosystems

In Chapter 1 we will dive in nanosystems' world. A general discussion of the nanosystems' realm will be presented in Sections 1.1 and 1.2. The first Section deals with the strategies for the fabrication of nanomaterials. The *bottom-up* approach, which will be analyzed thoroughly, involves the employment of functional components, namely the *building blocks*. In Section 1.2 we will discuss the main properties of nanosystems and a brief hystorical perspective will be presented. Finally, a summary of the principal application of nanosystems and nanotechnology will be examined in Section 1.3.

1.1 The Building Blocks

The fabrication of nanomaterials falls into one of two categories: *top-down* or *bottom-up*. In the top-down approach the key idea is to miniaturize the macroscopic structures, components and systems towards a nanoscale of the same. In the bottom-up approach the atoms and molecules constituting the Molecular Building Blocks (MBBs) are the starting point to build the desired nanostructure.

The top-down method involves carving nanomaterials out of bulk matter. The methods folling in this category are referred to as various forms of lithography. Lithography can be understood through the concepts of *writing* and *replication* [8]. Writing deals with the design of a pattern on a negative (usually a mask), while replication involves transferring the pat-

tern on the negative to a functional material. There are several types of lithography. Photolithography, which uses different kinds of electromagnetic radiation, is currently used to manufacture computer chips and other microelectronic devices [9]. Photolithography, as currently used, is not an effective tool for fabricating structures with features below 100 nanometers. E-beam lithography, a technique that employs beams of electrons to write, can produce some nanostructures with high resolution, albeit in an essentially serial fashion [10, 11, 12, 13, 14]. Soft lithographic techniques, such as printing, molding, and embossing, involve the physical or chemical deformation of the functional material to yield the desired structure. While soft lithography can be used to construct less planar nanostructures, it may be less precise than other techniques [15, 16, 17].

A second method of producing nanomaterials, the already mentioned the bottom-up approach, describes techniques for coaxing atoms and molecules to form nanomaterials [18]. One bottom-up technique, referred to as "positional assembly" involves using a probe to move atoms into certain arrangements. The use of an atomic force microscope to individually position xenon atoms to spell "IBM" is an example of this approach (see Figure 1.1). Although positional assembly allows control over individual atoms, it is time-consuming, cannot presently be used to create complex nanostructures, and does not represent an efficient means for commercial production. Positional assembly, as realized today, is largely a serial process: each step is performed after the previous one is completed. Photolithography, by way of contrast, is a massively parallel procedure — a very large number of features are created in each step. Both methods are, however, largely restricted to planar constructions or stacks thereof.

Self-assembly is another chemical bottom-up approach [19, 20, 21, 22]. Different atoms, molecules, or nanomaterials are mixed together and, because of their unique geometries and electronic structures, spontaneously organize into stable, well-defined structures. Since self-assembly methods are based on chemical reactions, they are simple and relatively inexpensive. However, they do not always offer the precision necessary for constructing designed, interconnected patterns that top-down approaches currently do.

Several categorization strategies have been employed to define the build-

ing blocks of nanotechnology. For example, some scientists categorize the building blocks into “soft” and “hard” categories [23]. Others describe two different, popular ways of classifying nanomaterials. Nanomaterials are often classified in the literature based on dimensionality [24]. Crucial to this classification is the concept of confinement, which may be roughly interpreted as a restriction in the ability of electrons to move in one or more spatial dimensions [25, 26]. 0D nanomaterials, such as quantum dots and nanoparticles, are confined in all three dimensions. Obviously, depending on their size these nanosystems, they can be also classified as 3D objects [27, 28]. 1D nanomaterials are confined in two directions and extended in only one: electrons flow almost exclusively along this extended dimension. Examples of one-dimensional nanomaterials are nanotubes and nanowires [29]. Finally, 2D nanomaterials, which are confined in one dimension and extended in two, include thin films, surfaces, and interfaces [30]. Interestingly, material structures currently used as elementary semiconductor devices fall under this category [31]. Nanomaterials can also be divided into inorganic and organic classes.

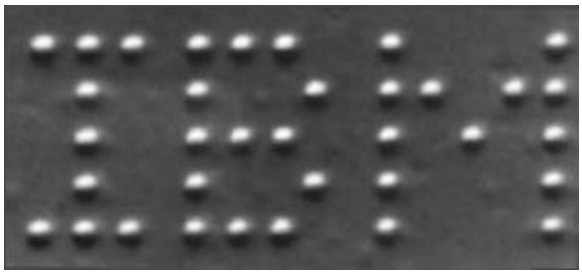

Figure 1.1: Xenon atoms on a nickel substrate positioned by STM. From http://muller.lbl.gov/.

The most fundamentally important aspect of the bottom-up approach is that the nanoscale building blocks, because of their sizes of a few nanometers, impart to the nanostructures created from them new and possibly preferred properties and characteristics heretofore unavailable in conventional materials and devices. Metals [32, 33, 34] and ceramics [35, 36, 37] produced by consolidating nanoparticles or micron-sized materials with controlled nanostructures are shown to possess properties substantially different

from materials with coarse microstructures. Such differences in properties include greater hardness, higher yield strength, and ductility in ceramic materials. The band gap of nanometer-scale semiconductor structures increases as the size of the microstructure decreases, raising expectations for many possible optical and photonic applications. Considering that nanoparticles have much higher specific surface areas, thus in their assembled forms there are large areas of interfaces. One needs to know in detail not only the structures of these interfaces, but also their local chemistry and the effects of segregation and interaction among MBBs and also between MBBs and their surroundings. Knowledge on means to control nanostructure sizes, size distributions, compositions, and assemblies are important aspects of the nanoscience and nanotechnology. The building blocks of all materials in any phase are atoms and molecules. All objects are comprised of atoms and molecules, and their arrangement and how they interact with one another define properties of an object. Nanotechnology is the engineered manipulation of atoms and molecules in a user defined and repeatable manner to build objects with certain desired properties. To achieve this goal a number of molecules are identified as the appropriate building blocks of nanotechnology. These nanosized building blocks are intermediate systems in size lying between atoms and small molecules and microscopic and macroscopic systems. These building blocks contain a limited and countable number of atoms. They can be synthesized and designed atom-by-atom. They constitute the means of our entry into new realms of nanoscience and nanotechnology. Nanotechnology molecular building blocks are distinguished for their unique properties. They include, for example, graphite, fullerene molecules made of variety number of carbon atoms (C_{60}, C_{70}, etc.) [38], carbon nanotube, diamondoids [39, 40], nanowires, nanocrystals and amino acids. The above mentioned building blocks have quite unique properties which are not found in rather small molecules. Some of these MBBs are electrical conductors, some are semiconductors, some are photonic and the characteristic dimension of each is a few nanometers. For example, carbon nanotubes are about five times lighter and five times stronger than steel. Many nanocrystals are photonic and they guide light through air since their spacing of the crystal pattern is much smaller than the wavelength of light being controlled.

Nanowires can be made of metals, semiconductors, or even different types of semiconductors within a single wire. They are upwards of ten nanometers and they can be made to be conductor or semiconductor [41, 42, 43]. Amino acids and DNA, the basis for life, can also be used to build nanomachines. Adamantane (a diamondoid) is a tetrahedrally symmetric stiff hydrocarbon that provides an excellent building block for positional (or robotic) assembly as well as for self-assembly. In fact, over 20,000 variants of adamantane have been identified and synthesized and even more are possible, providing a rich and well-studied set of MBBs. The applications of MBBs would enable the practitioner of nanotechnology to design and build systems on a nanometer scale. The controlled synthesis of MBBs and their subsequent assembly (self-assembly, self-replication or positional-assembly) into nanostructures is one fundamental theme of nanotechnology. These promising nanotechnology concepts with far reaching implications (from mechanical to chemical processes, from electronic components to ultra-sensitive sensors; from medical applications to energy systems, and from pharmaceutical to agricultural and food chain) will impact every aspect of our future.

1.2 The Importance of Being Nanosized

The Greek word "nano" refers to a reduction of a quantity — like size or time — by 10^{-9}, which is one thousand times smaller than a micron. One nanometer (nm) is one billionth of a meter and it is also equivalent to ten Ångströms. As such a nanometer is 10^{-9} meter and it is 10,000 times smaller than the diameter of a human hair. A human hair diameter is about 50 microns (i.e. 50×10^{-6} meter) in size, meaning that a 50 nanometer object is about 1/1000th of the thickness of a hair. One cubic nanometer (nm^3) is roughly 20 times the volume of an individual atom. A nanoelement compares to a basketball, like a basketball to the size of the earth. Nanoscience and nanotechnology can be defined through three factors:

- **Dimension** - At least one dimension from 1 to 1000 nanometers (nm).
- **Process** - Designed with methodologies that shows fundamental control over the physical and chemical attributes of molecular-scale struc-

tures.

- **Building block property** - They can be combined to form larger structures. Nanoscience, in a general sense, is quite natural in microbiological sciences considering that the sizes of many bioparticles dealt with (like enzymes, viruses, etc.) fall within the nanometer range.

Nanoscale is a magical point on the dimensional scale. Structures in nanoscale (called nanostructures) are considered at the borderline of the smallest of human-made devices and the largest molecules of living systems. Our ability to control and manipulate nanostructures will make it possible to exploit new physical, biological and chemical properties of systems that are intermediate in size, between single atoms, molecules and bulk materials.

There are many specific reasons why nanoscale has become so important some of which are as the following:

- The quantum mechanical (wavelike) properties of electrons inside matter are influenced by variations on the nanoscale. By nanoscale design of materials it is possible to vary their micro and macroscopic properties, such as charge capacity, magnetization and melting temperature, without changing their chemical composition.

- A key feature of biological entities is the systematic organization of matter on the nanoscale. Developments in nanoscience and nanotechnology would allow us to place man-made nanoscale things inside living cells. It would also make it possible to make new materials using the self-assembly features of nature. This certainly will be a powerful combination of biology with materials science.

- Nanoscale components have very high surface to volume ratio, making them ideal for use in composite materials, reacting systems, drug delivery, and chemical energy storage (such as hydrogen and natural gas).

- Macroscopic systems made up of nanostructures can have much higher density than those made up of microstructures. They can also be

better conductors of electricity. This can result in new electronic device concepts, smaller and faster circuits, more sophisticated functions, and greatly reduced power consumption simultaneously by controlling nanostructure interactions and complexity.

1.2.1 Atomic and Molecular Basis of Nanotechnology

The molecular theory of matter starts with quantum mechanics and statistical mechanics. According to the quantum mechanical Heisenberg *Uncertainty Principle* the position and momentum of an object cannot simultaneously and precisely be determined [44]. Then the first question that may come into mind is, how could one be able to brush aside the Heisenberg Uncertainty Principle to work at the atomic and molecular level, atom by atom as is the basis of nanotechnology.

The Heisenberg Uncertainty Principle helps determine the size of electron clouds, and hence the size of atoms. According to Werner Heisenberg "The more precisely the position is determined, the less precisely the momentum is known":

$$\Delta p \cdot \Delta x \geq \hbar \tag{1.1}$$

Where Δp is the error associated the measurement of a particle momentum, Δx is the error associated with the measurement of the particle position and $\hbar$ is the Planck's constant. It does not forbid the possibility of nanotechnology, which has to do with the position and momentum of such large particles like atoms and molecules. This is because the mass of the atoms and molecules are quite large and the quantum mechanical calculation by the Heisenberg Uncertainty Principle places no limit on how well atoms and molecules can be held in place.

Although we have long been aware of, and many investigators have been dealing with, "nano" sized entities the historic birth of the nanotechnology is commonly credited to Feynman. Historically nanotechnology was for the first time formally recognized as a viable field of research with the landmark lecture delivered by Richard P. Feynman, the famous Noble Laureate physicist on December 29th 1959 at the annual meeting of the American Physical Society [1]. His lecture was entitled "There's Plenty of Room at

the Bottom - An invitation to enter a new field of physics". Feynman stated in his lecture that the entire encyclopedia of Britannica could be put on the tip of a needle and, in principle, there is no law preventing such an undertaking. Feynman described then the advances made in this field in the past and he envisioned the future for nanotechnology. His lecture was published in the February 1960 issue of Engineering & Science quarterly magazine of California Institute of Technology.

In his talk Feynman also described how the laws of nature do not limit our ability to work at the molecular level, atom by atom. Instead, he said, it was our lack of the appropriate equipment and techniques for doing so. Feynman in his lecture talked about *"how do we write small?"*, *"information on a small scale"*, possibility to have *"better electron microscopes"* that could take the image of an atom, doing things small scale through *"the marvelous biological system"*, *"miniaturizing the computer"*, *"miniaturization by evaporation"* example of which is thin film formation by chemical vapor deposition, solving the *"problems of lubrication"* through miniaturization of machinery and nanorobotics, *"rearranging the atoms"* to build various nanostructures and nanodevices, and behavior of *"atoms in a small world"* which included atomic scale fabrication as a bottom-up approach as opposed to the topdown approach that we are accustomed to.

It is important to mention that almost all of the ideas presented in Feynman's lecture and even more, are now under intensive research by numerous nanotechnology investigators all around the world. For example, in his lecture Feynman challenged the scientific community and set a monetary reward to demonstrate experiments in support of miniaturizations. Feynman proposed radical ideas about miniaturizing printed matter, circuits, and machines. "There's no question that there is enough room on the head of a pin to put all of the Encyclopedia Britannica" he said. He emphasized "I'm not inventing antigravity, which is possible someday only if the laws (of nature) are not what we think". He added "I am telling what could be done if the laws are what we think; we are not doing it simply because we haven't yet gotten around to it." Feynmans challenge for miniaturization and his unerringly accurate forecast was met forty years later, in 1999, [45] by a team of scientists using Atomic Force Microscope (AFM) to perform

Dip-Pen Nanolitography (DPN). The results are shown in Figure 1.2. In this DPN an AFM tip is simply coated with molecular "ink" and then brought in contact with the surface to be patterned. Water condensing from the immediate environment forms a capillary between the AFM tip and the surface. Work is currently under way to investigate the potential of the DPN technique as more than a quirky tool for nanowriting, focusing on applications in microelectronics, pharmaceutical screening, and biomolecular sensor technology [46].

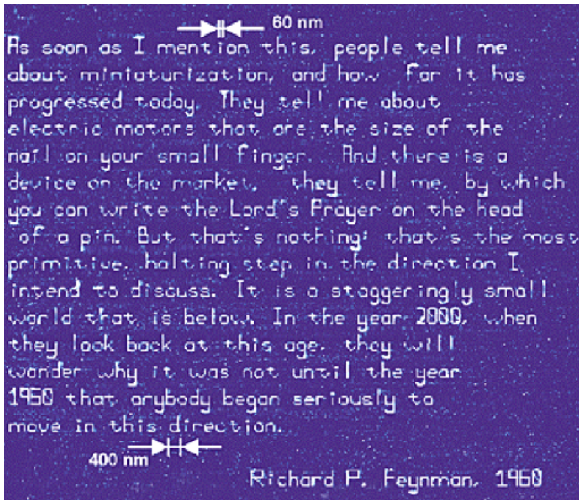

Figure 1.2: Demonstration of lithography miniaturization challenge by the scientists at the Northwestern University [45] as predicted by Feynman in 1959 using an AFM tip to write a paragraph of nanometer-sized letters with a single layer of mercaptohexadecanoic acid on a gold surface. Contrast is enhanced by surrounding each letter with a layer of a second "ink", namely octadecanethiol.

Feynman in 1983 talked about a scaleable manufacturing system, which could be made to manufacture a smaller scale replica of itself [47]. That, in turn would replicate itself in smaller scale, and so on down to molecular scale. Feynman was subscribing to the "Theory of Self-Reproducing Automata" proposed by von Neumann the 1940's eminent mathematician and physicist who was interested in the question of whether a machine can self-replicate, that is, produce copies of itself (see [48] for details). The study of man-

made self-replicating systems has been taking place now for more than half a century. Much of this work is motivated by the desire to understand the fundamentals involved in self-replication and advance our knowledge of single-cell biological self-replications.

Some of the other recent important achievements about which Feynman mentioned in his 1959 lecture include the manipulation of single atoms [49], positioning single atoms with a scanning tunneling microscope [50] and the trapping of single, 3 nm in diameter, colloidal particles from solution using electrostatic methods [51].

In early 60s there were other ongoing research on small systems but with a different emphasis. The experimental efforts for the study of the nanoworld thus necessitated of new theoretical tools. Nowadays, thermodynamics of small systems is now called "nanothermodynamics" [52].

Finally, it must be pointed out that in 1960s — when Feynman recognized and recommended the importance of nanotechnology — the devices necessary for nanotechnology were not invented yet. At that time, the world was intrigued with space exploration, discoveries and the desire and pledges for travel to the moon, partly due to political rivalries of the time and partly due to its bigger promise of new frontiers that man had also not captured yet. Research and developments in small (nano) systems did not sell very well at that time with the governmental research funding agencies and as a result the scientific community paid little attention to it.

1.3 Nanotechnology Today

The atomic-scale and cutting-edge field of nanotechnology which is considered to lead us to the next industrial revolution is likely to have a revolutionary impact on the way things will be done, designed and manufactured in the future.

We have known for many years that several existing technologies depend crucially on processes that take place on the nanoscale. Adsorption, lithography, ion-exchange, catalysis, drug design, plastics and composites are some examples of such technologies. The "nano" aspect of these technologies was not known and, for the most part, they were initiated accidentally by mere

luck. They were further developed using tedious trial-and-error laboratory techniques due to the limited ability of the times to probe and control matter on nanoscale. Investigations at nanoscale were left behind as compared to micro and macro length scales because significant developments of the nanoscale investigative tools have been made only recently.

The above mentioned technologies, and more, stand to be improved vastly as the methods of nanotechnology develop. Such methods include the possibility to control the arrangement of atoms inside a particular molecule and, as a result, the ability to organize and control matter simultaneously on several length scales. The developing concepts of nanotechnology seem pervasive and broad. It is expected to influence every area of science and technology, in ways that are clearly unpredictable.

Nanotechnology will also help solve other technology and science problems. For example, we are just now starting to realize the benefits that nanostructuring can bring to:

- Wear-resistant tires made by combining nanoscale particles of inorganic clays with polymers as well as other nanoparticle reinforced materials [53, 54, 55, 56, 57].
- Greatly improved printing brought about by nanoscale particles that have the best properties of both dyes and pigments as well as advanced ink-jet systems [58].
- Vastly improved new generation of lasers, magnetic disk heads, nanolayers with selective optical barriers and systems on a chip made by controlling layer thickness to better than a nanometer .
- Design of advanced chemical and bio-sensor [59].
- Nanoparticles to be used in medicine with vastly advanced drug delivery and drug targeting capabilities [60, 61, 62, 63, 64].
- Chemical-mechanical polishing with nanoparticle slurries, hard coatings and high hardness cutting tools [65].

The following selected observations regarding the expected future advances are also worth mentioning at this juncture:

- Photolithographic patterning of matter on the micro scale has led to the revolution in microelectronics over the past few decades. With nanotechnology, it will become possible to control matter on every important length scale, enabling tremendous new power in materials design.

- Biotechnology is expected to be influenced by nanotechnology greatly in a couple of decades. It is anticipated that, for example, this will revolutionize healthcare to produce ingestible systems that will be harmlessly flushed from the body if the patient is healthy but will notify a physician of the type and location of diseased cells and organs if there are problems.

- Micro and macro systems constructed of nanoscale components are expected to have entirely new properties that have never before been identified in nature. As a result, by altering and design of the structure of materials in the nanoscale range we would be able to systematically and appreciably modify or change selected properties of matter at macro and micro scales. This would include, for example, production of polymers or composites with most desirable properties which nature and existing technologies are incapable of producing.

- Robotic spacecraft that weigh only a few pounds will be sent out to explore the solar system, and perhaps even the nearest stars. Nanoscale traps will be constructed that will be able to remove pollutants from the environment and deactivate chemical warfare agents. Computers with the capabilities of current workstations will be the size of a grain of sand and will be able to operate for decades with the equivalent of a single wristwatch battery.

- There are many more observations in the areas of inks and dyes, protective coatings, dispersions with optoelectronic properties, nanostructured catalysts, high reactivity reagents, medicine, electronics, structural materials, diamondoids, carbon nanotube and fullerene products and energy conversion, conservation, storage and usage which are also worth mentioning.

Presently nanotechnology and its associated research discipline of nanoscience, together, constitute the complete spectrum of activities towards the promised next industrial revolution. They span the whole spectrum of physical, chemical, biological and mathematical sciences needed to develop the purposeful capabilities of nano manipulations, nano structural modifications, miniaturization and bottom-up technology originally proposed by Richard Feynman in his well-known 1959 lecture. The emerging fields of nanoscience and nanotechnology are also creating the necessary experimental and computational tools for the design and fabrication of nano-dimension electronic, photonic, biological and energy transfer components, such as quantum dots, atomic wires, operating on nanoscopic length scales, etc.

Nanoscience and nanotechnology should have major impacts on several key scientific and technological activities in a not too distant future. Expansions on these subjects will have a lot to do on the technological advances in instruments and tools of fabrication and manipulation in nano scale. Such instruments and tools are the means for live visualization and manipulation in nano world. They are presently expensive and, as a result, not available to many investigators. Technological advances are always followed with reduction of prices as has been the case with the electronic and communication industry products in recent decades.

The decisive and important leading role of molecular-based techniques for the study of matter in the fields of nanoscience and nanotechnology is well understood. Any development in this filed will have a great deal to do with advances in these techniques. Advances in molecular based study of matter in nanoscale will help to understand, simulate, predict and formulate new materials utilizing the fields of quantum and statistical mechanics, intermolecular interaction, molecular simulation and molecular modeling. We may then be able to understand how to design new molecular building blocks which could allow self-assembly or self-replication to advance the bottom-up approach of producing the necessary materials for the advancement of nanotechnology. The past trend of the contributions of molecular based study of matter in macroscopic technologies is indicative of the fact that its future influence into nanoscience and nanotechnology is quite promising.

Chapter 2

Piezoceramics

Piezoelectric materials — a subclass of *ferroelectric* materials — are used to convert mechanical energy into electrical energy and vice versa. Due to their ability to be tailored towards the requirements of particular applications their application range is continuously expanding. The aim of this Chapter is to provide a clear and useful introduction to *piezoceramics* — ceramic materials which show piezoelectric activity. After a brief description of the piezoceramic materials development and their properties — which will be given in Section 2.1 — the correlation between the crystalline structure and piezoelectric properties will be discussed in Section 2.2. Furthermore, the physical costants that quantify the piezoelectric activity of piezoresponsive materials will be examined. The most performing piezoelectric, PZT, will be introduced in Section 2.3, where a brief discussion of key concepts — such as the *morphotropic phase boundary* and the *polarization rotation* in ferroelectrics — will be given. Finally, the problems connected to *nanosized* ferroelectrics will be explored in Section 2.4.

2.1 An Introduction to Piezoceramics

The word "piezo" is a Greek language word, which means "push". The first experimental demonstration of a connection between macroscopic piezoelectric phenomena and crystallographic structure was published in 1880 by Pierre and Jacques Curie, who measured the surface charge appearing on

specially prepared crystals (tourmaline, quartz and Rochelle salt) which were subjected to mechanical stress.

The piezoelectricity is a property existing in many materials, which, subjected to mechanical forces, develop electrical charges on their surface (direct piezoelectric effect) and, conversely, subjected to an applied electric field, exhibit a mechanical deformation (inverse piezoelectric effect)(see Figure 2.1).

Piezoelectric materials — or piezoelectrics — are a subclass of *ferroelectric* materials. Ferroelectricity is a spontaneous electric polarization of a material that can be reversed by the application of an external electric field. The term is used in analogy to ferromagnetism, in which a material exhibits a permanent magnetic moment. Ferromagnetism was already known when ferroelectricity was discovered in 1920 in Rochelle salt by Valasek. Ferroelectric materials are thus also piezoelectric, but the opposite — as in the case of quartz — is not true.

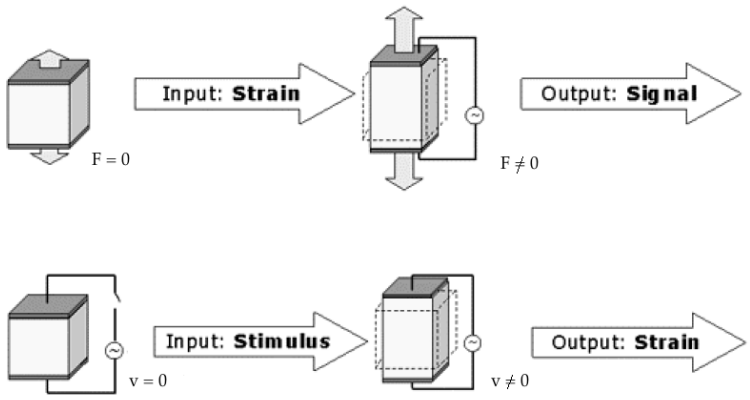

Figure 2.1: Direct piezoelectric effect: a mechanical input (force or vibration) produces an electric voltage in output. Inverse piezoelectric effect: an electric input (voltage) results in strain output.

The first serious application of the piezoelectricity was carried out during the First World War by Langevin, who constructed the first underwater ultrasonic source (sonar) consisting of piezoelectric quartz elements sandwiched between steel plates. The success of sonar stimulated intense development activity on all kinds of piezoelectric devices. Crystal frequency

control became essential for the growing broadcasting and radio communication industry. Between the two world wars, most of the classic piezoelectric applications (microphones, accelerometers, ultrasonic transducers, bender element actuators, phonograph pick-ups, signal filters, etc.) were conceived and developed even if the materials available at the time often limited the device performances and thus the commercial exploitation. In fact, the single crystals used at that time had low piezoelectric properties. The discovery during the Second World War of the possibility to induce piezoelectricity, by applying a strong electric field to sintered metallic oxides to align their dipole domains, allowed new piezoelectric applications and opened the way to intense research on piezoceramics.

The first piezoceramic was barium titanate ($BaTiO_3$), which exhibits dielectric constants up to 100 times higher than common cut crystals. Its crystalline structure is similar to that of perovskite mineral ($CaTiO_3$). Above the Curie temperature (130 °C) the elementary cell is cubic and symmetric, while, below the Curie temperature it is slightly distorted and tetragonal, exhibiting a dipole momentum different from zero. Barium titanate was widely used soon after the Second World War for the generation of acoustic and ultrasonic vibrations and for actuators, but today it has been generally replaced by lead zirconate titanate (PZT) for its superior piezoelectric properties and higher operating temperatures [66]. $BaTiO_3$ shows a greater resistance than other piezoceramics like PZT to depoling by compressive stresses and this resistance is particularly strong in cobalt-doped material, especially after a period of aging. For this reason, the use of cobalt-doped $BaTiO_3$ for producing high acoustic powers has continued in some applications despite its inferior piezoelectric activity.

The major limitation of barium titanate, i.e. the low operating temperatures, was overcome in the 1950s by the discovery of piezoelectric effects in lead zirconate titanate, $Pb(Zr,Ti)O_3$, and lead metaniobate, $PbNb_2O_6$, which can be used at least to 250 °C. Lead zirconate titanate $Pb(Ti_xZr_{1-x})O_3$, commercially called PZT, is a solid solution of orthorhombic $PbZrO_3$ and tetragonal $PbTiO_3$ with a perovskite structure. The Morphotropic Phase Boundary (MPB) between the tetragonal and rhombohedral phase, corresponding to the optimum compositional range where, due to the coupling

between two equivalent energy states, the piezoelectric performances peak, is almost vertical in PZT. For compositions near this boundary a large number of polarization directions are available, leading to high values of electromechanical coupling coefficients and electrical permittivity [67, 68, 69, 70]. We will discuss the details of these aspects in following Section.

By controlling chemistry and processing, a large quantity of compositions and geometrical shapes can be optimized for specific applications. By adding different kinds of dopants (donor or acceptors), PZT properties can be strongly modified [71].

Lead titanate $PbTiO_3$, the solid solution end member of PZT family, has a Curie temperature of about 470 °C and a tetragonal structure similar to $BaTiO_3$. As in the case of PZT, a large number of modifications have been developed to optimize specific electrical and mechanical performances. Many commercial compositions involve doping with samarium or calcium for use in hydrophones, with the side effect of lowering the Curie temperature to around 240 °C. Other compositions, doped with other elements, have Curie temperature values near 470 °C and have found applications in knock sensors for automobile engines. The higher operating temperature of lead titanate allows it to be mounted closer to the combustion chamber, thus giving a faster response time compared to PZT [67].

Other well known piezoceramics that must be mentioned are bismuth titanate ($Bi_4Ti_3O_{12}$) (see References [72, 73, 74, 75, 76]) and lead metaniobate ($PbNb_2O_6$) (see References [77, 78, 79]). Since they were not involved in this study will not deal with them. Many information are available in the literature.

From each piezoceramic previously described a family of piezoceramic materials is derived; in each family a controlled variation of composition allows wide range of properties. Big efforts have been still doing to optimize the composition and to control the manufacturing process of piezoceramics [80, 81].

The possibility of tailoring the composition and shape of piezoceramics for a specific application has been the reason of their success. Furthermore, scaling down the size of piezoceramics to nanometers offers even more opportunities for shaping piezoelectric devices. Compared to single crystals,

ceramics offer also the advantage of high strength, high electromechanical transformation efficiency, easy processing, especially into complex shapes and large area pieces, and mass production, leading them to become leader in the market.

The conventional manufacturing process of piezoceramics consists in the metal oxides mixing, calcinating, milling to a predetermined particle size, forming by means of dry press, or isostatic press or slip casting and sintering. After sintering the piezoelectric ceramic is machined to its target dimensions, grinded, lapped. But a few disadvantages, such as compositional inhomogeneity resulting from the incomplete reaction of the starting materials, volatilization of lead oxide due to the high processing temperatures, and impurities from the grinding media can severely affect the performances of the piezoceramic. In Section 4.2 a detailed description of the most powerful synthetic approaches for the synthesis of piezoceramics — in their nanostructured forms — will be discussed.

Because of the reciprocal coupling between mechanical and electrical energy, piezoelectric materials are used in a wide application range, which is continuously increasing with the improvement and development of new materials. They can be used as sensors, converting the mechanical into electrical energy (with a frequency range from 1 Hz to several MHz), or as actuators, converting the electric into mechanical energy (with force changes from mN to kN) or they function as both sensors and actuators. The number of piezoceramic applications is so high that it is not possible to mention all in a single paper. A snapshot with few examples is reported in Figure 5.4.

In the daily life, the piezoelectric effect is exploited in heaters and lighters, where a lever applies a pressure to a piezoceramic, inducing an electric field, which is strong enough to create a spark, and as signal filters in television remote control and communications.

In automotive engineering, piezosensors are used for occupant safety and intelligent engine control solutions, such as reversing sensors helping for parking or knock sensors to monitor the engine vibrations. In underwater applications, the echo sounders range from small individual transmitters for pleasure boats to professional systems used in large ships to sound the water depth or to locate schools of fish.

Military	Commercial	Medical
Hydrophones	Ultrasonic cleaners	Ultrasonic cataract removal
Depth sounders	Ultrasonic welders	Ultrasonic therapy
Range finders	Ultrasonic drilling	Ultrasonic transducers
Security systems	Ultrasonic degreasers	Insulin pumps
Automotive	Ultrasonic probes for NDT	Fetal heart detectors
Knock sensor	Level indicators	Flowmeters
Airbag sensors	Flaw detection	Ultrasonic imaging
Vibration control	Seismic sensors	Nebulizers
Spark ignition	Geophones	Consumer
Keyless door entry	TV and radio resonators	Gas igniters
fuel atomisation	Ink printings	Cigarette lighters
Computer	Alarm systems	Smoke detectors
Microactuators for hard disk	Strain gauges	Phonograph cartridges
Transformers for notebook	Ignition systems	Speakers
	Fish finders	Musical instruments
	Microphones	

Figure 2.2: Some applications of piezoelectric ceramics.

In aircraft engines, gas turbines and power generators ultrasonic sensors are used for dynamic monitoring. Sensors strategically mounted on the machine detect destructive conditions of imbalance or unequal loading of the rotor, enabling the possibility of corrective measures to be implemented. The sensor converts the associated mechanical energy of the vibration into electrical energy, which can be amplified and monitored [82, 67].

In ultrasonic systems, piezoceramics devices can generate powerful ultrasonic waves used for cleaning, drilling and welding, as well as to stimulate chemical processes. Moreover, they act as transmitters and receivers of ultrasonic waves in medical diagnostic equipment and non-destructive material testing, being a valuable tool for locating defects within a structure. In a non-destructive testing, a piezoceramic transducer generates an acoustic signal at ultrasonic frequencies that is transmitted through the test specimen. When the acoustic wave reaches an interface of the sample, it is reflected back to the transmitter/sensor, which, therefore, acts as a receiver. If, however, the acoustic wave impinges upon a flaw, a portion of the wave is reflected and thus reaches the sensor ahead of the original wave [83].

The reverse piezoelectric effect is used in micro-positioning, where an electric field applied to a piezoceramic is used to produce precise motion. Examples of applications are: fibre optic alignment, machine tool align-

ment, active damping, image enhancement through mirror tilting and so on. Piezoceramic actuators are used also in hydraulic and pneumatic valves and in medical devices such as lithotripters, surgical knives or inhalators with ultrasonic nebulizers [67]. Piezoelectric materials are also exploited in microscopes such as AFM and Scanning Tunneling Microscopy (STM) [84].

2.2 Crystalline Structure and Piezoelectric Properties

The ability of piezoelectric materials to transform electrical in mechanical energy and vice versa depends on their crystalline structure. The necessary condition for the occurrence of piezoelectric effect is the absence of a centre of symmetry in the crystal. This condition is necessary to have charge separation between positive and negative ions and for the formation of Weiss domains, i.e. dipole groups with parallel orientation. By applying an electric field to a piezoelectric material, the Weiss domains align proportionally to the field (see Figure 2.3). Consequently, the material dimensions change, increasing or decreasing if the direction of Weiss domains is the same or opposite to the electric field. After the sintering stage, poly-

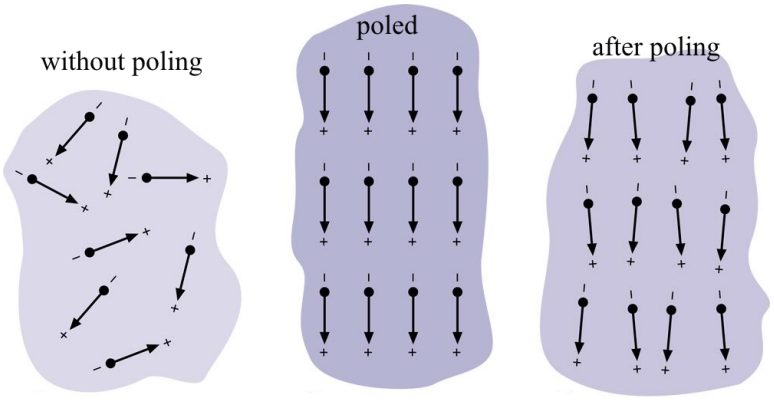

Figure 2.3: Electric dipoles in Weiss domains.

crystalline piezoceramics, consist of a huge number of randomly oriented dipoles without piezoelectric properties. In these isotropic materials the piezoelectricity is induced by a poling process, consisting in the application

of a strong electric field at high temperatures, which aligns the molecular dipoles in the same direction of the applied field. The dipole moment remains unchanged after removing the electric field, and the ceramic exhibits piezoelectric properties unless an excessively high voltage or high stress is imposed upon it or unless it is heated to very high temperatures. If either of these conditions is reached, the energy input to the domains exceeds the internal binding force holding the domains in alignment and the material once again becomes unpoled [85]. As previously mentioned, most of piezoceramics ($BaTiO_3$, $PbTiO_3$, PZT) belong to the simple crystal structure of perovskite. In Figure 2.4 the elementary cell of a PZT crystal is represented. Lead atoms are positioned at the corners of the unit cell and oxigens at the

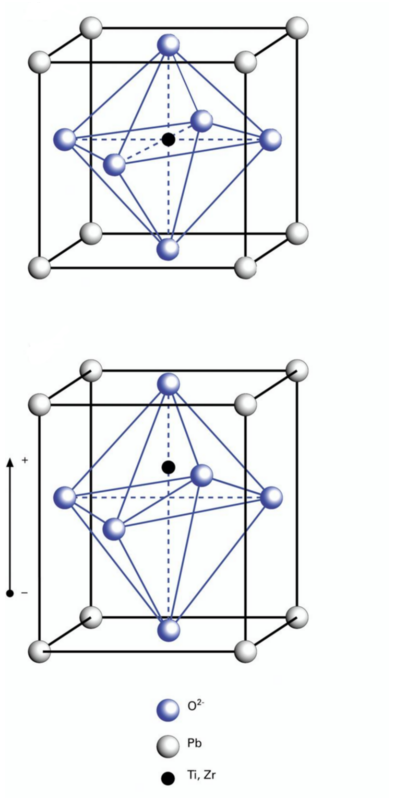

Figure 2.4: Piezoelectric elementary cell of a PZT ceramic above and below the Curie temperature.

face centers. Above a specific temperature, called Curie temperature, the lattice has a cubic structure, i.e. it consists of regularly arranged oxygen

octahedrons in the centre of which the titanium or zirconium ion is placed. Below the Curie temperature the lattice structure reorders to a mixture of rhombohedral and tetragonal crystals in which the titanium or zirconium ion is no longer placed in the centre but shifts from its central location along one of several allowed directions. Due to this displacive phase transformation with atomic displacements of about 0.1 Å, a separation of charges takes place and produces an electric dipole with a single axis of symmetry [86].

In order to provide a deeper and more quantitative knowledge on the piezoelectric properties of piezoceramics, a number of interrelated coefficients, many of which have been standardized by the Institute of Electrical and Electronics Engineers (IEEE) will be introduced. Because of the anisotropic nature of piezoceramics, the effects are strongly dependent upon the orientation with respect to the poled axis. This latter represents the direction of polarization and is generally designated as the z-axis of an orthogonal crystallographic system. The axes x, y and z are respectively represented as 1, 2 and 3 directions and the shear directions around these axes are represented as 4, 5 and 6. To link electrical and mechanical quantities, double subscripts are introduced. The first subscript gives the direction of the electrical field associated with the voltage applied or the charge produced. The second subscript gives the direction of the mechanical stress or strain. Superscripts “S”, “T”, “E”, “D” describe an electrical or mechanical boundary condition:

- S = strain = constant (mechanically clamped)
- T = stress = constant (not clamped)
- E = field = constant (short circuit)
- D = electrical displacement = constant (open circuit)

It should be clearly understood that the piezoelectric coefficients described here are not independent constants but vary with temperature, pressure, electric field, form factor, mechanical and electrical boundary conditions etc. The coefficients only describe material properties under small signal conditions.

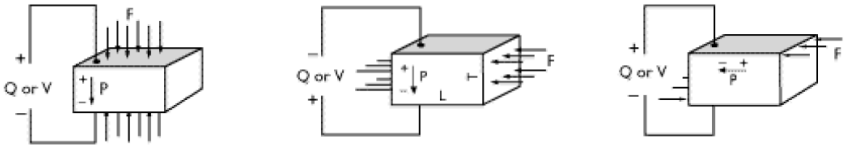

Figure 2.5: Relationships between force and electric charge for different vibration modes of piezoelectric crystals.

Piezoelectric Charge (or Strain) Constant d

It represents the mechanical strain produced by an applied electric field:

$$d = \frac{s}{V}, \tag{2.1}$$

where s is the strain development and V is the applied electric field. Large d_{ij} constants relate to large mechanical displacements, which are usually sought in motional transducer devices. Conversely, the coefficient may be viewed as relating the charge collected on the electrodes, to the applied mechanical stress.

$$d = \frac{q}{F}, \tag{2.2}$$

where q is the short circuit charge density and F is the applied mechanical stress. According to the different modes with which the stress can be applied, it is possible to have different d constants (see Figure 2.5). d_{33} (direct d) is used when the force is in the 3 direction (along the polarization axis) and is impressed on the same surface on which the charge is collected (Fig. 9.a); in this case the mechanical stress is parallel to the dipole moment, producing an enhancement of the spontaneous polarization along the 3 axis. d_{31} (transverse d) is used when the charge is collected on the same surface as before, but the force is applied perpendicularly to the polarization axis. d_{15} (shear d)is used when the charge is collected on electrodes perpendicular to the original poling electrodes and the applied mechanical stress is shear that tilts the dipoles.

Piezoelectric Voltage Constant g

It represents the electric field produced at open circuit by a mechanical stress:

$$g = \frac{E}{F}, \tag{2.3}$$

where E is the open circuit electric field. The g constant is a measure of the sensitivity of a piezoelectric material, because it is proportional to the open circuit voltage. The sensitivity needs to be sufficiently high so that the generated signal can be detected above the background noise. The sensitivity is maximized when the g coefficient is maximized. Therefore, high g_{ij} constants are required for sensors. Although the g coefficients are called voltage coefficients, it is also correct to say that g_{ij} is the ratio of strain developed over the applied charge density:

$$g = \frac{l}{c}, \tag{2.4}$$

where l is the strain developed and c is the applied charge density. As in the case of the d constant the direct, transverse and shear piezoelectric voltage constants can be measured depending on the angle between the polarization and the mechanical stress direction.

Electromechanic Coupling Coefficient k

It describes the conversion of energy from electrical to mechanical form or vice versa representing a sort of piezoelectric efficiency of the material. It measures how strong the coupling is between the vibration mode and the excitation. Since this coefficient is an energy ratio, it is dimensionless. Subscripts denote the relative directions of electrical and mechanical quantities and the kind of motion involved. Large k_{ij} coefficients provide a more efficient energy transfer and are required in the piezoelectric actuators. k_{ij} determines the bandwidth of filters and transducers.

$$k = \frac{E_{ael}}{E_{smc}}, \tag{2.5}$$

or

$$k = \frac{E_{amc}}{E_{sel}}, \tag{2.6}$$

where E_{amc} and E_{ael} are the accumulated mechanical energy and the accumulated electrical energy, respectively, while E_{smc} and E_{sel} are the supplied mechanical energy and the supplied electrical energy.

Dielectric Constant ε_r

The relative dielectric constant is the ratio of the permittivity of the material, ε, to the permittivity of free space, ε_0, in the unconstrained condition, i.e., well below the mechanical resonance of the part.

$$\varepsilon_r = \frac{\varepsilon}{\varepsilon_0}, \tag{2.7}$$

Large dielectric constants are required for sensors in order to overcome the losses associated with the cables, but an excessive value of ε_0 decreases the voltage coefficients and thus the sensitivity according this relationship between d and g coefficients:

$$g_{ij} = \frac{d_{ij}}{\varepsilon\varepsilon_0}, \tag{2.8}$$

Curie Temperature

It is the critical temperature at which the crystal structure changes from a non-symmetrical (piezoelectric) to a symmetrical (non-piezoelectric) form in which the piezoelectric properties are lost. Upon cooling the dipoles don't realign unless they are subjected to a strong electric field. Other consequences of increasing temperature are changes in the value of electromechanical coefficients and the process called "thermally activated aging". As a practical rule, the maximum operating temperature of a piezoceramic is about half the Curie temperature.

Young's Modulus

The Young's modulus of a piezoelectric material, i.e. the ratio of stress (force per unit area) to strain (change in length per unit length), changes with the electric load. Because mechanical stressing of the ceramic produces an electrical response, which opposes the resultant strain, the effective Young's Modulus with electrodes short-circuited is lower than with the

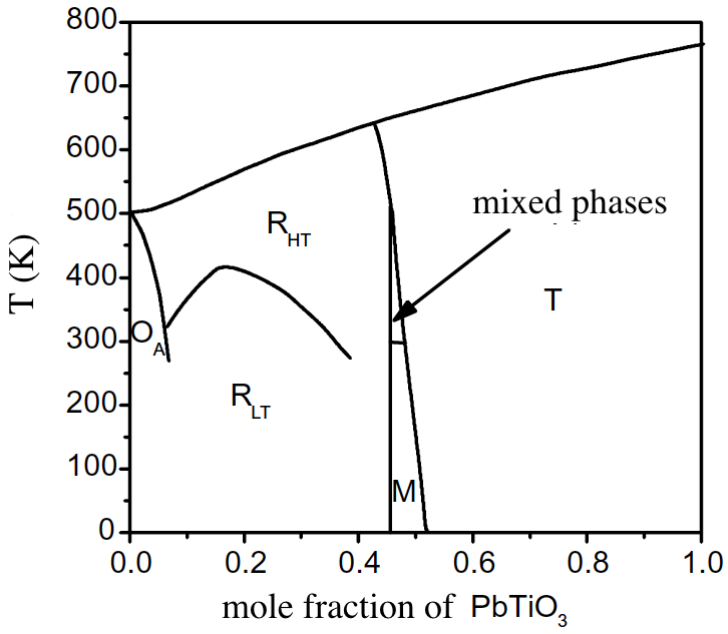

Figure 2.6: The phase diagram of $Pb(Ti_xZr_{1-x})O_3$ modified from Jaffe, Cook and Jaffe [70] to include the monoclinic phase [87].

electrodes open circuited. In addition, the stiffness is different in the 3 direction from that in the 1 or 2 direction. Therefore, in expressing such quantities, both direction and electrical conditions must be specified. The Young's Modulus of a piezoceramic is about one quarter that of steel.

2.3 PZT

Lead zirconate titanate ($PbTi_xZr_{1-x}O_3$) has been the leading, high activity ferroelectric material for over 40 years and consequently is at the heart of the majority of piezoelectric actuators and sensors in production today [70]. For the majority of applications of PZT, the optimum performance is found at the boundary between the tetragonal and rhombohedral perovskite phases (see Figure 2.6) often known as the MPB [70].

Conventional wisdom suggests that for compositions close to the MPB, the piezoelectric coefficients maximize due to (i) a peak in the spontaneous polarization, to which the intrinsic piezoelectric coefficient is proportional

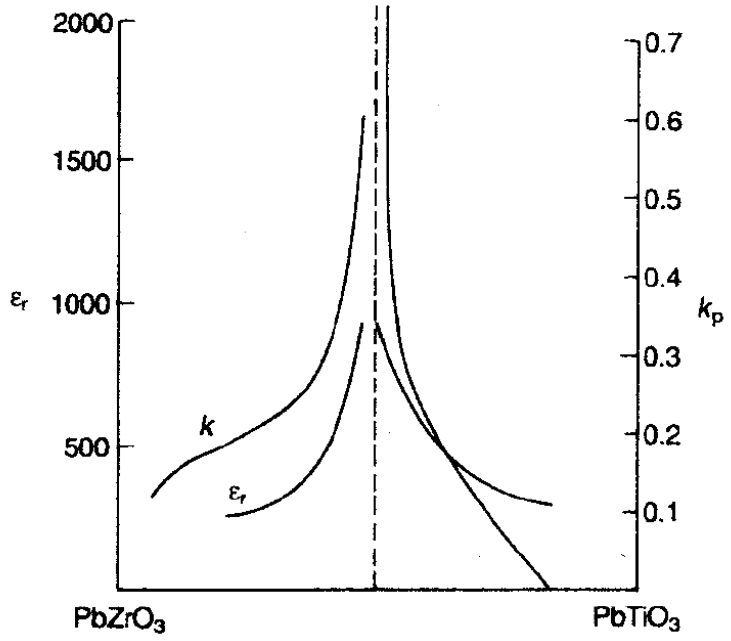

Figure 2.7: Coupling coefficient k_P and ε_r values across the PZT compositional range [70].

and (ii) near degeneracy of the tetragonal and rhombohedral states, which allows for ease of reorientation of domains under applied fields and stresses, thereby maximizing the extrinsic piezoelectric contributions (see Figure 2.7). Consequently, much of the past research and development work on PZT has focused on the management of domain wall mobility through the control of defect chemistry. The discussions in this paper, however, focus mainly on the intrinsic contribution.

Since the morphotropic phase boundary in PZT ceramics is seen as central to their outstanding piezoelectric performance, the search for new or improved materials focuses on systems which possess a similar phase boundary. However, a number of relatively recent discoveries have driven a reassessment of our understanding of the MPB in PZT; these are:

- The unprecedented performance of complex perovskite single crystals, such as [001]-oriented $Pb(Zn_{1/3}Nb_{2/3})O_3$-$PbTiO_3$ compositions on the rhombohedral side of their MPB; the mechanism appears to rely on a field-induced rotation of the polarization vector in the (110) plane

from the [111] to the [001] axis [88];

- A previously undetected monoclinic phase at the morphotropic phase boundary in PZT [87] with polarization in the (110) plane and the presence of monoclinic [89] and orthorhombic [90] phases at the phase boundary in the complex-perovskites;

- The local atomic displacements in PZT appear to differ from those consistent with the macroscopic symmetry [91]: for example, in the rhombohedral phase the lead cation displacements seem to be composed of local, short-range, random arrangements of tetragonal type displacements superimposed on the average, long range rhombohedral order.

2.3.1 Polarization Rotation

Asimplistic treatment of the intrinsic component of piezoelectricity might suggest that the piezoelectric effect is greatest parallel to the polar axis. That is, on applying an electric field parallel to the spontaneous polarization, P_s, it is augmented by an induced polarization, P_{ind}, which adds to the lattice strain, x:

$$\Delta x = x - x_s \approx 2QP_s\varepsilon E, \tag{2.9}$$

where x_s is the spontaneous strain and Q is the relevant electrostriction coefficient. For small fields, the induced strain, x, is proportional to the electrostriction coefficient, the spontaneous polarization and the permittivity, ε, where E is the applied electric field; the intrinsic piezoelectric coefficient, d_{int}, is given by:

$$d_{int} = 2QP_s\varepsilon. \tag{2.10}$$

As the direction of P_s is normally taken to be the direction of maximum spontaneous polarization, this textbook treatment can lead to the fallacy that the maximum intrinsic piezoelectric effect occurs parallel to the polar axis. Whilst this may be true for simple compounds well removed from phase transitions, it does not necessarily hold close to phase transitions at which the direction of the spontaneous polarization changes (for example at the morphotropic phase boundary in PZT or at the tetragonal-orthorhombic

transition in barium titanate). The misconception is highlighted by the large piezoelectric effect in "domain-engineered" complex perovskite single crystals [88]. It was noted that close to the MPB, in [001]-poled rhombohedral crystals, the piezoelectric coefficient is much greater parallel to [100] than it is along the polar [111] axis. It was proposed and confirmed [92] that on applying a field parallel to [001], the polarization rotated from the [111] axis continuously through the (110) plane to lie parallel, at a sufficiently high field, to the [001] axis. This "polarization rotation" was accompanied by a large induced strain. Support for this type of mechanism came in the form of calculations, from both the *ab initio* [93] and thermodynamic [94] schools, using $BaTiO_3$ as a prototype. In the latter case, the Landau-Ginzburg-Devonshire (LGD) approach was used to show how the piezoelectric coefficients parallel to the nonpolar low-index axes could exceed those parallel to the zero-field polar axes, again due to field induced rotation of the polarization vector. Furthermore, Damjanovic [95] calculated that in barium titanate the direction of maximum piezoelectric coefficient itself rotates as a function of temperature close to the tetragonal-orthorhombic transition. A number of *ab initio* calculations for PZT have also supported the rotation hypothesis [96, 97].

2.4 Nanosized Ferroelectrics

The ferroelectric polarization results from the sum over all dipole moments within a unit cell and is equivalent to a surface charge density which rapidly drops with shrinking lateral dimensions. In principal one may assume that bulk ferroelectricity lasts all the way down to the unit cell capacitor. But as ferroelectricity is a cooperative phenomenon of interacting dipoles, deviations from bulk behaviour are expected as the number of contributing unit cells decreases. The ultimate (shape dependent) volume below which spontaneous polarization ceases is referred to as the *superparaelectric limit*. The search for the superparaelectric limit is fundamental but closely linked to rather technological issues like the impact of grain shape and aspect ratio [98], substrate strain [99], polarization tilting under biaxial strain [100], dislocations [101, 102, 103], extended defects [104, 105], do-

main formation and pinning [106, 107, 108, 109], electrode and perimeter effects [110, 111], chemical (de-)composition and measurement limitations [112, 113]. In a recent paper Glinchuk and coworkers [114] have proved that under the favorable conditions ensemble of noninteracting nanoparticles possesses superparaelectric features.

In summary, the conditions of superparaelectric phase appearance in the ensemble of noninteracting ferroelectric particles of spherical shape and their properties, which can be considered as characteristic features of Superparaelectric (SPE) phase, can be summarized as it follows; (i) The superparaelectric phase can appear in ferroelectric nanoparticles of average radius $R_{cr} < R < R_c$ at temperatures $T_f(R) < T < T_{cr}(R)$. Here R_c is the correlation radius (which can be calculated through the fluctuation-dissipation theorem) and R_{cr} is the critical radius which defines size-driven ferroelectric-paraelectric phase transition. $T_f(R)$ is the freezing temperature (which can be estimated from the condition $\Delta F(T_f, R) = k_B T_f$, where $\Delta F(T_f, R)$ is the potential barrier for polarization reorientation) while T_{cr} is the temperature of size-driven ferroelectric-paraelectric phase transition. In this region:

- All nanoparticle dipole moments are aligned due to the correlation effects.
- Potential barrier of polarization reorientation is smaller than the thermal activation energy $\approx k_B T$
- Langevin-like law for polarization dependence on external field is valid at temperatures higher than the freezing temperature $T_f(R)$, but lower than the temperature $T_{cr}(R)$ of size-driven ferroelectric-paraelectric phase transition.
- Hysteresis loop and remnant polarization (frozen SPE) appear at temperatures $T < T_f(R)$.
- The observation time of the experiment t should be larger than characteristic time τ of particle reorientation in external field. The time τ is given by the Arrhenius law:

$$\tau = \tau_0 e^{\frac{\Delta F}{k_B T}} \tag{2.11}$$

where the barrier height ΔF is proportional to the particle volume V.

(ii) The favorable conditions or the superparaelectricity observation in small ferroelectric nanoparticles at room temperatures are small Curie-Weiss constant, high nonlinear expansion coefficients (see Reference [114] for details) and narrow distribution function of particle radii. Remarkably, the ensemble of noninteracting ferroelectric nanoparticles could be realized in nanoporous nonferroelectric matrix with the porous filled at least partly by some ferroelectric material.

Chapter 3

Geotextiles and Composite Materials

Composite materials (or *composites* for short) are engineered materials made from two or more constituent materials with significantly different physical or chemical properties which remain separate and distinct on a macroscopic level within the finished structure. *Geotextile composites* (or shortly *geotextiles*) are permeable fabrics which, when used in association with soil or masonry, have the ability to separate, filter, reinforce, protect, or drain. When they are properly functionalized they can be also applied for the detection of environmental conditions. Overall, these materials are referred to as *geosynthetics* and each configuration — geonets, geogrids and others — can yield benefits in geotechnical and environmental engineering design. Geotextiles and related products have many applications and currently support many civil engineering applications including roads, airfields, railroads, embankments, retaining structures, reservoirs, canals, dams, bank protection, coastal engineering and construction site silt fences. In this Chapter we will briefly introduce geotextiles (3.1) and their applications (3.2). Finally, piezoelectric composite materials will be presented in Section 3.3.

3.1 A Brief Introduction to Geotextiles

Technical textiles are extensively used in construction, which is one of the main application sectors [115, 116, 117, 118, 119]. The most important application in terms of volume of textile material is concerning the application of geotextiles used for the strengthening and stabilization of earthworks, including embankments for roadways and railroads, natural slopes, airports pavements.

The principal functions of geosynthetics are filtration, drainage, separation, reinforcement, provision of a fluid barrier, and environmental protection. Expanded use of geosynthetics will likely occur as design and installation procedures continue to be refined, but their application can be significantly increased only if more definitive economic benefits and integration of functions are introduced and demonstrated. Effectively, geotextiles containing sensor fibers are still an exception. Though there have been made efforts to integrate nonoptical sensor systems into textiles, by now it was not possible to create solutions for measuring deformations over extended areas or at several points by using single integrated sensor fibers.

Another application where technical textiles are used is for the retrofitting of infrastructure members, including bridge piers and columns of buildings. The principal function in this case is the increase of strength of the structural member and state-of-the-art solution is to use bidirectional woven textiles of uniform thickness. For reinforced masonry it is possible to use textile material as load-bearing part of the building. When the building is loaded in case of earthquake the reinforced structure shows a better shear and bearing behaviour.

Common techniques for retrofitting of masonry so far include the construction of jackets made of steel-reinforced shot-concrete, external post-tensioning with steel ties, polymer rods stuck into milled grooves and strips made of fibre reinforced polymer or steel glued and potentially mechanically anchored on the walls surface.

Each of these techniques suffers from diverse disadvantages. Heavy jackets add considerable mass to the structure resulting in increased dynamic loads. Post-tensioning is only applicable if the masonry offers sufficient

reserves for additional vertical loading. Jackets as well as milled grooves require a huge amount of work input and steel components suffer from the danger of corrosion damage. Furthermore due to its low tensile strength, masonry is very sensitive regarding stress concentrations caused by surface-glued strips yielding to brittle failure.

These aspects have led to the idea of strengthening existing masonry by the large-area application of Fibre Reinforced Composites (FRC) on the wall surfaces. Because of the materials little weight this technique is easy to apply and yields no extra loads. However up to now the combination of common fibre fabric structures with resin matrices represents the standard case in FRC-strengthening of masonry. These fibre reinforced polymers were originally introduced in the aircraft and automotive industry to build up extremely lightweight and high strength construction materials. But for structural strengthening of masonry they are only conditionally applicable.

Both the applications mentioned (earthworks and masonry structures) are very important for the technical textile industry, but it is needed to advance beyond the state of the art solutions, to make the textile structure able to integrate different functions and to provide cost effective solutions in the medium-long term. In fact, except for the geotextiles with glass-fibre based Bragg grating sensors, in literature no others experiences regarding to integration of optical sensor fibers in textile area-measured material are known. Particularly the integration of polymer optical sensor fibers with their outstanding material properties in knitted fabrics does not exist up to now. We want to point out that the most promising technologies for the intended application (geotextiles and masonry structures) include the use of optical fibers and piezoelectric materials. The latter can be used for monitoring deformations, stresses and structural integrity.

3.2 Geotextile Functions and Applications

Geotextiles perform one or more basic functions [120]: filtration, drainage, separation erosion control, sediment control, reinforcement, and (when impregnated with asphalt) moisture barrier. In any one application, a geotextile may be performing several of these functions [121, 122, 123].

The use of geotextiles in filter applications is probably the oldest, the most widely known, and the most used function of geotextiles. In this application, the geotextile is placed in contact with and down gradient of soil to be drained. The plane of the geotextile is normal to the expected direction of water flow. The capacity for flow of water normal to the plane of the geotextile is referred to as permittivity. Water and any particles suspended in the water which are smaller than a given size flow through the geotextile. Those soil particles larger than that size are stopped and prevented from being carried away. The geotextile openings should be sized to prevent soil particle movement. The geotextiles substitute for and serve the same function as the traditional granular filter. Both the granular filter and the geotextile filter must allow water (or gas) to pass without significant buildup of hydrostatic pressure. A geotextile-lined drainage trench along the edge of a road pavement is an example using a geotextile as a filter. Most geotextiles are capable of performing this function. Slit film geotextiles are not preferred because opening sizes are unpredictable. Long term clogging is a concern when geotextiles are used for filtration [124, 125, 126].

A geotextile serves to control sediment when it stops particles suspended in surface fluid flow while allowing the fluid to pass through. After some period of time, particles accumulate against the geotextile, reducing the flow of fluid and increasing the pressure against the geotextile. Examples of this application are silt fences placed to reduce the amount of sediment carried off construction sites and into nearby water courses. The sediment control function is actually a filtration function.

When functioning as a drain, a geotextile acts as a conduit for the movement of liquids or gases in the plane of the geotextile [127, 128]. Examples are geotextiles used as wick drains and blanket drains. The relatively thick nonwoven geotextiles are the products most commonly used. Selection should be based on transmissivity, which is the capacity for in-plane flow. Questions exist as to long term clogging drains. They are known duration applications.

In erosion control, geotextile protects soil surfaces from the tractive forces of moving water or wind and rainfall erosion [129, 130, 131]. Geotextiles can be used in ditch linings to protect erodible fine sands or cohesionless

silts. The geotextile is placed in the ditch and is secured in place by stakes or is covered with rock or gravel to secure the geotextile, shield it from ultraviolet light, and dissipate the energy of the flowing water. Geotextiles are also used for temporary protection against erosion on newly seeded slopes. After the slope has been seeded, the geotextile is anchored to the slope holding the soil and seed in-place until the seeds germinate and vegetative cover is established. The erosion control function can be thought of as a special case of the combination of the filtration and separation functions.

In the most common reinforcement application, the geotextile interacts with soil through frictional or adhesion forces to resist tensile or shear forces. To provide reinforcement, a geotextile must have sufficient strength and embedment length to resist the tensile forces generated, and the strength must be developed at sufficiently small strains (i.e. high modulus) to prevent excessive movement of the reinforced structure. To reinforce embankments and retaining structures, a woven geotextile is recommended because it can provide high strength at small strains [132, 133, 134, 135, 136].

Separation is the process of preventing two dissimilar materials from mixing. In this function, a geotextile is most often required to prevent the undesirable mixing of fill and natural soils or two different types of fills. A geotextile can be placed between a railroad subgrade and track ballast to prevent contamination and resulting strength loss of the ballast by intrusion of the subgrade soil. In construction of roads over soft soil, a geotextile can be placed over the soft subgrade, and then gravel or crushed stone placed on the geotextile. The geotextile prevents mixing of the two materials [137].

Both woven and nonwoven geotextiles can serve as moisture barriers when impregnated with bituminous, rubber-bitumen, or polymeric mixtures. Such impregnation reduces both the cross-plane and in-plane flow capacity of the geotextiles to a minimum. This function plays an important role in the use of geotextiles in paving overlay systems. In such systems, the impregnated material seals the existing pavement and reduces the amount of surface water entering the base and subgrade. This prevents a reduction in strength of these components and improves the performance of the pavement system.

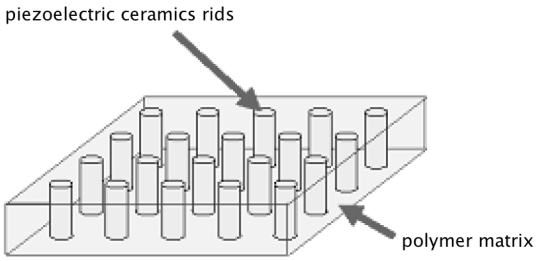

Figure 3.1: An example of a multifunctional textile structure.

3.3 Sensing Technologies: Piezoelectric Composites

As already discussed in Chapter 2 piezoelectric materials, like Lead Zirconate Titanate (PZT) and polyvinylidene fluoride (PVDF), can be used as sensors and/or actuators. One of drawbacks associated with the use of piezoelectric materials is that due to their crystalline structure, they are brittle and therefore are not suitable for situations where they are primarily subjected to large tensile stress. The piezoelectric effect offers the possibility for utilization in mechanical micro- and nanosensors such as pressure and acceleration sensors. When these pressure sensors are incorporated into masonry constructions, structural damage to masonry structures and earthworks can be detected.

The set-up of piezocomposites, compounds of polymer and piezoceramic, has extended the range of piezoceramic performances and applications. The 1-3 structure, which is nowadays mostly used as a transducer material, refers to parallel ceramic rods incorporated in an epoxy-resin matrix (see Figure 3.1). Piezocomposites have higher efficiency than pure ceramic so that a higher signal amplitude is obtained. Moreover the type of polymer used affects the mechanical and acoustical features of the piezocomposite element. Depending on the application, rigid or flexible polymers can be used in order to change the internal damping of the element. Piezocomposites are used in those applications where broadband transducers and high penetration capability are required [138, 139].

A promising technique to apply and cure nanopiezoelectric particles over the fabric is by encapsulation with acrylate. Acrylates particles are building from the monomer stage up to the desire particle size, which usually range from 50 nm up to 1 micrometer. Acrylates can be tailor-made according to the application demands: one can control the building blocks of the polymeric chain or surfactants type and quantities. Those options immediately influence the chemical and physical properties of the binder. Thus the major controlled properties are hydrophilic/hydrophobic, flexibility, strength, foaming, elongation and film appearance. A schematization of a piezoelectric geotextile is reported in Figure 3.2.

In order to bind the nanopiezoelectric particles to the fabric, for better weathering stability properties, it is crucial to develop stable nanosystem that will function both as binding and carrying element. Thus the encapsulation system should take care about the fabric nature, final fabric properties and the way of applying the material (spraying, printing, padding etc.) as well as maintaining the activity of the electric properties of the particles. The combination of geotextiles and mortars for masonry structures, demands for compatible materials to control the interface properties.

Unreinforced masonry structures are ranked among the oldest buildings of mankind and are spread throughout the world due to their various advantages. But in seismic regions they are highly vulnerable because being originally designed mainly for gravity loads they often cannot withstand the dynamic horizontal loads in case of strong earthquakes. But also defective workmanship or strong decay of material by exposure to climate conditions enhance the seismic vulnerability of masonry. Damage up to collapses of whole buildings associated with loss of life and property are the consequences. Hence the necessity arises to develop efficient methods for the strengthening of endangered masonry buildings. New practical measures and technologies in the range of modern surface-applied fiber-composite materials to strengthen or retrofit endangered or predamaged masonry structures have to be found. Durable materials easy to applicate combined with a neutral physical, long-term and environmental behaviour must fulfill all mechanical demands.

Novel 2D textile fabrics will be introduced in the future. These textiles

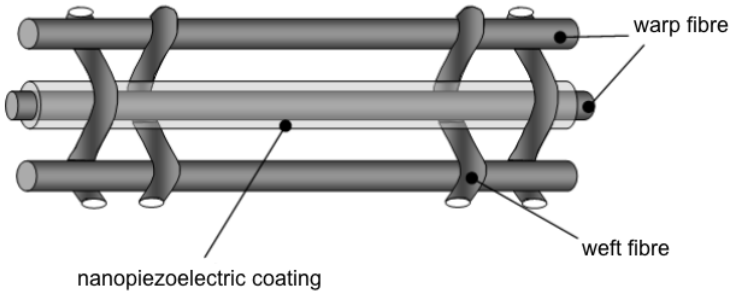

Figure 3.2: An example of a multifunctional textile structure.

will have embedded optical fibers for constant on-line health monitoring of the structure. Moreover several fibers will have piezoelectric ceramic coatings so as to generate electric pulses as they are loaded and yield some indication of the internal stressing of the building.

Application of multifunctional technical textiles for the reinforcement of masonry structures is schematically depicted in Figure 3.3. In this case real-time, in-service health monitoring techniques can be harnessed to reduce costs and improve safety. The new health monitoring technique relies on the use of piezoelectric materials, surface bonded or embedded onto the textile structure which behave as a support to actively conduct on-line health monitoring.

Despite the efforts of the recent years, new nano-structured mortars and adhesive materials suitable for the specific application — featuring a neutral behaviour under fire and providing suitable mechanical properties — must be developed. Also advancements in the range of fibre structures have to be made. Materials have to be developed which are durable in the environmental matrix. Moreover these textiles will have embedded sensors for constant on-line monitoring and damage detection in order to assess the structural health of the retrofitted structure after an earthquake.

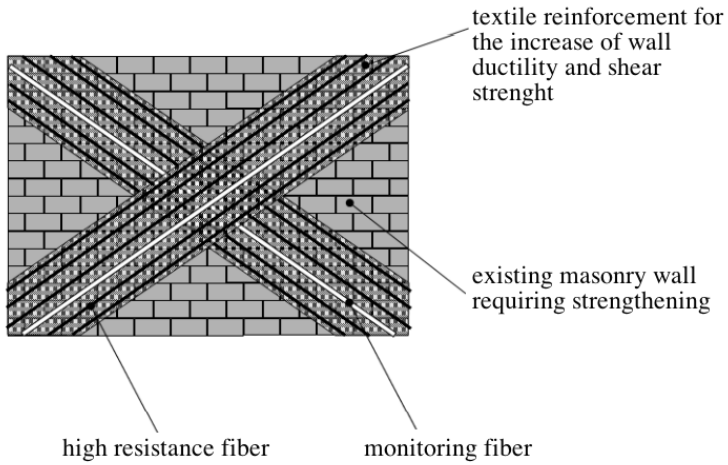

Figure 3.3: A schematization of the application of multifunctional technical textiles to masonry retrofitting.

Chapter 4

PZT Nanoparticles

In this Chapter we will briefly discuss the chemical properties of lead, titanium and zirconium, their coordination and organometallic chemistry, and how these relate to the synthetic approach for PZT nanosystems (Section 4.1). These concepts will provide in Section 4.2 the basis for a general discussion of the methods for the synthesis of PZT nanosystems. The experimental procedures for the synthesis of perovskite-like PZT nanocrystals will be explored and the experimental results will be presented in Sections 4.3 and 4.4. Section 4.5 is devoted to the study of PZT nanoparticles dispersions in water and to the characterization of the colloidal suspensions.

4.1 Chemistry of Lead, Titanium and Zirconium

Lead, titanium and zirconium, the cationic ingredients of PZT powders, belong to the 14^{th} and the 4^{th} groups of the periodic table respectively. Combining these elements in their cationic form into a unique water-based system is a task that requires a deep knowledge of their behavior in water solution. As it will be discussed in the following, the development of a water-based approach for the synthesis of PZT nanoparticles was chosen, requiring the cations to be present in a water solution in stable forms at the same time. Despite the different properties that they have (Table 4.1), Pb^{II}, Ti^{IV} and Zr^{IV} — the last two are extremely hard ions — can be combined in water solution with the aid of only one complexing agent.

Cation	Radius (pm)
Pb^{II}	119
Ti^{IV}	60.5
Zr^{IV}	72

Table 4.1: Ionic radii for 6-coordinated Pb^{II}, Ti^{IV} and Zr^{IV}[140].

4.1.1 Lead

Lead is one of the oldest metals known to mankind. It is by far the most abundant of the heavy elements (13 ppm), being approached amongst these only by thallium (8.1 ppm) and uranium (2.3 ppm). This abundance is related to the fact that three of the four naturally occurring isotopes of lead (206, 207 and 208) arise primarily as the stable end products of the natural radioactive series.

It is well recognized as a heavy metal poison binding to oxo groups in enzymes and affecting virtually all steps in the process of heme synthesis and porphyrin metabolism. Lead is also an inhibitor of acetylcholineesterase, acid phosphatase, ATPase, carbonic anhydrase, etc. In addition to oxygen complexation, Pb^{II} also inhibits SH-enzymes, especially interacting with cysteine residues in proteins. Typical symptoms of lead poisoning are cholic, anaemia, headaches, convulsions, chronic nephritis of the kidneys, brain damage and central nervous system disorders. Complexing and sequestering Pb^{II} using a strong chelating agent such as any anionic forms of ethylenediamine tetra-acetic acid (EDTA) or *(RS)*-2,3-disulfanylpropan-1-ol (BAL) is a common treatment.

Lead forms alkoxides mainly in +2 oxidation state. $Pb(OMe)_2$ was first reported by Szilard in 1906 as a product of anodic oxidation of metal in the NaOMe solution in MeOH. Chablay in 1917 succeeded in preparing $Pb(OR)_2$ with the aid of metathesis reactions of lead iodide or nitrate with NaOR in liquid ammonia. Recently volatile and hydrocarbon soluble $Pb(OR)_2$-derivatives of ramified radicals [141] and also bimetallic t-butoxides of lead and divalent metals have been described and structurally characterized. Un-

luckily Pb^{II} alkoxides are not commercially available. As it will be discussed in the following sections this aspect of lead organometallic chemistry will be extremely important when a source of Pb^{II} will be chosen for the synthesis of PZT nanoparticles.

The coordination chemistry of Pb^{II} is, amongst *p*-block elements, particularly broad, since it can adopt many different coordination geometries, allowing a high degree of tolerance for ligand conformations which is not seen in *d*-block elements [142]. Furthermore, despite its ionic radius and charge — which make of it a typical soft cation — Pb^{II} binds well to both hard and soft donor atoms [143, 144]. These properties make Pb^{II} an interesting cation which can form stable complexes with ligands such as the already mentioned EDTA.

4.1.2 Titanium and Zirconium

Titanium and zirconium have been considered in the past unfamiliar due to the difficulties involved in the preparation of the pure metals and also to their rather diffuse occurrence (6320 and 162 ppm respectively on the lithosphere). The most noticeable feature of these metals in the elementary massive form at room temperature is their outstanding resistance to corrosion, which is due to the formation of a self-healing oxide film. This is particularly striking in the case of zirconium. With the exception of hydrofluoric acid (which is the best solvent because of the formation of soluble fluoro-complexes) mineral acids have little effect unless hot.

Their cations are classified as type "a", since they bind strongly hard ligands, and are found as silicates and oxides in many siliceous materials. These are frequently resistant to weathering and so often accumulate in beach deposits. The most important oxidation state in the inorganic chemistry of these elements is the group oxidation state of +4. This is too high to be ionic, but zirconium, being larger, have oxides which are more basic than those of titanium and give rise to a more extensive and less hydrolyzed aqueous chemistry.

A huge number of coordination compounds of the M^{IV} cations have been studied [145, 146, 147, 148] and complexes such as $[MF_6]^{2-}$ and those with

O- or N-donor ligands are particularly stable [149, 150, 151]. The M^{IV} ions are sufficiently large, bearing in mind their high charge, to attain a coordination number of 8 or more, which is certainly higher than is usually found for most transition elements. Eight is not a common coordination number for the first member, titanium, but is very well known for zirconium, and the spherical symmetry of the d^0 configuration allows a variety of stereochemistries. Moreover, a well known, sensitive method for estimating titanium is to measure the intensity of the typical orange colour produced when H_2O_2 is added to acidic solutions of Ti^{IV}. The colour is due to the peroxo complex, $[Ti(O_2)(OH)(H_2O)]^+$. The peroxo ligand is apparently bidentate with oxygen atoms being equidistant from the metal ion.

Concerning alkoxides, complexes with both tetravalent cations are well characterized but those of titanium are particularly important. The solvolysis of $TiCl_4$ with an alcohol yields a dialkoxide:

$$TiCl_4 + 2ROH \rightarrow TiCl_2(OR)_2 + 2HCl.$$

Dry ammonia can be added to remove the HCl; then the tetraalkoxides are produced:

$$TiCl_4 + 4ROH + 4NH_3 \rightarrow Ti(OR)_4 + 4NH_4Cl.$$

These titanium alkoxides are liquids or sublimable solids with octahedral coordination of the titanium by polymerization, unless steric effects due to the alkyl chain prevent it. Lower alkoxides are particularly sensitive to moisture and hydrolyzation to the dioxide. Applying *organic titanates* (as they are frequently described) on surfaces can produce a thin, transparent, and adherent layer of TiO_2 to a variety of materials just by exposure to the atmosphere. They are consequently used in waterproof fabrics and also in heat-resistant paints. However, the most important commercial application is in the production of thixotropic paints which do not "drip" or "run". For this purpose the $Ti(OR)_4$ is chelated with ligands such as β-diketonates to give products of the type $[Ti(OR)_2(L\text{-}L)_2]$. These are water soluble and can be more resistant to hydrolysis. Titanium tartrate complexes, probably dimeric species such as $[Ti_2(tartrate)_2(OR)_4]$, are also useful catalysts in asymmetric epoxidations of allylic alcohols. As we

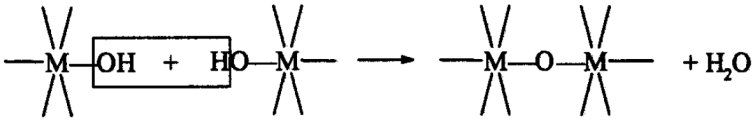

Figure 4.1: A schematization of the condensation process of two metal alkoxides: starting from hydrated metal alkoxides, water and M–O–M chains are obtained.

will discuss in the following these aspects will have an important impact on the synthesis strategy for PZT nanoparticles. Not surprisingly, in view of its greater size, zirconium shows a greater preference than titanium for O-donor ligands as well as for high coordination numbers, and this is shown by the greater variety of β-diketonates, carboxylates and sulfato complexes which it forms. Bis-β-diketonates such as $[MCl_2(acac)_2]$ of both metals are made by the reaction of MCl_4 and the β-diketonate in inert solvents such as toluene. They are octahedral with cis-chlorides. In addition, Zr^{IV} forms the monomeric, 7-coordinate $[MCl(acac)_3]$ complexes which have a distorted pentagonal bipyramidal stereochemistry. Also, in alkaline conditions, Zr^{IV} will yield the tetrakis complexes, $[M(acac)_4]$, in aqueous solution.

Hydrolysis of metal alkoxides is the basis for the sol-gel method of preparation of oxide materials; for this reason reactions of metal alkoxides with water in various solvents, principally alcohols, may be considered as their most important chemical property. Formation of M–O–M bonds in the hydrolysis products may follow mainly in two different paths. The first one is the typical aging process of hydrated oxides; their metal ions are coordinated by hydroxo, oxo, and aqua groups. Dehydration — which is sketched in figure 4.1 — of such product results in irregular amorphous oxide structures. The second way is characteristic only of metal alkoxides and involves the elimination of ethers as shown in figure 4.2. The principles of metal alkoxide hydrolysis were formulated by Livage and Sanchez [152]. A schematization of the hydrolysis process is shown in figure 4.3. On the addition of water or a mixture of water and alcohol to the solutions of alkoxides in organic solvents, nucleophillic attack of molecule at the positively charged metal atom occurs (a), which leads to an intermediate state

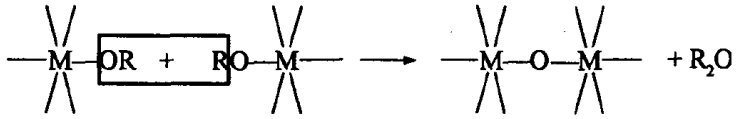

Figure 4.2: A schematization of the condensation process of two metal alkoxides: when metal alkoxides are not hydrated the final products of the reaction are M–O–M chains and ethers.

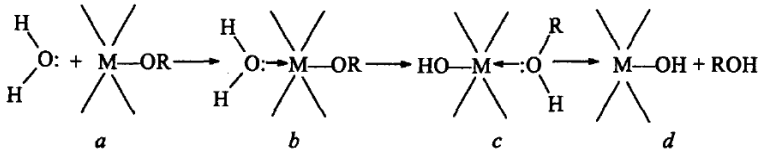

Figure 4.3: Metal alkoxide hydrolysis via nucleophilic attack of water on the electrophilic metal center.

(b). The shift of the proton from water molecule to the negatively charged oxygen atom of the neighboring OR-group results in the intermediate state (c) followed by elimination of an alcohol molecule. Thus, the whole process follows the mechanism of nucleophillic substitution. The thermodynamics of the reaction is determined by the nucleophilicity of the attacking group and the electrophilicity of the metal atom. The rate of the substitution process depends on the insaturation of the metal atom coordination sphere in the metal alkoxide, the stability of the transition state (b) and the possibility of the proton transfer within the transition state. $Ti(OR)_4$ and $Zr(OR)_4$ are definitively the most throughly studied alkoxides from the point of view of their hydrolytic decomposition. Depending on the hydrolysis technique, different products such as thin layers, fibers, glasses, and particles of $Ti(O)_2$ and $Zr(O)_2$ — but also more complex oxides — may be obtained. Several preparation techniques are described in the literature. On the other hand the physico-chemical aspect of hydrolysis received considerably less attention. The study of the hydrolysis and condensation of titanium n-butoxide by means of ^{17}O-NMR spectroscopy has shown that formation of oxo bridges occurs immediately after addition of water, proving the extremely high rates of both reactions. These rates are comparable even in the presence of re-

action inhibitors like acids and complexing agents [153]. Condensation of metal alkoxides occurring as a result of uncontrolled hydrolysis greatly influences further hydrolysis. Therefore, the properties of the products are highly dependent on the content of residual water in the solvent used for the preparation of the alkoxide solutions, as well as on the time and conditions of storage of the solutions prior to hydrolysis. This fact was demonstrated by the study of $Zr(OR)_4$ hydrolysis of which are especially sensitive to water [154, 155]. Acetic acid (HAc) has been reported to act as an acidic catalyst, increasing gelation time and leading to the formation transparent homogeneous gels. This effect can be explained by partial substitution of OR- by OAc- groups chelating metal atoms [156]. In the course of hydrolysis, the OAc-groups remain bonded to tetravalent cation and consequently hinder formation of gels. Acetylacetone and other β-diketonates are much stronger chelating agents. In this case precipitation does not occur even with a big excess of water, as chelating ligands cannot be completely eliminated. Blanchard and Sanchez used complex formation to slow down condensation in the course of hydrolysis [153].

4.2 PZT Synthesis

The synthesis of PZT products involves the use of different reactants and several steps, including a high temperature treatment. The conventional method for the preparation of a PZT powder is the solid-state mechanical mixing of carbonates, hydroxides and oxides. Although this process is feasible, several drawbacks have been reported in the literature: non-homogeneity of the final products, lack of control of the cation stoichiometry, abnormal grain growth, high temperature formation of perovskite phase, and poor sintering behavior [157, 158, 159, 160]. For these reasons the final electro-mechanical properties of the PZT material may not attain the requested standard. In order to avoid the problems arising with the common solid-state methods, several wet-chemistry routes were proposed for the preparation of nanostructured PZT materials [161]. All wet-chemistry methods involve the mixing of the starting materials at the molecular level, thus determining high compositional homogeneity, stoichiometry control and low

sintering temperatures [162, 163]. The common methods for the production of PZT nanoparticles include the *hydrothermal* synthesis [158, 164, 165], *co-precipitation* [159, 166], *sol-gel* techniques [160, 167, 168, 169], and *complexes combustion* (or *ligand burning*) process [157, 170, 171, 172, 173]. Sol-gel methods have been widely used for producing crystalline PZT nanoparticles. However, this synthetic route often involves the use of titanium and zirconium alkoxides, requiring then the use of nonaqueous solvents in the preparation of the piezoelectric powders. On the other hand, complexes combustion syntheses are based on the chelating properties of specific ligands, e.g. tartaric acid and citric acid, and are carried out in water. Here the starting materials are lead nitrate, titanium and zirconium oxides. Because of the low solubility in water of these compounds, a treatment with hydrofluoric acid is necessary to dissolve them. Afterwards, fluoride anions must be carefully removed to obtain the crystalline powders [174].

4.2.1 Sol-gel Methods

Sol-gel processing refers to the hydrolysis and condensation of alkoxide-based precursors. The earliest examples of such reactions was reported by Ebelmen in 1846 [175]. Sol-gel processing did not gather wide attention till Geffcken and Berger developed a method for the preparation of oxide films from sol-gel precursors in 1939 [176], which proved to be useful in the manufacturing of stained glass. The versatility and general usefulness of modern sol-gel processing is reflected in the huge volume of available literature.

Disregarding the nature of the precursors, the sol-gel process can be characterized by a series of distinct steps:

- **Step 1** - Formation of stable solutions of the alkoxide or solvated metal precursor (the sol).
- **Step 2** - Gelation resulting from the formation of an oxide- or alcohol-bridged network (the gel) by a polycondensation or polyesterification reaction that results in a dramatic increase in the viscosity of the solution. If so desired, the gel may be cast into a mold during this step.

- **Step 3** - Aging of the gel (syneresis), during which the polycondensation reactions continue until the gel transforms into a solid mass, accompanied by contraction of the gel network and expulsion of solvent from the gel pores. Ostwald ripening and phase transformations may occur concurrently with syneresis. The aging process of gels can exceed 7 days and is critical to the prevention of cracks in gels that have been cast.

- **Step 4** - Drying of the gel, when the solvents are removed from the gel network. This process is complicated due to fundamental changes in the structure of the gel. The drying process has itself been broken into four distinct steps: (i) the constant rate period, (ii) the critical point, (iii) the first falling rate period, and (iv) the second falling rate period. If isolated by thermal evaporation, the resulting monolith is termed a xerogel. If the solvent is extracted under supercritical or near-supercritical conditions, the product is an aerogel.

- **Step 5** - Dehydration, during which surface-bound M–OH groups are removed thereby stabilizing the gel against rehydration. This is normally achieved by calcining the monolith at temperatures up to 1000 °C.

- **Step 6** - Densification and decomposition of the gels at high temperatures ($T > 1000$ °C). The pores of the gel network are collapsed, and remaining organic species are volatilized. This step is normally reserved for the preparation of dense ceramics or glasses.

The sol-gel method has been widely used in preparing materials as nanoparticles, films and bulk forms. It is one of the most common synthesis technique for the preparation of ferroelectric materials — including PZT nanoparticles — and it offers several advantages [177, 178, 179]:

- Materials can be easily shaped into complex geometries in the gel state.

- Usually low temperatures, 200–600 °C, are required for the calcination step.

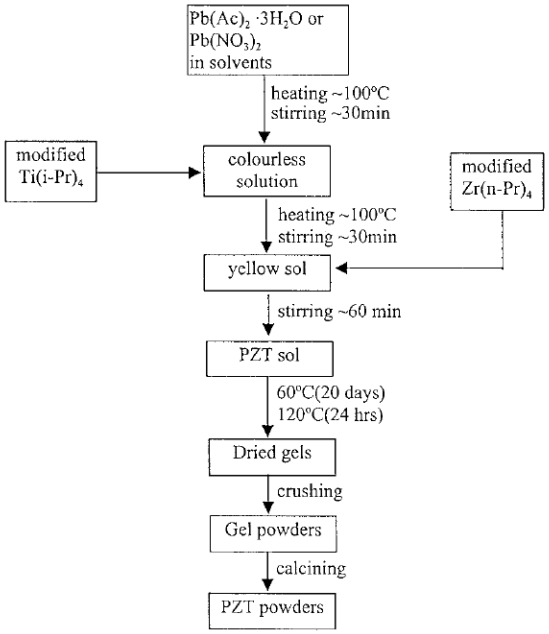

Figure 4.4: Flow chart of the sol-gel process developed by Wu *et al.* [160] for the production of PZT nanopowders. Acetic acid and 1,2-propanediol were used to dissolve the lead acetate. Ethylene glycol, 2-propanol and distilled water were used as solvents for the $Pb(NO_3)_2$.

- High purity products can be produced because the starting material can be mixed, dissolved in a specific solvent at the molecular level.

Despite these good points also some drawbacks have been reported. The sol-gel method necessitate of quite a long time — several days — to completed. In figure 4.4 we report a flow chart of the sol-gel method proposed by Wu *et al.* [160] for the synthesis of 52:48 PZT powders.

Many sol-gel methods reported in the literature for the preparation of PZT materials require nonaqueous solvents or reactants that are not commercially available [168, 180, 181, 182, 183]. These considerations limit the application of the method to small-scale production of PZT precluding the implementation of PZT synthesis in large-scale industry. The flow charts in figures 4.5 and 4.6 are just two of the many examples reported in the literature. Moreover, the calcination step — which inevitably leads to the agglomeration of the particles — must be cited.

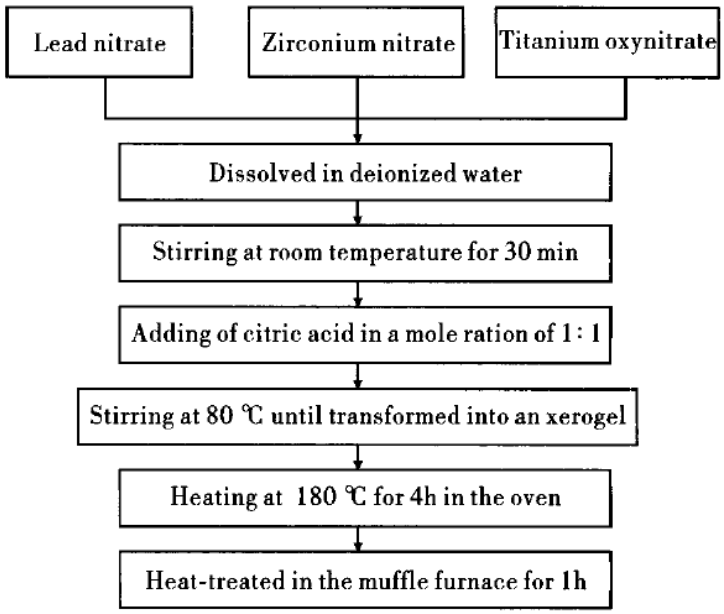

Figure 4.5: Flow chart of the synthesis of PZT nanopowders proposed by Li *et al.* [180]. Titanium oxynitrate and Zirconium nitrate can not be easily found on the market.

4.2.2 The Pechini Method

In 1967, Pechini developed a modified sol-gel process for metals that are not suitable for traditional sol-gel approaches because of their unfavorable hydrolysis equilibria [184]. Even though Pechini's original method was developed specifically for the preparation of thin films, it was later adapted to the synthesis of powdered materials. The Pechini method, as it is now referred to, relies on the formation of complexes of alkali metals, alkaline earths, transition metals, or even nonmetals with bi- and tridendate organic chelating agents such as citric acid. A polyalcohol like ethylene glycol is added to establish linkages between the chelates by a polyesterification reaction, resulting in gelation of the reaction mixture. A schematization of the early stages of the process is reported in figure 4.7. ^{13}C and ^{87}Sr Nuclear Magnetic Resonance (NMR) studies of some gelled precursors have also been published [185, 186, 187]. After drying, the gel is heated to initiate pyrolysis of the organic species, resulting in agglomerated submicron oxide

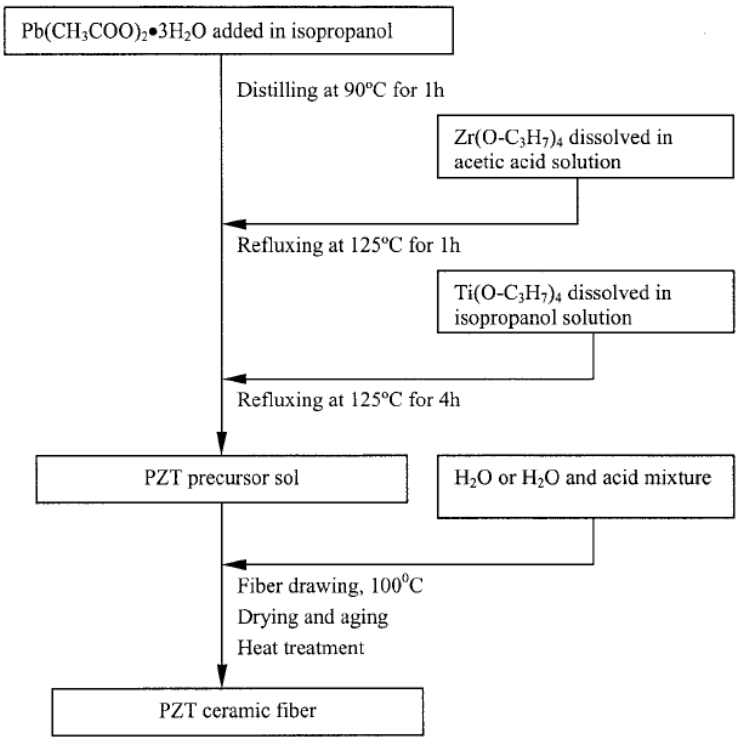

Figure 4.6: Flow chart for the preparation of PZT fibers according to procedure developed by Zhang *et al.* [182].

particles. The advantage of the Pechini method lies in the elimination of the requirement that the metals involved form suitable hydroxo complexes. Chelating agents tend to form stable complexes with a variety of metals over fairly wide pH ranges, allowing for the relatively easy synthesis of oxides of considerable complexity.

The literature contains numerous variations of the Pechini method, most of them involving alternative chelating agents. Several examples of complexing agents have been reported from EDTA [188] to the already cited citrate [187] and many others. EDTA is widely used as a complexing agent for quantitative complexometric titrations due to its ability to bind almost any cation. The four carboxylate groups allow the molecule to behave as either a bi-, tri-, tetra-, penta-, or hexadendate ligand, depending of course on the pH of its solution. Although EDTA's binding ability tends to increase with increasing pH, the polyesterification reaction between carboxylic acids and

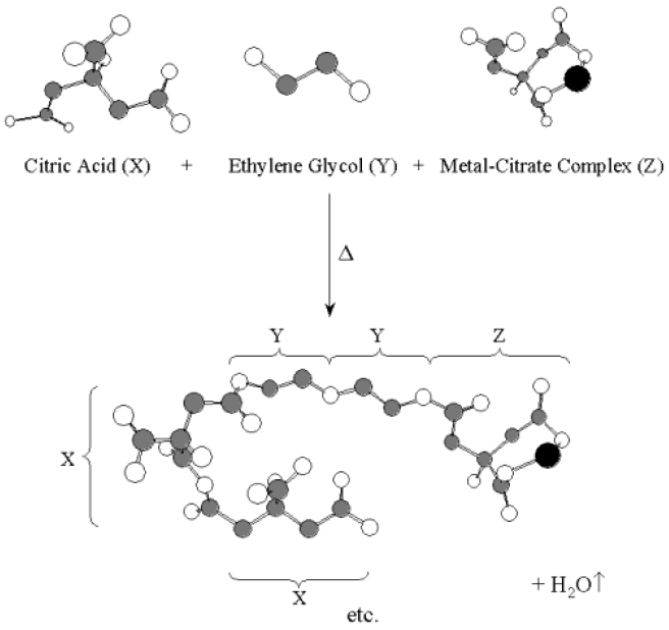

Figure 4.7: A representation of the early stages of the Pechini method: the condensation between a metal complex, citric acid and a polyol.

polyalcohols that is necessary for gelation is acid catalyzed. Fortunately, due to its zwitterionic character, EDTA will still bind many metals as a bidentate ligand, even under highly acidic (pH < 4) conditions. Oxalic acid and polymeric alcohols such as polyvinyl alcohol (PVA) have also been used as chelating agents for Pechini type syntheses [189]. In the case of polymer alcohols, given the 3D network provided by the polymer, addition of a polyol and subsequent esterification are not necessary. The polymer is simply combined with the metal cations in solution to form a precursor that is subsequently calcined to pyrolyze the organic species. These reactions are sometimes referred to as polymer combustion syntheses. There are a number of syntheses reported in the literature that, while similar to the Pechini method in their use of carboxylic acid-based chelating agents and pyrolysis of the resulting precursors, forego the use of a polyol or similar reagent to induce polymerization [190]. It must be stressed that it is not clear whether these solutions are in fact forming gels or simply contain precipitated metal-citrate complexes. Furthermore the products of such reactions tend to exhibit relatively large crystallite sizes with irregular morphologies

Preparative condition for the synthesis of fine PZT powders through the various methods
DEA method Stoichiometric amount of hydrated metal oxides (Pb, Zr, Ti) were reacted with 4–5 moles of DEA per mole of PZT at 200°C to produce a homogeneous red colored solution of metal ion–DEA complex.
Oxalate method 1 mole of Pb(EDTA) was mixed with stoichiometric amount of Ti-oxalate and Zr-oxalate solution to produce a homogeneous solution.
Tartarate method 1 mole of Pb(EDTA) was mixed with stoichiometric amount of Ti-tartarate and Zr-tartarate solution to produce a homogeneous solution.
The homogeneous precursor solutions obtained through each of the preparative methods were evaporated to complete dryness to result in a fluffy carbonaceous powders which were calcined to produce the PZT phase.

Figure 4.8: A summary of the complexes combustion method developed by Das *et al.* [174].

[191].

4.2.3 Complexes Combustion Approach

Despite the success of sol-gel processes, the moisture sensitivity of the starting material metal alkoxides and organo-metallic compounds limits their commercial application to the powder synthesis. A complex based precursor solution method was thereby proposed for the preparation of nanocrystalline powders such as PZT by Das *et al.* [174]. In this method and its developments [171] a complexing agent, such as diethanolamine (DEA), oxalic acid or tartaric acid, is used to keep the metal ions in homogeneous solution, which leaves sufficient flexibility for the system to remain homogeneous throughout the synthesis without any precipitation. A schematization of the complexes combustion approach is reported in figure 4.8.

Highly crystalline PZT nanosystems were synthesized according to this method at relatively lower heat treatment temperature compared to that of the solid-state method. Among all the other methods investigated by the authors, tartarate and DEA methods resulted to be the better methods to produce nanocrystalline PZT powders giving higher dielectric values at relatively low temperatures, namely 200 °C and 450 °C. Using DEA or tartaric acid in the system provided a homogeneous distribution of metal ions preventing their precipitation or segregation from the solution during the dehydration process. After complete dehydration, the exothermic decomposition of metal complexes — a mere combustion involving atmospheric oxygen — produced sufficient heat for nanophase formation. Thus, the PZT phase formation occurred at relatively low external temperature in the DEA and tartarate-based methods, in comparison to other reported methods — with only exception of hydrothermal methods which are not discussed here. Furthermore, the exothermic decomposition of precursors was accompanied by the evolution of various gases such as NH_3, CO, CO_2 and water vapor, which could not only protect the particles from agglomeration, but also dissipate the heat of combustion, thus inhibiting the sintering of nanocrystalline powders. The only disadvantage of this approach, as already mentioned above, is related to the starting materials involved in the synthesis. In fact, the most common sources of Ti^{IV} and Zr^{IV} — namely TiO_2 and $ZrCl_2$ — are extremely inert chemicals which can not be easily dissolved in water solution. A procedure for obtaining water soluble Ti^{IV} and Zr^{IV} chemical necessitates of a tedious chemical treatment of TiO_2 and $ZrCl_2$ with hydrofluoric acid to produce the hydrated water-soluble oxides $TiO_2 \cdot nH_2O$ and $ZrO_2 \cdot nH_2O$. This methodology, which is sketched in figure 4.9, may also introduce in the final water solution fluoride anions thus compromising the electro-mechanical properties of the piezoelectric powder.

4.2.4 Experimental

High positive charges on the metal tend to stabilize the transition state during hydrolysis. Consequently, the rate of hydrolysis for the titanium and zirconium alkoxides is rapid, to the extent that special handling precautions

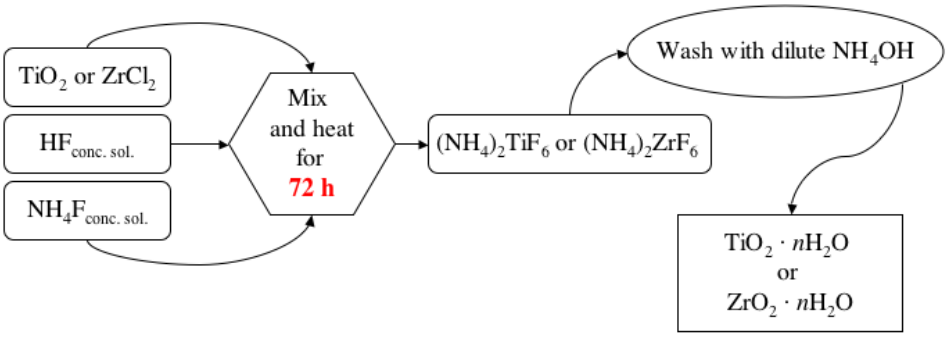

Figure 4.9: A sketch of the common procedure for the preparation of water soluble $TiO_2 \cdot nH_2O$ and $ZrO_2 \cdot nH_2O$.

must be taken to protect the complexes from water and moisture. A strategy, the *standard alkoxides* approach, for the production of PZT nanoparticles using Ti- and Zr-alkoxides as starting material was thus studied. The aim of this approach was to determine the effects of the ligands involved in the stabilization of the cations in the water solution. Afterwards, based on the results of the characterization of the powders obtained with standard alkoxides method, the *EDTA* approach was developed. In this section we present and discuss both methods.

Chemicals

Zirconium propoxide ($Zr(OCH_2CH_2CH_3)_4$, 70 wt % in 1-propanol, Aldrich), titanium isopropoxide ($Ti[OCH(CH_3)_2]_4$, purum, Fluka), lead acetate trihydrate ($Pb(CH_3COO)_2 \cdot 3H_2O$, puriss., Riedel-de Haën), ethylenediamine tetra-acetic acid (H_4EDTA, 99.5%, Aldrich), lead nitrate ($Pb(NO_3)_2$, 99+%, Aldrich), acetic acid ($\geq$ 99.7 %, Sigma-Aldrich), 2,4-pentanedione (Hacac, $\geq$ 99.5%, Aldrich), DL-tartaric acid (99%, Aldrich) and Atlox 4912 (Uniqema, now Croda International; MW $\approx$ 5000 g/mol) were used without any further purification. Water was purified with a Millipore (Billerica, MA) system (resistivity 18 M$\Omega \cdot$ cm).

The Standard Alkoxides Approach

The standard alkoxides approach is resumed in Figure 4.10. The same general procedure was used to prepare solutions containing Ti^{IV} or Zr^{IV} and the ligand. The proper amount of the selected ligand was dissolved in water to obtain a 6 M solution. The alkoxide was then added at 40 °C under magnetic stirring. In order to avoid hydrolysis and condensation of the metal complexes, ligands were used in excess, and solutions added slowly. Furthermore, catalytic amounts of H_2O_2 were added to the ligand solution to enhance the formation of the complexes. The concentrations of the ligand and the metal ion in the final solution were 2 M and approximately 0.8 M respectively. Lead nitrate was dissolved in a solution of fully protonated ethylenediamine tetra-acetic acid (H_4EDTA) with a equimolar ratio Pb^{II}:EDTA. A catalytic amount of ammonium hydroxide (100 μL) was added. The final concentration of the Pb^{II}-EDTA complex was 1.6 M. Proper amounts of the cations solutions were mixed, heated in a flask at 80 °C with a heating mantle and the solvent evaporated. The temperature of the heating mantle was raised. As soon as the burning process started, the heating treatment was stopped. The combustion of the organic ligands brought about the evolvement of large amounts of dark brown gases. A gray, fine-grained precursor powder was obtained. The precursors were then calcinated in a muffle oven.

The EDTA Approach

A flowchart of the EDTA method is reported in Figure 4.11. 5 g of titanium isopropoxide were added to 10 mL of acetic acid. A proper amount of zirconium propoxide was added. Lead acetate was dissolved in a small amount of water, the concentration of Pb^{II} was equal to the overall concentration of Ti^{IV} and Zr^{IV}. The water and acetic acid solutions were mixed quickly, and finally EDTA was added in equimolar amount with respect to the total cations. Upon shaking, the solution became clear, and water was evaporated by heating. After drying the the ligand was burned, and the heating was stopped as soon as the combustion gases started developing. The precursor powders, which are shown in Figure 4.12, obtained were

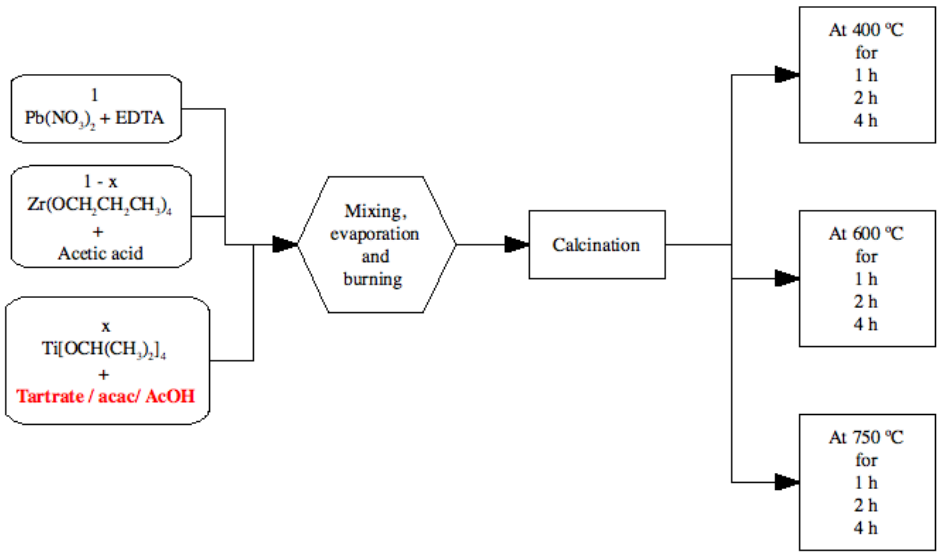

Figure 4.10: A schematization of the standard approach for the synthesis of PZT nanoparticles.

finally calcinated for 15 min at 450 °C.

4.2.5 Few Comments on the Synthesis Methods and Summary

Both methods we present can be defined as hybrid approaches. While the typical starting material of the Pechini method or sol-gel synthesis are involved the key ideas of complexes combustion methods are applied. The advantage of this modus operandi is that the duration of whole process, from starting materials to the final crystalline product, is remarkably reduced. On top of that, the best characteristic of both methods — complexes combustion and sol-gel or Pechini methods — are mixed. Commercially available starting materials which do not need any chemical modification or purification are required. Nonaqueous solvents are not necessary and the combustion of the ligands can be considered — compared to the pyrolysis step of sol-gel and Pechini methods — as an energy saving solution. As already pointed out, the heat released by the burning material let the heating to be switched off in the early stages of the combustion step. The calcination step is also shorter

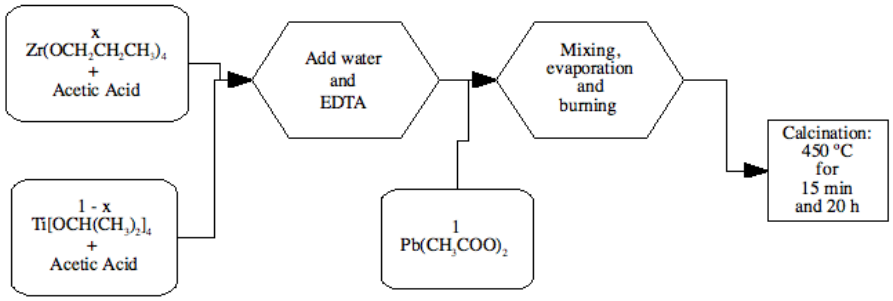

Figure 4.11: A schematization of the EDTA approach for the synthesis of PZT nanoparticles.

than the well known methods reported in the literature thus contributing to the overall energy saving. In Table 4.2 we report a summary of the sample which were produced according to the standard alkoxides method and the EDTA method. All these precursor powders were produced keeping the molar ratio $Ti^{IV} : Zr^{IV} = 48 : 52$. Moreover, in order to check the influence of the $Ti^{IV} : Zr^{IV}$ molar ratio on the electro-mechanical properties of the PZT crystalline powders, as it will be discussed in the following Chapter, two more samples with molar ratio $25 : 75$ and $75 : 25$, were produced according to the EDTA method. The calcination conditions were the same as those reported in Table 4.2 for precursor D. The pictures of these precursors and crystalline powders are reported in Figures 4.12 and 4.13, respectively.

4.3 Precursors Characterization

As already mentioned in the foregoing, the techniques we developed for the preparation of crystalline PZT nanoparticles — as well as those reported in the literature — necessitate of a thermal treatment to assure to formation the perovskite-like structure. The best conditions of the thermal treatment where determined by means of Differential Thermal Gravimetry (DTG). The morphological features of the precursor powders were investigated through Transmission Electron Microscopy (TEM) measurements.

Precursor ID	Ti^{IV} Ligand	Synthesis Method	Calcination Temperature (°C)	Calcination Duration
A	tartaric acid	standard	450	1, 2 and 4 h
			600	1, 2 and 4 h
			750	1, 2 and 4 h
B	acetic acid	standard	450	1, 2 and 4 h
			600	1, 2 and 4 h
			750	1, 2 and 4 h
C	acetyl acetone	standard	450	1, 2 and 4 h
			600	1, 2 and 4 h
			750	1, 2 and 4 h
D	H_4EDTA	EDTA	450	15 min and 20 h

Table 4.2: A list of the precursor prepared according to the standard alkoxide and the EDTA methods and the calcination conditions which were used for the production of all the samples.

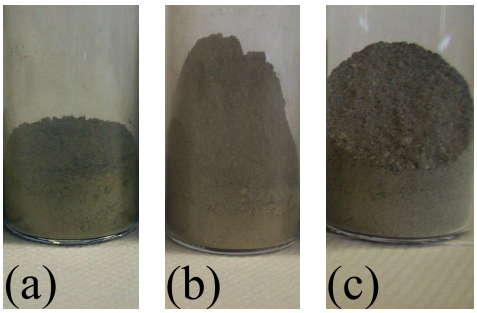

Figure 4.12: Pictures of precursor powders obtained from the EDTA method. Three stoichiometries with different Ti^{IV} : Zr^{IV} molar ratio were prepared. (a): $Pb(Ti_{0.25}Zr_{0.75})O_3$; (b): $Pb(Ti_{0.48}Zr_{0.52})O_3$; (c): $Pb(Ti_{0.75}Zr_{0.25})O_3$.

4.3.1 Experimental Methods

TEM

TEM measurements were carried out with a Philips electron microscope (model EM201C).

DTG

Differential Thermal Gravimetry measurements were performed with an SDT Q600 apparatus (TA Instruments, Milan, Italy) between 50 and 800 °C with a heating rate of 10 °C/min. The samples were kept under an air flux of 100 mL/min.

4.3.2 Results

TEM Measurements

All the synthetic routes lead to the formation of amorphous precursors. The precursor powders were obtained before the calcination step. The TEM images of these samples (Figures 4.14, 4.15 and 4.16) show the presence of small-sized particles embedded in the carbonaceous material due to ligands which were only partially burned. The calcination step is therefore fundamental for obtaining a highly crystalline powder. The presence of carbona-

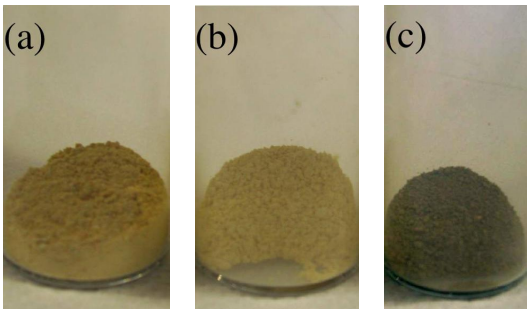

Figure 4.13: Pictures of PZT powders obtained from the EDTA method. Three stoichiometries with different Ti^{IV} : Zr^{IV} molar ratio were prepared. (a): $Pb(Ti_{0.25}Zr_{0.75})O_3$; (b): $Pb(Ti_{0.48}Zr_{0.52})O_3$; (c): $Pb(Ti_{0.75}Zr_{0.25})O_3$.

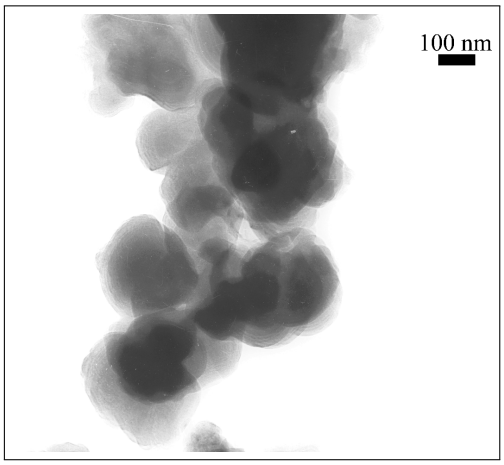

Figure 4.14: TEM image obtained from the precursor powder A.

ceous residues is especially remarkable in sample A (Figure 4.14), where no nanostructure can be detected after this synthetic step. On the other hand, the samples prepared using low molecular weight ligands, such as HAc and 2,4-pentanedione, acetyl acetone (Hacac), exhibit the presence of highly agglomerated nanoparticles that are still embedded in the carbonaceous residues.

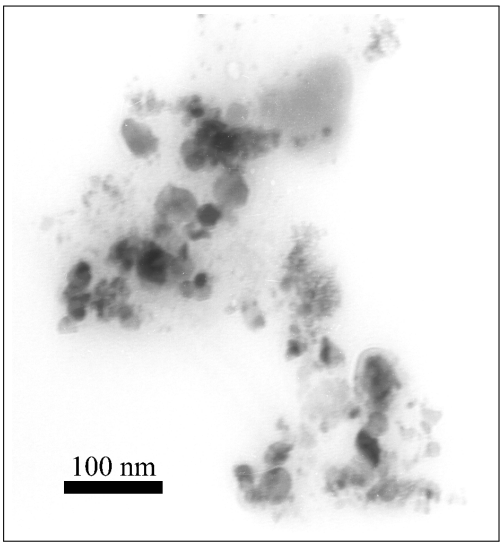

Figure 4.15: TEM image obtained from the precursor powder B.

DTG Measurements

DTG data confirm the presence of carbonaceous residues in the precursor powders: in fact all samples show a significant mass loss during the temperature ramp. This feature is particularly evident in samples A and D, with a mass loss of about 35% before a first plateau is reached around 730 °C. The combustion of the ligand residues determines the evolvement of gas (CO_2, H_2O, and NH_3). High molecular weight ligands lead to a larger production of combustion gasses. This process prevents particle sintering through the dissipation of the combustion heat [165].

The thermogravimetric measurements performed on the precursors also reveal if PbO loss due to volatilization at high temperature occurs and how the calcination treatment may affect the properties of the final powder, depending on the temperature and the duration of the thermal treatment. Between 20 °C and 200 °C the thermogram indicates the loss of solvent molecules, see Figure 4.17, at a relatively slow rate. Temperature increments result in the decomposition of the residues of the ligands that were only partially burned. The thermal stability of a ligand thus sets the temperature at which the calcination leads to a crystalline pure material. Comparing the data of samples A, B, C and D, and the thermograms obtained from the

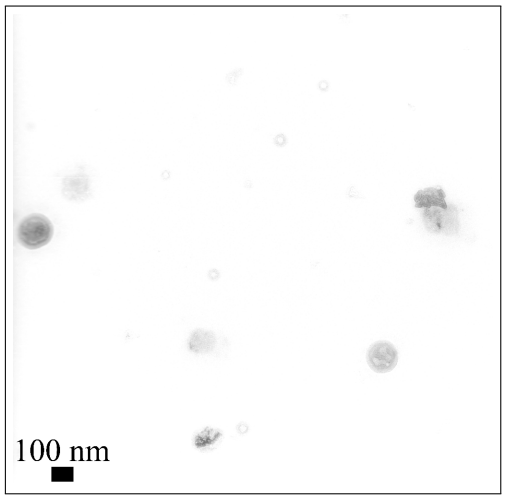

Figure 4.16: TEM image obtained from the precursor powder C.

pure ligands, each peak can be easily related to the decomposition of the particular ligand. All the samples show a plateau at 730 °C. A mass decrease, due to the loss of PbO, takes place above 790 °C. At lower temperatures all the samples show one or more peaks between 350 °C and 700 °C, due to the decomposition of EDTA (the only peak in sample D), tartrate (sample A), acetic acid (sample B), or acac (sample C) and their residues. The only exception is sample D, where the plateau is already reached at 550 °C and the decomposition of EDTA does not lead to the formation of any residue. Furthermore, no mass loss due to PbO volatilization is observed above 790 °C. The analysis of the thermal behavior of the precursors was investigated in order to assess which ligand can provide the necessary thermal energy to sustain the burning step. The results (Figure4.17, red curves) obtained for sample A and D are particularly interesting, as they show that the peak at lower temperature, corresponding to the decomposition of tartrate and EDTA residues, are characterized by the highest combustion enthalpy (4.6 and 5.5 kJ/g, respectively). On the other hand, the decomposition of acetic acid residues does not produce any release of heat (sample B), while the enthalpy calculated for sample C is only 0.9 kJ/g. A summary of the DTG data is reported in Table4.3. The temperature of combustion (T_c) was calculated from the first maximum of the mass loss derivative curve (which is

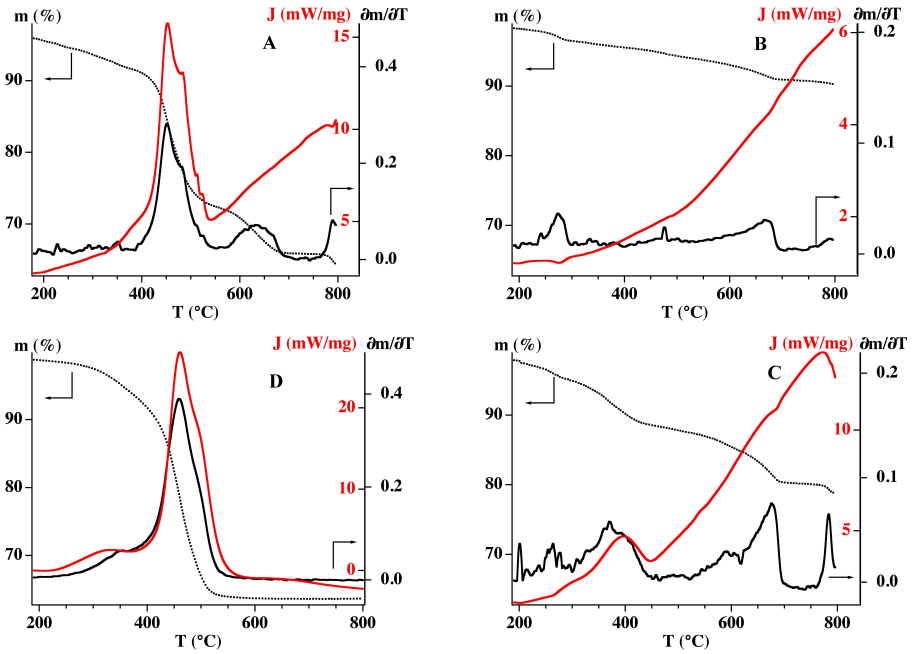

Figure 4.17: DTG data form sample A, B, C and D. The left y-axis represents the weight (%) of the sample, the black right y-axis indicates the ∂m/∂T derivative, and the red right y-axis the heat flow used to determine the enthalpy involved in the combustion process. All data were plotted vs. the temperature (T). To ease comparison the ∂m/∂T data were rescaled.

associated with enthalpy development). At higher temperatures, a positive heat flow was recorded for samples A, B and C, due to particle sintering. This aspect will discussed in the following.

4.4 PZT Powders Characterization

In this Section we discuss and compare the results of the novel hybrid syntheses — the alkoxides approach and the EDTA approach — where, as it was described in the previous Sections, the concepts of the complexes combustion methods are applied to starting materials such as titanium and zirconium alkoxides. The crystalline and chemical purity of the PZT powders were evaluated by means of X-Ray Diffraction (XRD) and Proton In-

Sample ID	Ligand Molecular Formula	MW (g/mol)	ΔH (kJ/g)	T_c (°C)
A	$C_4H_6O_6$	150.09	4.6	450
B	$C_2H_4O_2$	60.05	-	-
C	$C_5H_8O_2$	100.13	0.9	370
D	$C_{10}H_{16}N_2O_8$	292.24	5.5	450

Table 4.3: A summary of the thermal data obtained form DTG.

duced X-Ray Emission (PIXE), respectively. The morphological feature of the crystalline powders were checked through Scanning Electron Microscopy (SEM) measurements. The temperature and duration of the calcination step strongly affect the morphological and the crystalline properties of the powders, depending on the chemical and thermal properties of the ligands involved in each synthetic pathway. All the results presented in this Section refer to the samples with stoichiometry $Pb(Ti_{0.48}Zr_{0.52})O_3$.

4.4.1 Experimental Methods

PIXE

PIXE measurements were performed at the 3 MV Tandetron accelerator of INFN-LABEC laboratory in Florence. Samples were bombarded with a 3.2 MeV proton beam. The beam was collimated to dimensions of 2 $\times$ 1 mm^2; anyway, using a scanning mode, most of the area of the sample has been analyzed. X-rays were revealed by two detectors, optimised for low and medium-high X-ray energies; the first one is a Silicon Drift Detector (SDD), the latter is a Si(Li) detector and their energy resolutions are 145 and 190 eV at 5.9 keV, respectively. The experimental set-up is described in detail elsewhere [192]. PIXE spectra were analyzed with the GUPIX software [193].

XRD Measurements

XRD data were recorded using a Bruker D8 Advance Diffractometer (Bruker axs), equipped with a ceramic X-ray tube and a copper anode, theta-theta goniometer and Bragg-Brentano geometry. The crystallite size was calculated by means of a built-in software. The band broadening due to instrumental response was thus subtracted.

SEM

SEM images were collected with a Stereoscan S360 instrument, (Cambridge, UK). Samples were coated with gold by sputtering under vacuum.

4.4.2 Results

PIXE

Since the molar ratio between titanium and zirconium cations is extremely important for the piezoelectric response of PZT powders, PIXE measurements (Figure 4.18) were carried out to assess the quantities of both Ti^{IV} and Zr^{IV} ions in the PZT nanoparticles obtained from the EDTA method. PIXE is a well-established analytical method for multielemental determination that is based on ion bombardment to produce characteristic X-rays of the elements present in the material. Therefore it offers the possibility of an very interesting investigation of the chemical composition of the samples. The measurements were repeated for six times on samples with theoretical molar ratio $Zr^{IV} : Ti^{IV} = 52 : 48$ (corresponding to 1.08). The mass ratios obtained are summarized in Table 4.4. The error associated with the measurements is 8%.

A molar $Zr^{IV} : Ti^{IV}$ ratio of 1.02 ± 0.08 was thus calculated with few algebraic step. This result clearly confirm that the EDTA method allows a satisfactory control of the chemical composition of the final nanopowders.

XRD Measurements

Figure 4.19 show the X-Ray Diffraction profiles of the calcinated powders obtained from precursors A, B, and C. As suggested by the DTG measure-

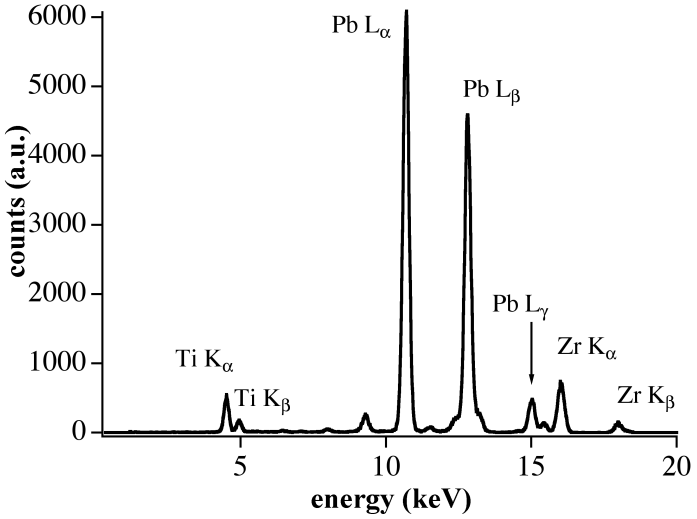

Figure 4.18: PIXE data for the $Pb(Ti_{0.48}Zr_{0.52})O_3$ sample prepared according to the EDTA method.

Cations	Mass Ratio
Ti^{IV}/Pb^{II}	0.115
Zr^{IV}/Pb^{II}	0.223
Zr^{IV}/Ti^{IV}	1.94

Table 4.4: Cations mass ratios calculated from PIXE data. The error associated with the measurements is 8%.

ments, calcination at low temperatures may not lead to crystalline pure PZT powders. When the samples are treated at 450 °C (Figure 4.19 (a) and (b)), the only powders that show the typical PZT diffraction patterns — although with some impurities — are those obtained from precursor B, where acetic acid was used as stabilizer for both Ti^{IV} and Zr^{IV} ions. Although the temperature is relatively low, the limited mass fraction of carbonaceous residues leads to the formation of crystalline PZT, with some degree of impurity, after at least 1 hour of calcination in the muffle furnace. No crystalline PZT phase can be detected in the samples obtained from precursors A and C, where the amount of residues from tartaric acid (A) and acac (C) is much

higher, due to their larger molecular weight. This evidence agrees with the mass loss of the precursors as recorded through DTG measurements.

The calcination of the precursors at 600 °C (Figure 4.19 (c)) results in the formation of crystalline materials (from sample B) or partially crystalline powders as in the case of samples A and C, where pyrochlores and PbO signals are detected. This behavior can be ascribed to the different thermal properties of the ligands used as stabilizers for Ti^{IV} and Zr^{IV}. Unlike the combustion of tartrate residues, which involves a significant release of heat, the burning of acac is not so efficient. This may lead to a heterogeneous removal of the carbonaceous matrix, and determine the formation of $PbTiO_3$, $PbZrO_3$ and PbO. On the other hand the combustion of high molecular weight ligands, like tartrate, necessitate of longer calcination times if the heat generated in the burning process is not large enough to assure the removal of the whole carbonaceous matrix. Therefore the thermal properties of the ligands involved in the stabilization of Ti^{IV} and Zr^{IV} do affect strongly the crystalline purity of the final powder. This picture is confirmed by XRD data obtained for precursor D. Figure 4.20 shows a pure crystalline PZT phase after calcination at 450 °C for 15 min only. Hence, the presence of the same ligand (EDTA) for the cations inhibits the formation of crystalline impurities even when the calcination is carried out for such a short period of time. On the basis of the discussion above concerning the effects of the molecular weight of the ligand and those of the heat released in the combustion, it is clear that the large enthalpy of combustion of EDTA is fundamental to achieve crystalline pure powders.

The crystallite sizes were calculated according to the Scherrer equation, and are reported in Table 4.5. As expected, the crystallite size grows raising the temperature and the duration of the calcination step.

SEM

The morphology and the micro-structure of the calcinated powders were investigated through Scanning Electron Microscopy. Figures 4.21, 4.22, 4.23 and 4.24 show the SEM images of the samples produced with the different synthetic paths. A long thermal treatment of the precursors results in sin-

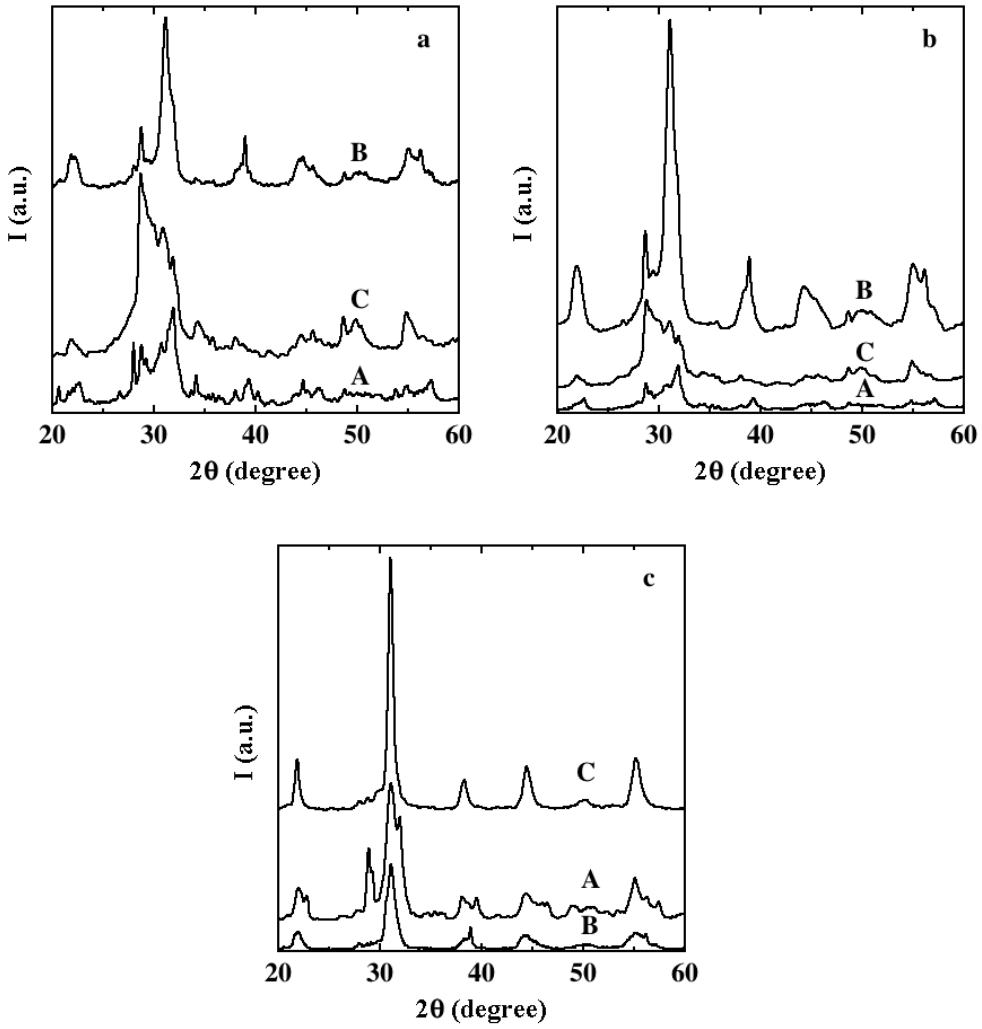

Figure 4.19: XRD profiles from the powders obtained calcinating precursors A, B and C at 450 °C for 1 h (a), 2 h (b) and at 600 °C for 1 h (c).

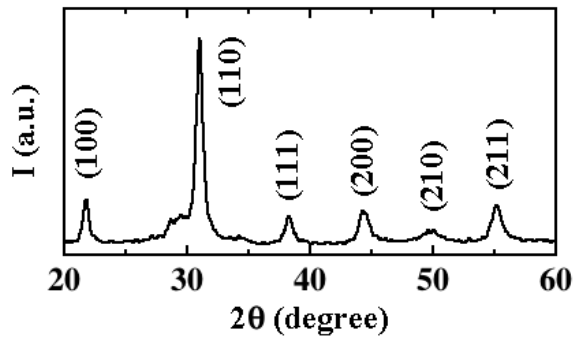

Figure 4.20: XRD pattern from sample D after calcination at 450 °C for 15 min.

Precursor ID	Calcination	Mean Crystallite Size (nm)
C	600 °C - 1 h	19.4 ± 1.5
C	750 °C - 1 h	26 ± 3.7
D	450 °C - 15 min	16.3 ± 1.7

Table 4.5: Mean crystallite size calculated according to the Scherrer equation from XRD measurements.

tered powders (see Figures 4.21 and 4.22 on pages 82 and 83, respectively). The powder obtained from precursor A after 1 hour of calcination at 450 °C still reveals a very fine structure embedded in the carbonaceous matrix. After 2 hours, free standing particles with an average diameter ranging between 100 and 600 nm are formed. When the samples are calcinated for 4 h, sintering strongly occurs and only a few free standing particles are found.

This behavior is common in all the investigated samples and the presence of high molecular weight ligands prevents particle sintering. In Figure 4.22 we compare the effects of calcination at 450 °C for 2 hours on samples B and C. Calcination of sample B (see Figure 4.22 (a)) leads to highly sintered domains that contain free standing particles with a diameter of about 600 nm. Instead in sample C (see Figure 4.22 (b)) no free standing particles are found.

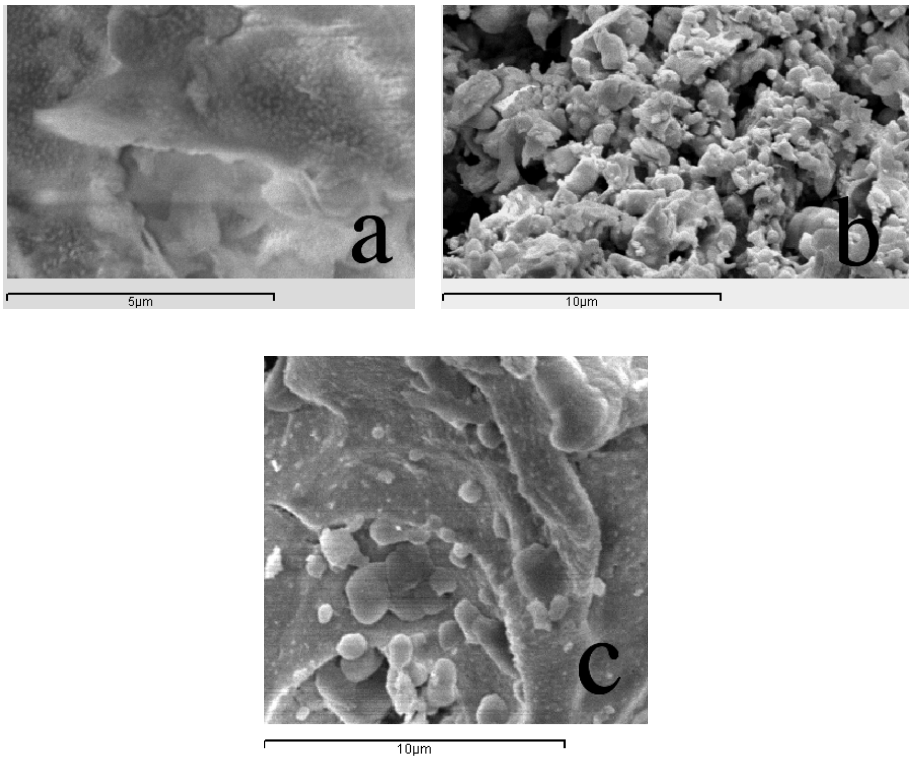

Figure 4.21: SEM images of samples A calcinated at 450 °C for 1 hour (a), 2 hours (b), and 4 hours (c).

These considerations are confirmed by SEM investigation of the powders produced by calcinating the precursor A at 750 °C for 1 h: Figure 4.23 shows the presence of free standing particles, with an average diameter of about 150 nm.

Finally, SEM on sample E (Figure 4.24) shows the presence of small agglomerated particles. In order to evaluate their size, we carried out Dynamic Light Scattering (DLS) measurements after dispersing the sample in a surfactant aqueous solution. The next Section is devoted to the discussion of these dispersions.

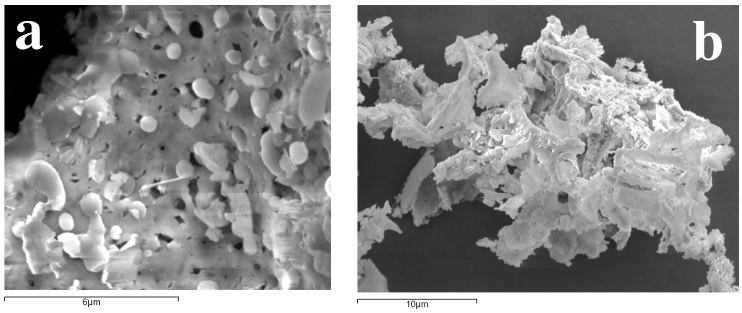

Figure 4.22: SEM images of the samples from precursors B (a) and C (b), calcinated at 450 °C for 2 hours.

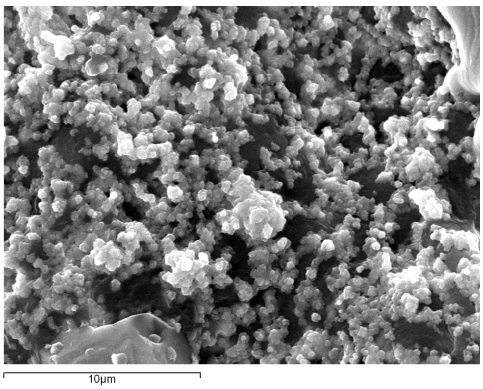

Figure 4.23: SEM image of sample A after calcination at 750 °C for 1 hour.

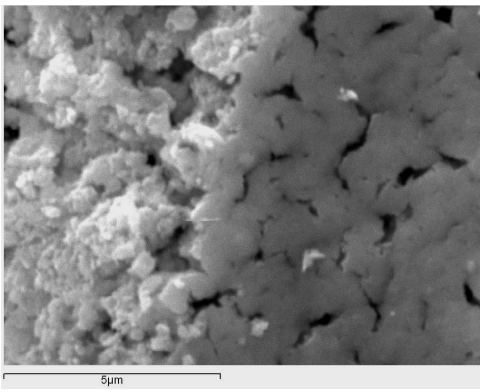

Figure 4.24: SEM image of sample E after calcination at 450 °C for 15 min.

4.5 Dispersion and Coating

Once the properties of PZT powders were well characterized we looked into the possibility of preparing stable colloidal dispersions of PZT nanopowders. This point is extremely important in order to apply the piezoelectric powders mixed with any kind of polymeric dispersion for the production of piezoelectric devices acting as sensors. On the other hand having an *ad hoc* stable water dispersion can be also exploited for the functionalization of any kind of surface. The PZT water-based dispersions were characterized by means of DLS and zeta potential.

4.5.1 Experimental Section

Preparation of PZT Water-Based Formulations

PZT water dispersions were prepared with a two-step method. The powders (≈5% wt/wt) were placed in a vial with Atlox 4912, see Figure 4.25, (≈1% wt/wt) and water (15 ml). The surfactant was dissolved at 60 °C. A pre-dispersion step was carried out with a sonicator (S-450 Sonifier®, Branson Ultrasonics Corporation, 41 Eagle Rd., Danbury, CT) equipped with a micro-tip for small volumes. Then the dispersions were size-reduced through microfluidization at high pressure, up to 930 bar, for 15 min with a M-110S Microfluidizer®(Microfluidics International Corporation, 30 Ossipee Road, Newton, MA). A picture of a dispersion is shown in Figure 4.26.

DLS

DLS measurements were performed with a Brookhaven apparatus (Brookhaven Instruments Corporation, 750 Blue Point Road, Holtsville, NY) equipped with a BI200SM goniometer, a BI9000AT digital correlator card, an EMI 9863B/350 photomoltiplier and an index-matching liquid (decahydronaphthalene) filtration and circulation system. The light source ($\lambda = 532$ nm) was the second harmonic of a diode pumped Nd:YAG laser (Compass 350M-20, Coherent Inc., Santa Clara, CA), linearly polarized in the vertical direction and impinging on the sample with 68 mW power. The laser long-term power stability was ± 0.5%. The light scattered from the sample was col-

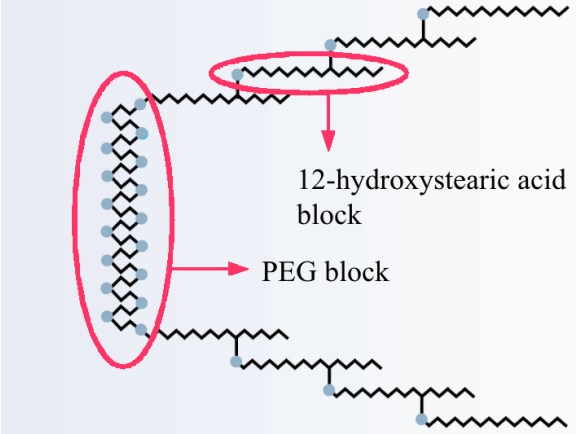

Figure 4.25: A schematization of the structure of Atlox 4912. Atlox 4912 is an ABA block copolymer. 'A' block is made of 12-hydroxystearic acid units while 'B' block is polyethylene glycol.

Figure 4.26: A picture of the water-based PZT dispersion with Atlox 4912.

lected at 90° with respect to the impinging laser light radiation. A water circulating bath temperature control system was used to maintain a constant temperature during the experiment. In order to avoid multiple scattering, the samples were diluted 1:1000 with MilliQ water, directly into cylindrical scattering glass tubes (Hellma®, Müllheim, Germany). To obtain the size distribution histograms of the scattering objects, the field autocorrelation functions were Laplace inverted using the CONTIN routine [194]. All CONTIN analyses were number weighted.

Zeta Potential

Zeta potential was determined with a ZetaPals (Brookhaven Instruments Corporation, 750 Blue Point Road, Holtsville, NY). About 1.6 ml of each sample were added in a disposable cuvette and the temperature stabilized at 25 °C for 5 minutes. The zeta potential was then determined by measuring the direction and velocity that the particles or aggregates moving in the applied electric field. The Smoluchowsky mathematical model was used ware to convert the electrophoretic mobility measurements into zeta potential values.

4.5.2 Results

DLS and Zeta Potential

DLS analysis of the dispersions produced with Atlox 4912 reveals the presence of small particles with a diameter centered at 40 nm. The autocorrelation function for the PZT water dispersion is reported in figure 4.27. The histogram reported in figure 4.28 was plotted according to the fitting parameters extracted with the CONTIN procedure from the autocorrelation functions.

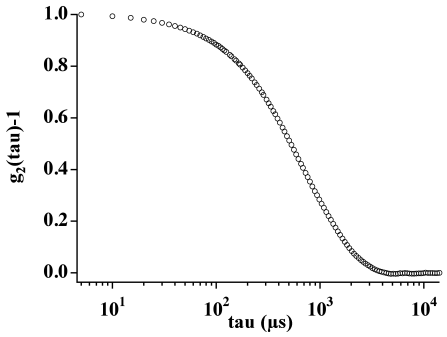

Figure 4.27: Normalized autocorrelation function of the PZT in water dispersion with Atlox 4912.

This result ensure both colloidal stability and high electro-mechanical properties, thus confirming that our procedures can be applied for the production of piezoelectric nano-devices. The small particle size may prevent particle sedimentation while the piezoelectric properties of PZT powders

can guaranteed on the basis of the recent works published in the literature ([195, 196, 197, 114], in particular those by Glinchuk *et al.*). In fact, a further reduction of the particle size may result in ferroelectricity quenching as already suggested by several authors like Jian [198] and Zhong [199].

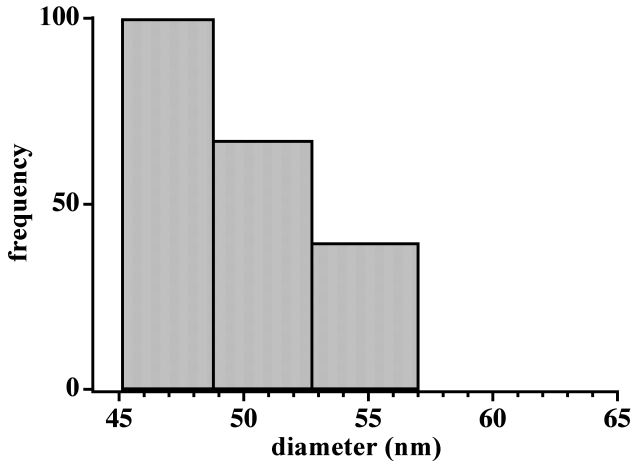

Figure 4.28: Particle size distribution histogram (hydrodynamic diameter) for the PZT in water dispersion with Atlox 4912.

Furthermore, concerning colloidal stability, zeta potential measurements indicate that the average zeta potential is ≈ -20 mV. This result demonstrate that electrostatic interactions and steric effects (due the the surfactant chemical structure) play a role in determining the colloidal stability of the dispersions.

Chapter 5

PZT Nanocomposites

Chapter 5 is devoted to the presentation of the PZT *nanocomposites* which were prepared in our labs (Section 5.2) and to the discussion of results of the electro-mechanical characterization which was performed (Section 5.4). An introduction to the key ideas beyond the science of nanocomposites is given in Section 5.1, while the experimental setup for the electro-mechanical characterization of the nanocomposites is thoroughly described in Section 5.3.

5.1 Introduction to Nanocomposites

Nanostructured composites — or *nanocomposites* — are multicomponent materials in which at least one of the constituents has one or more characteristic dimensions (length, width, or thickness) in the nanometer size range — from 1 to 1000 nm. The main difference between nanocomposites [200, 201, 202, 203] and conventional composite materials is that the former are characterized by an extremely high surface to volume ratio of the reinforcing phase. In fact, the area of the interface between the matrix and reinforcement phase is usually at least an order of magnitude greater than for conventional composite materials, while the reinforcing material can be made up of 3D- (e.g. minerals nanoparticles), 2D- (e.g. exfoliated clay stacks) or 1D-objects (e.g carbon nanotubes or electrospun fibers) [204]. The field of nanocomposite materials has had the attention of both scientists

and engineers in the last decades. This scrutiny results from the simple and fascinating premise that using nanosized building blocks makes it possible to design and fabricate new smart materials with unprecedented flexibility and improvements in their physical properties. In general, nanocomposite materials can demonstrate different mechanical, electrical, optical, electrochemical, catalytic, and structural properties than those of each individual component. The multifunctional behavior for any specific property of the material is often more than the sum of the individual components. The ability to tailor composites by using nanosized building blocks of different chemical species has found applications in several interdisciplinary fields.

Nature was the inspiriting muse of the art and the science of nanocomposites. The most convincing examples of such designs are structures such as bones, which are hierarchical nanocomposites built from ceramic tablets and organic binders. Because the constituents of a nanocomposite have different structures and compositions and hence properties, they may serve various functions. Thus, the materials built from them can be *multifunctional*. Taking some clues from nature and based on the demands that emerging technologies put on building new materials that can satisfy several functions at the same time for many applications, scientists have been devising synthetic strategies for producing nanocomposites. These strategies have clear advantages over those used to produce homogeneous large-grained materials. Behind the push for nanocomposites is the fact that they offer useful new properties compared to conventional materials combining different components with different properties.

The idea of enriching properties and improving characteristics of materials through the development of multiple-phase nanocomposites is not recent. This purpose has been practiced ever since civilization started and humanity began producing more efficient materials for functional aims. Apart from the large variety of nanocomposites found in nature an excellent example of the use of synthetic nanocomposites in antiquity is the discovery of the structure of Mayan paintings developed in the Mesoamericas. State-of-the-art characterization of these paintings samples reveals that they consisted in a matrix of clay mixed with a bluish organic colorant — namely indigo (see Figure 5.1) — molecules. They also contained inclusions of metal nanoparticles

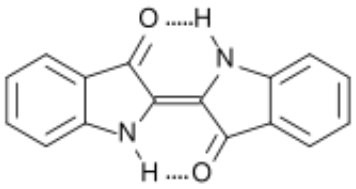

Figure 5.1: An indigo molecule.

encapsulated in an amorphous silicate substrate, with oxide nanoparticles on the substrate. The nanoparticles were formed during heat treatment from impurities — like Fe, Cr and Mn — present in the raw materials such as clays, but their content and size also affected the optical properties of the final paint. The combination of intercalated clay forming a superlattice in conjunction with metallic and oxide nanoparticles embedded on the amorphous substrate made this paint one of the earliest synthetic materials resembling modern functional nanocomposites [205].

As already stated above, nanocomposites can be considered as solid structures with at least one nanometer-scale characteristic dimension. These materials typically consist of an inorganic (host) solid containing an organic component or vice versa. Or they can comprise two or more inorganic/organic phases in any combinatorial form with the constraint that at least one of the phases or features be in the nanosize range. Extreme examples of nanocomposites can be porous media, colloids, gels, and copolymers. In the following we will present composites made of two inorganic components and others were oxides nanoparticles are embedded in organic matrixes.

Both simple and complex approaches for the production of nanocomposite exist. A practical dual-phase nanocomposite system, such as supported catalysts used in heterogeneous catalysis (e.g. metal nanoparticles placed on ceramic supports), can be prepared simply by evaporation of metal onto chosen substrates or applying a dispersion on the support surface. On the other hand, material such as bone, which has a complex hierarchical structure with coexisting ceramic and polymeric phases, is difficult to duplicate entirely by existing synthesis techniques. The methods used in the prepara-

tion of nanocomposites range from chemical means to vapor phase deposition.

5.1.1 Ceramic Nanocomposites

Nanocomposite technology can be also applied to functional ceramics such as ferroelectric and piezoelectric materials [206, 207, 208]. Incorporating small amounts of ceramic or metallic nanoparticles into $BaTiO_3$, ZnO, or cubic ZrO_2 can significantly improve their mechanical strength and hardness, which are very important for the production of highly reliable electric devices operating in critical environmental conditions. Dispersion of soft materials into a hard ceramic generally decreases its mechanical properties (e.g., hardness). However, in nanocomposites, soft materials added to several kinds of ceramics can improve their mechanical properties. For example, adding hexagonal boron nitride to silicon nitride ceramic can enhance its fracture strength not only at room temperature but also at very high temperatures up to 1500 °C. In addition, some of these nanocomposite materials exhibit superior thermal shock resistance and machinability because of the characteristic plasticity of one of the phases and the interface regions between that phase and the hard ceramic matrices. Processing is of course a key factor for the fabrication of nanocomposites with optimized properties. Some examples of commonly used processes for creating nanocomposites are discussed in the following.

Nanocomposites by Mechanical Alloying

Mechanical alloying was invented to shape small-particle dispersion strengthened metallic alloys. In this high-energy ball milling process, alloying occurs as a result of repeated breaking up and joining (welding) of the component particles. The procedure can prepare metastable systems such as polyfunctional amorphous alloys and nanocomposites. One the major advantages of this approach is the easy scaling up of the process to industrial quantities. On the other hand purity and homogeneity of the structures produced remain a challenge. Furthermore, high-energy ball milling can induce chemical reactions transferring mechanical energy to the system. This

concepts were used to prepare magnetic oxide-metal nanocomposites via mechanically induced displacement reactions between a metal oxide and a more reactive metal [209]. Ball milling can obviously induce chemical changes also in nonmetallurgical systems, like minerals, ceramics and organic compounds. In summary, the interest in mechanical alloying as a method to produce nanocrystalline materials is due to the simplicity of the method and the possibility for scaling up the process. Clearly these concepts can be also applied to composites made of two inorganic components.

Inorganic Nanocomposites for Electrical Applications

The functionalization of a piezoelectric material with a nonpiezoelectric component is unlikely to improve properties such as the strain per unit field or the charge per unit force. On the other hand, the dielectric loss of the nanocomposite material under high alternating electric fields is an interesting issue. Large dielectric loss at high fields may limit high-drive electrical applications, reducing their efficiency. A clear distinction has been shown between weak and strong field behavior in materials such as $BaTiO_3$. Above a critical field, due to hysteretic domain wall motion and the resultant reorientation by spontaneous polarization, the dielectric constant and dielectric loss increase dramatically. However, it is possible that incorporating nanosized particles (SiC of small volume percentages, 2.5%) into an electroceramic matrix ($BaTiO_3$) may hinder domain wall motion sufficiently to reduce dielectric losses at high fields. Accordingly, the microstructure requires the particles to be situated intragranularly. This concept is similar to that used in the development of hard ferromagnetic materials. In this case heat treatment is used to produce a fine dispersion of particles within the microstructure, increasing the resistance to domain wall motion. Furthermore, in addition to the possible effect of the particles on piezoelectric properties, other issues that must be taken into account include the effects of any secondary phases produced by solid-state reactions between the matrix and nanoparticles; in a $BaTiO_3$/SiC system, heat treatment and hot pressing can form new phases such as $Ba_2TiSi_2O_8$. When such phases are formed in the composite, the permittivity of the system decreases. Addition of silicon car-

bide leads to a change in the microstructure of the material and a decrease in grain size. This outcome has been reported in structural systems, which show corresponding improvements in mechanical properties. In addition, the fracture mode was transformed from transgranular for monolithic $BaTiO_3$ to intergranular for the nanocomposite. Many studies have been undertaken to fabricate piezoelectric particle-dispersed ceramic nanocomposites from other materials: $Pb(Ti_xZr_{1-x})O_3$ nanocomposites have been prepared from high-purity PZT powder and small amounts of oxides (Al_2O_3, MgO, etc.) [210]. Small additions of a second phase improve the mechanical properties, such as hardness and fracture toughness, of the PZT. The nanocomposites reduced grain size during processing with the second phase is responsible for the improved mechanical properties. The piezoelectric properties of these composites remain essentially unchanged, although for the MgO composites, the electromechanical coupling factor (which is important for actuator applications) becomes even larger.

On the other hand, one of key points of this work is to check the possibility of incorporating PZT nanoparticles in inert matrixes — such as inorganic materials or organic polymers — and to use them as sensors. The big issue is whether polarization is necessary to detect piezoelectric effects. Moreover, the effects of the incorporation of PZT nanoparticles in a matrix on the electro-mechanical response will have to be determined.

Nanocomposites can also be useful for such applications as electrical contact materials, particularly to replace the toxic Ag/CdO contacts. The reactive milling process has been used for manufacturing Ag/SnO_2 nanocomposites. A high-energy ball mill controls the reaction to obtain nanosized SnO_2 particles in an Ag matrix [211]. Then this powder is hot pressed into electrical contacts with superior erosion resistance and good thermal and electrical conductivity. Such cermet-like nanocomposites (in different configurations) have applications in other areas, like sensors. Many reports have appeared on gas-sensing technologies based on the measurement of changes in the electrical resistances of metal oxides (such as SnO_2, TiO_2) as the environment is changed [212, 213]. The sensitivity and selectivity of these metal oxide sensors can be affected by deposition of discontinuous metal films on their surface. Metals such as Pd, Pt, etc. have been used as

surface activators. Similarly, incorporating metal clusters into bulk oxides to form nanocomposites also makes it possible to tailor the effective bulk electrical response of sensor materials. This incorporation allows the range of resistivity changes caused by changes in the carrier concentration at the surface or bulk of the metal oxide sensor material to be altered. Although ceramic/metal composites are exciting mostly due to improved mechanical properties, the temperature-dependent electrical behavior of metal in ceramic nanocomposites is quite interesting [214].

5.1.2 Polymer-based and Polymer-filled Nanocomposites

Polymer composites are commercial materials with applications that include filled elastomers for damping, electrical insulators, thermal conductors and high-performance composites for use in aircraft [215]. Multifunctional materials are prepared combining components with tailored properties; for example, high-modulus but brittle carbon fibers are added to low-modulus polymers to create a stiff, lightweight composite with some degree of toughness [215]. These materials can be applied in aircraft industry but many others have been applied like filled elastomers for damping, electrical insulators and thermal conductors. Nevertheless, in recent years science and technology have reached the limits of optimizing composite properties of conventional micrometer-scale composite fillers.

Recently, new approaches have been investigated to overcome the limitations of traditional micrometer-scale polymer composites — nanoscale filled polymer composites — in which the filler is characterized by at least one dimension smaller than 1000 nm. Although some nanofilled composites have been used for more than a century, research and development of nanofilled polymers has greatly increased in the last decades [216]. First, unprecedented combinations of properties have been observed in some polymer nanocomposites [217]. A second reason for the dramatic increase in research and development of these materials was the “second” — nanotubes have been observed since the 1960s [218] — discovery of carbon nanotubes by Iijima in the early 1990s [219]. Starting from the mid-1990s they were made in the quantities required for property evaluation of composites. The

properties of these carbon nanotubes, particularly strength and electrical properties, are significantly different from those of graphite and offer exciting possibilities for new composite materials. Last but not least, a noteworthy development in the chemical processing techniques of nanoparticles and in the in situ processing of nanocomposites has led to unprecedented control over the morphology of such composites. It has also generated an almost unlimited ability to control the interface between the matrix and the filler. It is therefore an exciting time to study nanocomposites. Because of the unique combinations of properties that are achievable, because of the high potential for successful commercial development and also because of the powerful instruments that scientists posses for this purpose. We have at our fingertips, however, the ability to change the size, volume fraction, interface, and degree of dispersion or aggregation. Moreover the polymer-based nanocomposites approach offer the opportunity of an extremely easy shaping of the piezoelectric sensor. Thus, the opportunities may well become limitless when theory and experiment have assembled enough information to guide further development.

One of the key limitations in the commercialization of nanocomposites is processing. Early attempts at clay-filled polymers required processing that was not commercially feasible, but this situation has changed. Similarly, processing of other nanocomposites is becoming easier and more commercially viable as our understanding improves. A primary difficulty is proper dispersion of the fillers. Without proper dispersion and distribution of the fillers, the high surface area is compromised and the aggregates can act as defects, which limit properties. To facilitate discussion, we will define the state of aggregation in those nanocomposites. Distribution of a nanofiller describes the homogeneity throughout the sample, and the dispersion describes the level of agglomeration.

There are three general ways for dispersing nanofillers in polymers. The first one is the direct mixing of the polymer and the nanoparticles — either in the solid state or properly dispersed in a liquid phase. The second is in-situ polymerization in the presence of the nanoparticles, while the third is the parallel in-situ growth of the nanoparticles and in-situ polymerization. The latter can result in composites called hybrid nanocomposites because of

the intimate mixing of the two phases [220, 221, 222, 223, 224]. A detailed description of the processing of the nanocomposites which were developed in this work is reported in the next Section.

5.2 Preparation of PZT Nanocomposites

5.2.1 Materials

PZT powders were synthetized in our labs. $BaTiO_3$ (nanopowder (cubic crystalline phase), < 100 nm particle size (BET), $\geq 99\%$ trace metals basis) was bought from Sigma-Alrich and was used without any further purification. All the polymer dispersions were kindly supplied by BG Polymers (www.bgpol.co.il). $CaCO_3$ (SigmaUltra, $\geq 99.0\%$) was bought from Sigma-Alrich and was used without any further purification. Cements which were used for PZT nanocomposites were kindly supplied by Italcementi (Bergamo, Italy).

5.2.2 Pure Piezoelectric Discs

In order to evaluate the piezoelectric response of crystalline PZT powders — produced according to the EDTA method — small piezoelectric discs, of about 2 mm of thickness and 1 cm of diameter, were produced (See Figure 5.2). The discs were prepared weighting about 400 mg of the powder. The powders were placed between two aluminum foils and pressed at 7 tons for 15 minutes. The aluminum foils acting as electrodes were connected to the acquisition system which will be described in Section 5.3. This procedure was applied for the production of pure PZT samples obtained from the EDTA method (the same holds for all the others). A summary of the samples prepared with pure piezoelectric powders can be found in Table 5.1. Furthermore, pure $BaTiO_3$ discs were prepared as a reference for the evaluation of the electric response of PZT discs.

5.2.3 PZT/Polymer Nanocomposites

PZT/polymer nanocomposites were produced mixing 2 ml of PZT water dispersion with 2 ml of polymer dispersion. The mixture was placed in

Figure 5.2: A picture of a pure PZT disc which was used for the electro-mechanical measurements.

Powder Formula	Sample ID
$Pb(Ti_{0.48}Zr_{0.52})O_3$	DP1
$Pb(Ti_{0.25}Zr_{0.75})O_3$	DP2
$Pb(Ti_{0.75}Zr_{0.25})O_3$	DP3
$BaTiO_3$	DB4

Table 5.1: Pure piezoelectric discs. PZT were synthetized according to the EDTA method. $BaTiO_3$ (nanopowder (cubic crystalline phase), < 100 nm particle size (BET), $\geq 99\%$ trace metals basis) was bought from Sigma-Alrich and was used without any further purification.

a 2 cm sided plastic support and water was slowly evaporated keeping the sample on a orbital stirrer at room temperature. Once water was completely removed the plastic support was removed. A picture of one of the samples produced is reported in Figure 5.3. The polymers which were used are reported in Table 5.2 with the samples IDs.

5.2.4 PZT/Inorganic Matrixes Nanocomposites

Nanocomposites consisting of $Pb(Ti_{0.48}Zr_{0.52})O_3$ nanoparticles mixed with different inorganic matrixes were produced. The discs were prepared according to the same procedure described for pure piezoelectric powders after mixing the nanopowder with the matrixes.

PZT nanopowders were mixed with $CaCO_3$ in various ratios, to find out

Sample ID	Monomers Type	Particle Size (nm)
DO1	Et, MMA, AN	150
DO2	EA, BA	300

Table 5.2: A list of the polymers which were used for the preparation of PZT nanocomposites. All the polymer dispersions were kindly supplied by BG Polymers (www.bgpol.co.il).

Figure 5.3: A picture a nanocomposite prepared with PZT water dispersion and a polymer (DO2).

minimum quantity of piezoelectric material that is necessary to detect an electric response. A summary of the samples is reported in Table 5.3.

The PZT nanopowders were also mixed in a 1:1 ratio with dry cement. The mixture discs were again prepared with the same procedure (sample ID: DE1). Two discs were hydrated for 10 days. After the hydration, the samples was dried either with paper at room temperature (sample ID: DE2) or in an oven at 105 °C until the weight remained constant (sample ID: DE3). Finally, the PZT nanopowders were mixed with cement and sand in a 4:1:3 ratio respectively(sample ID: DS1). Two discs were hydrated for 10 days. After the hydration, the samples was dried either with paper at room temperature (sample ID: DS2) or in an oven at 105 °C until the weight remained constant (sample ID: DS3).

Sample ID	% of PZT
DC1	75
DC2	50
DC3	5
DC4	1

Table 5.3: A list of the nanocomposites prepared mixing PZT nanopowders with $CaCO_3$.

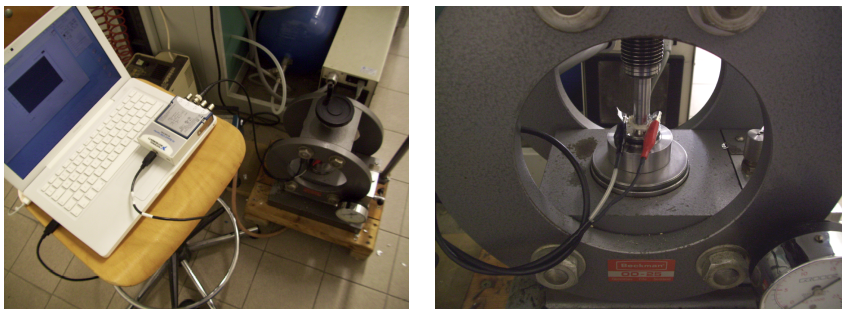

Figure 5.4: Pictures of the apparatus for the electro-mechanical measurements.

5.3 Piezoelectricity Tests: Experimental Setup

The electric response of the pure PZT discs was evaluated by means of a lab-made apparatus (see Figure 5.4). A piezoelectric disc was placed in a manual press and electrically insulated. The electrodes on the faces of the PZT disc were connected to a 24-Bit digital acquisition module (NI 9234, National Instruments, Austin, TX) coupled with a Hi-Speed USB Carrier (NI USB-9162). The electrical parameters were controlled with LabVIEW as it will be discussed in the following, sampling the signal at 50 kHz. A schematization of the "sandwich" is shown in Figure 5.5.

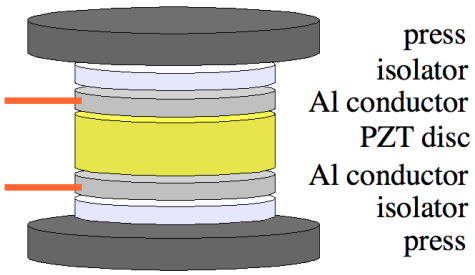

Figure 5.5: A schematization of the sandwich prepared for electromechanical measurements.

Figure 5.6: A picture of NI 9234 module.

5.3.1 Hardware

The piezoelectric response of the PZT powder and composites was checked by means of a 24-Bit National Instruments dynamic signal acquisition module (NI 9234, National Instruments, Austin, TX) with four analog input channels. A picture of the NI 9234 module is shown in Figure 5.6.

The module is designed for dynamic acquisition of signals which require high accuracy. The precision p of the instrument can be calculated according to following formula:

$$p = \frac{A}{2^{24}},$$

where A is the amplitude range of the signal recordable. Being $A = \pm 5$, the precision can be estimated in ± 600 nV.

A scheme of one of the four channels of the NI 9234 is reported in Figure 5.7. The signals within the passband have frequency-dependent gain or attenuation. The small amount of variation in gain with respect to frequency

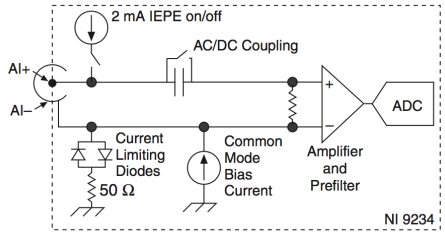

Figure 5.7: NI 9234 input circuitry for one channel.

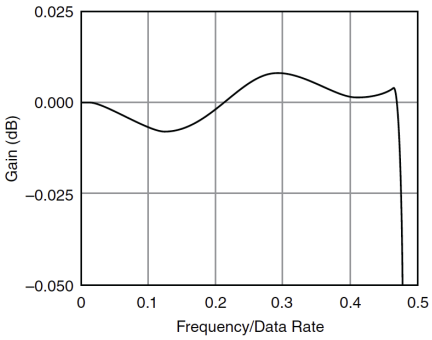

Figure 5.8: NI 9234 typical passband flatness.

is called the passband flatness. The digital filters of the NI 9234 adjust the frequency range of the passband to match the data rate. Therefore, the amount of gain or attenuation at a given frequency depends on the data rate. Figure 5.8 shows typical passband flatness for the NI 9234. The filter significantly attenuates all signals above the stopband frequency. The primary goal of the filter is to prevent aliasing.

Therefore, the stopband frequency scales precisely with the data rate. The stopband rejection is the minimum amount of attenuation applied by the filter to all signals with frequencies within the stopband. Any signal that appears in the alias-free bandwidth of the NI 9234 is not an aliased artifact of signals at a higher frequency. The alias-free bandwidth is defined by the ability of the filter to reject frequencies above the stopband frequency, and it is equal to the data rate minus the stopband frequency.

The frequency of a master timebase (f_M) controls the data rate (f_s) of the NI 9234. The NI 9234 includes an internal master timebase with a frequency of 13.1072 MHz.

5.3.2 Software

The software for the electro-mechanical measurements was developed with LabVIEW 8.6 (Copyright 2008 ©, National Instruments, Austin, TX) LabVIEW is a graphic interface programming language that uses icons instead of lines of code to create applications and virtual instruments (VIs). In contrast to text-based programming languages, where instructions determine program execution, LabVIEW uses dataflow programming, where the flow of data determines execution. In LabVIEW, the user builds an interface with a set of tools and objects. The user interface is known as the front panel. The code is then added using graphical representations of functions to control the front panel objects. The block diagram contains this code. In some ways, the block diagram resembles a flowchart.

LabVIEW programs are called VIs, because their appearance and operation imitate physical instruments, such as oscilloscopes and multimeters. Every VI uses functions that manipulate input from the user interface or other sources and display that information or move it to other files or other computers. A VI contains the following three components:

- The **front panel** which serves as the user interface.
- The **block diagram** which contains the graphical source code that defines the functionality of the VI.
- The **icon and connector pane** which identifies the VI so that user can load the VI in another VI. A VI within another VI is called a subVI. SubVIs correspond to the subroutines in text-based programming languages.

The VI developed for the electro-mechanical tests is made of two distinct parts: the driver and the data processing unit. A sketch of the first one — which is the driver that allows the operative system to handle the acquisition module — is reported in Figure 5.9. Following the flow from left to right, a channel and the 50 kHz clock are created. The excitation on the channel and the AC capacitor are disabled. In fact, order to keep the measurement offset the instrument was working in DC modality.

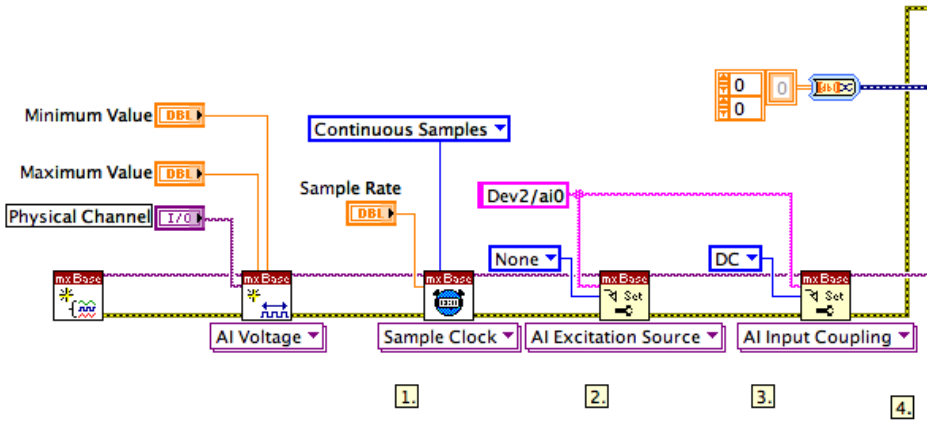

Figure 5.9: A schematization of the driver in the VI for the electro-mechanical measurements.

The data processing unit is shown in Figure 5.10. The data processing unit is in a while loop so that all the data measured are collected and stored properly. First, the output file is created and the acquisition starts. The picture is referred to the first iteration when the "case structure" in the gray box is "true". Its value is then set to "false" in the following iterations. The instruments starts reading the data from the buffer in the module. 50000 samples per second are read. Then the "sample compression" box calculates the mean value of 1000 points. This procedure is necessary in order to remove the noisy sinusoidal signal on the data.

5.4 Results

The piezoelectric response of PZT nanodevices can be exploited for producing electro-mechanical sensors to be applied in building industry, road constructions, and dikes' reinforcement. For this reason we checked the capability of PZT discs to convert mechanical inputs into electric signals. Since several data on PZT electro-mechanical properties are available in the literature (see References [225, 226, 227, 228, 229]), the aim of the measurements performed in this work is to confirm that the piezoelectric capacity

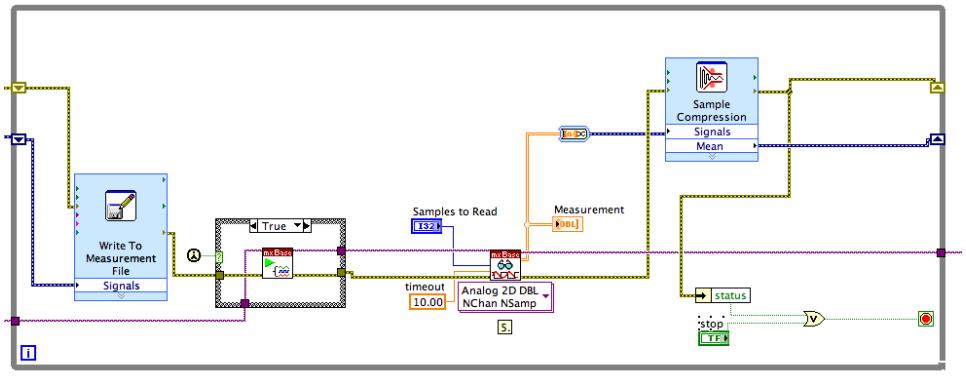

Figure 5.10: A schematization of the data processing unit in the VI for the electro-mechanical measurements.

of the synthesized PZT nanoparticles that can be exploited for building piezoelectric sensors.

In order to find out which composition of the PZT powder is optimal, electro-mechanical measurements have been made with selected PZT nanopowders with various compositions. The results of the tests are reported in Figure 5.11. They clearly show that PZT nanoparticles produce the strongest piezoelectric signal when the ratio between Ti^{IV} and Zr^{IV} cations is 48:52. In this case the voltage reaches ± 2 V with jumps of 1.55 ± 0.61 V. The sample DP2, which was prepared with $Pb(Ti_{0.25}Zr_{0.75})O_3$ powders, shows peaks of 0.42 ± 0.15 V with a maximum voltage of 0.75 V. The electric signals recorded from sample DP3 are even weaker with voltage jumps of 0.37 ± 0.16 V and a maximum voltage of 0.55 V. Moreover, when the same apparatus is used to test the electro-mechanical properties of $BaTiO_3$ nanoparticles a weaker signal — which can be compared to the one obtained from sample DP3 — is recorded. This results thus confirm the data reported in the literature [230, 231].

When PZT nanoparticles are embedded in $CaCO_3$ matrixes the electric signal is still recordable. The results of the PZT nanoparticles embedded in calcium carbonate are reported in Figure 5.12. PZT dilution in an inorganic matrix results in a slight progressive decrease of the electric signal recorded. However the 5% PZT in $CaCO_3$ still generates electric signals when pressed. On the other hand dilution down to 1% results in no signal

detection. The measurements on the samples prepared with polymers (samples DO1 and DO2) did not produce any electric response. This is probably due to the limited hardness of the matrixes which may lead to mechanical energy dissipation. Despite the efforts for improving the hardness of the nanoparticles-polymer composites the problem still held. We thus investigated the possibility of incorporating the PZT nanoparticles in extremely hard material like cement.

PZT-cement composites (see Figure 5.13) show electric activity. Samples DE1 and DE2 revel the best piezoelectric response with the voltage reaching ± 0.6 V. The mean value of the voltage is 0.40 ± 0.20 and 0.46 ± 0.21 V, respectively. The response obtained from sample DE3 is slightly weaker reaching a voltage of ± 0.5 with an average value of 0.28 ± 0.12. Cement hydration thus seams not to influence the piezoelectric properties of the composites. The same does not hold for drying in the oven which results in a slight decrease of the electro-mechanical response of the composite.

Finally, the nanocomposites with sand were tested. The measurements did not reveal any electric response. This is probably due to the size of the sand grains which do not allow a proper compacting of the disc.

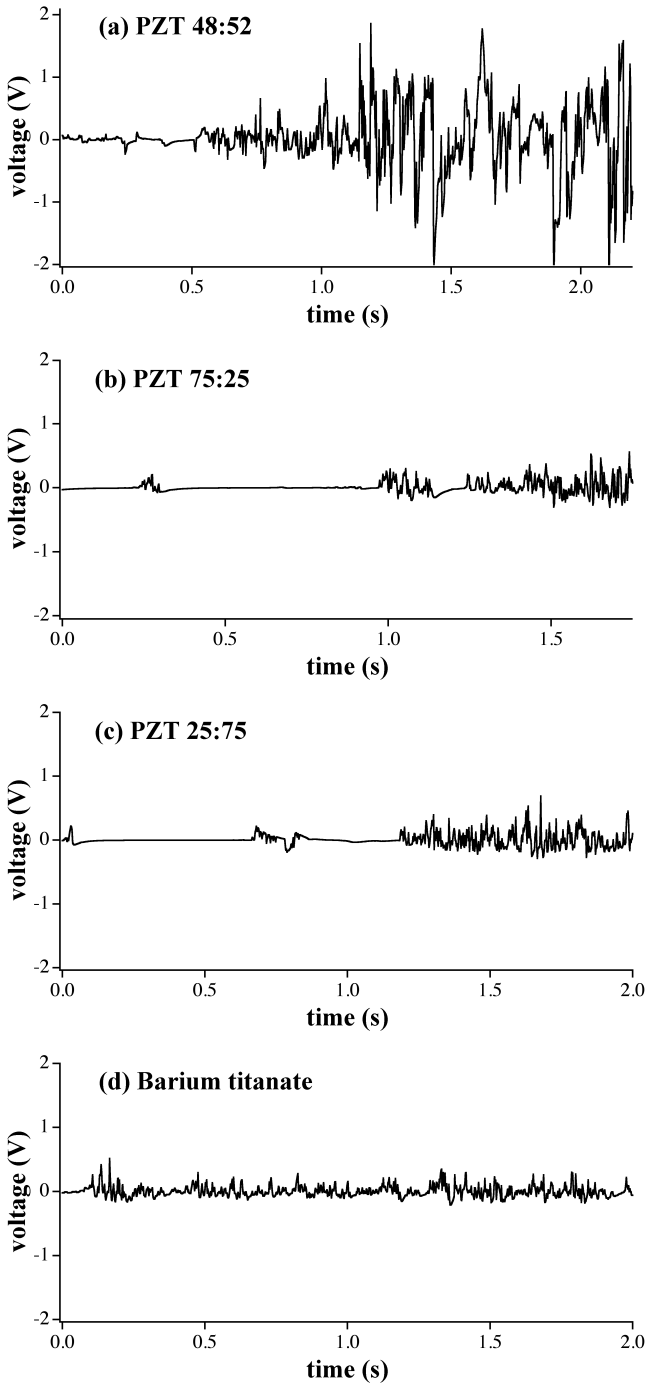

Figure 5.11: Electric voltage (in V) as a function of time, showing the piezoelectric response of the pure PZT nanopowders prepared with the EDTA method at different Ti:Zr ratios ((a) 48:52, (b) 75:25 and (c) 25:75), and of $BaTiO_3$ nanoparticles (d).

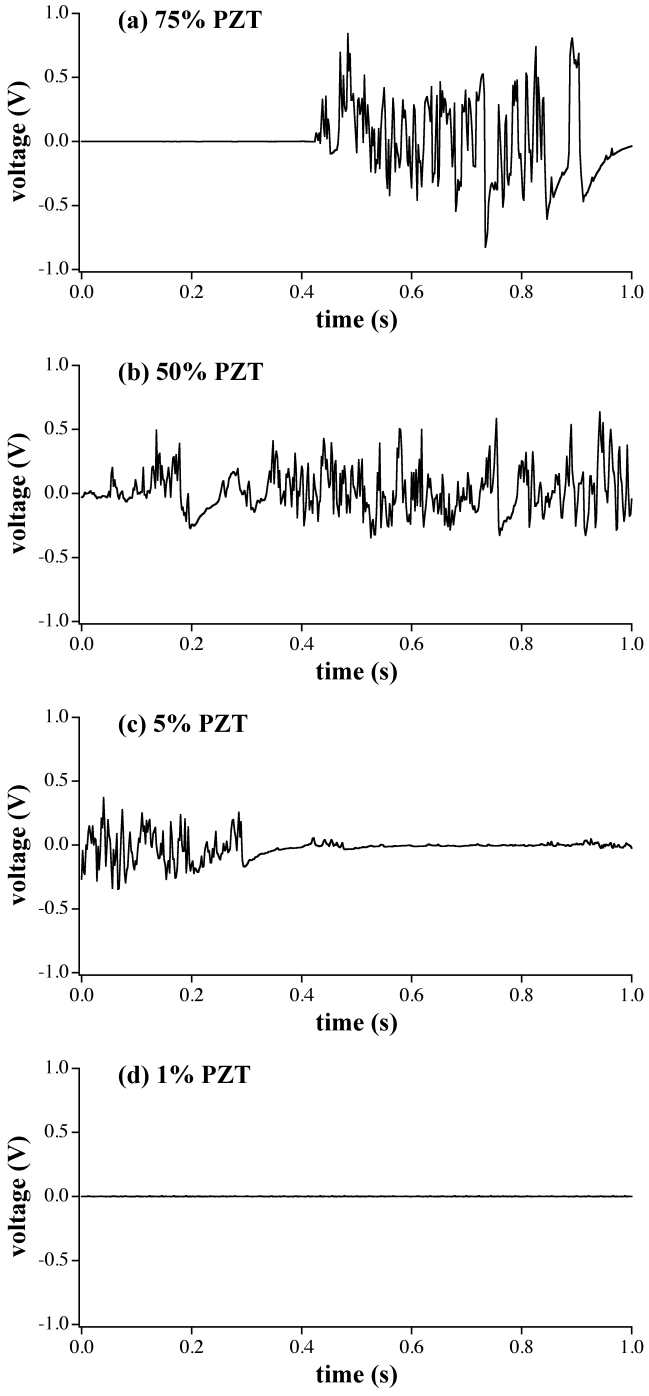

Figure 5.12: Electric voltage (in V) as a function of time, showing the piezoelectric response of the PZT nanopowders embedded in calcium carbonate with different ratios.

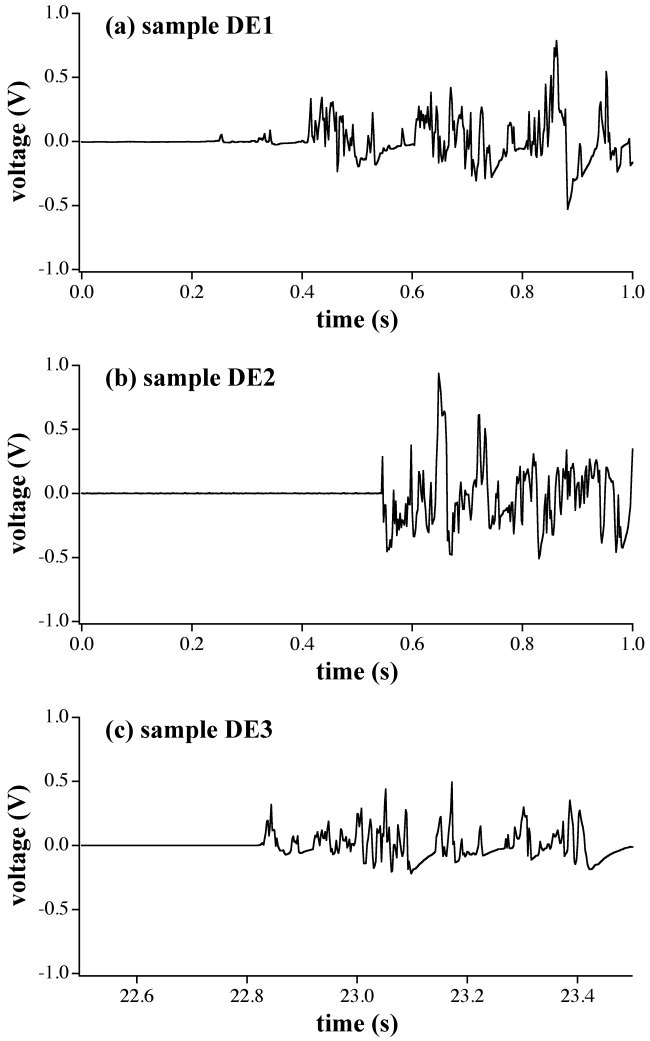

Figure 5.13: Electric voltage (in V) as a function of time, showing the piezoelectric response of the PZT nanopowders embedded in cement matrixes.

Conclusions

The work which was carried out in the three years of this Ph.D. thesis involved the development of a fast and smart synthetic procedure for the production of PZT nanoparticles, namely the EDTA method. This synthetic approach was developed in order to be easily scaled-up, starting from commercially available chemicals. A detailed characterization of the nanopowders was performed by means of SEM, XRD and PIXE. Furthermore, a lab-made equipment for the measurement of piezoelectric activity of the nanoparticles produced — embedded in various matrixes — was developed. The piezoelectric response of the nanoparticles prepared and those of several PZT-based nanocomposites were thus investigated. These studies required a deep knowledge of the chemical properties of Ti^{IV} and Zr^{IV} cations. The lab-made apparatus for the piezoelectric measurements was developed by means of the LabVIEW tools.

We applied a modified complex combustion procedure to titanium and zirconium alkoxides, in order to produce nanocrystalline PZT materials. DTG measurements on the precursor powders indicate that the thermal properties of the precursors, and the molecular weight of the ligands involved in the stabilization of the cations, strongly affect the crystalline purity of the final products. In fact, when the enthalpy of combustion of the organic matter (i.e. the ligand) is large, it is sufficient to trigger the combustion by first increasing the temperature, and then stop the heating. The heat released by the burning material will sustain the combustion. Moreover, for the same reason, a shorter calcination step will be required. Therefore, the advantage of this hybrid synthetic procedure includes a significant energy saving. PIXE measurements confirmed that the chemical composition of PZT nanopow-

ders — a key factor for the electro-mechanical properties of these systems — can be properly controlled with the EDTA method. The composition of the nanopowders which were produced was thus near the morphotropic phase boundary where the best piezoelectric response are detected. TEM measurements revealed that very small nanosized particles are produced before the calcination step. Obviously, they are subjected to sintering during the thermal treatment. In fact, scanning electron microscopy confirmed that calcination results in particle sintering or agglomeration. However, particle sintering can be limited due to the very short calcination time required in the EDTA method. The chemical composition of the starting solution, in particular the ligands involved in the stabilization of the Ti^{IV}, Zr^{IV} and Pb^{II} cations, plays a crucial role with respect to crystalline purity of the calcinated powders. With the EDTA method, highly crystalline powders were produced. When EDTA is the stabilizer for all cations, its combustion enthalpy is the key factor for producing homogeneous crystalline PZT nanoparticles.

The possibility of developing a colloidal dispersion on PZT nanoparticles was investigated. This aspect is extremely important when the piezoelectric properties of PZT must be exploited in nanocomposites. In this case PZT dispersions can be easily mixed with any kind of matrix precursor — like the polymer dispersions that we tested — which is dispersed in water. The agglomerated particles produced with the EDTA method can be easily dispersed in water, with the help of a suitable surfactant combining both electrostatic — as revealed by zeta potential measurements — and steric stabilizing effects. Stable water dispersions of PZT nanoparticles were produced by means of microfluidization process. These dispersions may be exploited for functional coating of nanocomposites and/or geotextiles.

The electro-mechanical tests clearly showed that the synthesized PZT nanoparticles possess a significant piezoelectric activity, greater or equivalent to that of $BaTiO_3$, depending on the chemical composition of the PZT nanopowder. The same piezoelectric capacity of the pure powder is retained in PZT/$CaCO_3$ mixtures for concentrations of PZT larger than 5% w/w and PZT/cement composites. These results appear to be very interesting and promising for future applications in remote monitoring of both masonry

structural integrity and geological activity.

List of Figures

List of Tables

Acronyms

acac acetylacetonate anion. 55

AFM Atomic Force Microscope. 16, 29

AN acrylonitrile. 99

BA butyl acrylate. 99

BAL *(RS)*-2,3-disulfanylpropan-1-ol. 52

cermet a composite material made of ceramic (cer) and metallic (met) materials. 94

DEA diethanolamine. 64

DLS Dynamic Light Scattering. 82, 84, 86

DPN Dip-Pen Nanolitography. 17

DTG Differential Thermal Gravimetry. 69, 71, 79

EA ethyl acrylate. 99

EDTA any anionic forms of ethylenediamine tetra-acetic acid. 52, 53

Et ethylene. 99

FRC Fibre Reinforced Composites. 43

H_4EDTA fully protonated ethylenediamine tetra-acetic acid. 66, 67

HAc acetic acid. 57, 72

Hacac 2,4-pentanedione, acetyl acetone. 66, 72

IEEE Institute of Electrical and Electronics Engineers. 31

MBB Molecular Building Block. 9, 12, 13

MMA methyl methacrylate. 99

MPB Morphotropic Phase Boundary. 25, 35, 36

MW Molecular Weight. 66

NMR Nuclear Magnetic Resonance. 56, 61

PIXE Proton Induced X-Ray Emission. 76, 77

PVA polyvinyl alcohol. 63

PVDF polyvinylidene fluoride. 46

PZT Lead Zirconate Titanate. 46

SEM Scanning Electron Microscopy. 76, 79, 82

SPE Superparaelectric. 39

STM Scanning Tunneling Microscopy. 29

TEM Transmission Electron Microscopy. 69, 71

VI virtual instrument. 103

XRD X-Ray Diffraction. 75, 77

Bibliography

[1] Hush, N. *Molecular Electronics III* **1006**, 1–20 (2003).

[2] Junk, A. & Riess, F. *American Journal of Physics* **74**(9), 825–830 September (2006).

[3] Kukowska-Latallo, J. *et al. Cancer Research* **65**(12), 5317–5324 June (2005).

[4] Wang, Z., Ruan, J. & Cui, D. *Nanoscale Research Letters* **4**(7), 593–605 July (2009).

[5] Herron, N. & Thorn, D. *Advanced Materials* **10**(15), 1173–1184 October (1998).

[6] Zhang, A. *Progress In Chemistry* **17**(1), 157–171 January (2005).

[7] Jones, R. *Nature Nanotechnology* **4**(2), 75–75 February (2009).

[8] Xia, Y., Rogers, J., Paul, K. & Whitesides, G. *Chemical Reviews* **99**(7), 1823–1848 July (1999).

[9] Whitesides, G. & Love, J. *Scientific American* **285**(3), 38–47 September (2001).

[10] Glass, R., Moller, M. & Spatz, J. *Nanotechnology* **14**(10), 1153–1160 October (2003).

[11] Milne, W. *et al. Journal of Materials Chemistry* **14**(6), 933–943 (2004).

[12] Solak, H. *et al. Microelectronic Engineering* **67-8**, 56–62 June (2003).

[13] Pfeiffer, F., David, C., Burghammer, M., Riekel, C. & Salditt, T. *Science* **297**(5579), 230–234 July (2002).

[14] Mendes, P. *et al. Langmuir* **20**(9), 3766–3768 April (2004).

[15] Guo, L. J. *Advanced Materials* **19**(4), 495–513 February (2007).

[16] Melin, J. & Quake, S. R. *Annual Review of Biophysics and Biomolecular Structure* **36**, 213–231 (2007).

[17] Zhong, Z., Gates, B., Xia, Y. & Qin, D. *Langmuir* **16**(26), 10369–10375 December (2000).

[18] Lu, W. & Lieber, C. M. *Nature Materials* **6**(11), 841–850 November (2007).

[19] Boeker, A., He, J., Emrick, T. & Russell, T. P. *Soft Matter* **3**(10), 1231–1248 (2007).

[20] Ryu, J.-H., Hong, D.-J. & Lee, M. *Chemical Communications* (9), 1043–1054 (2008).

[21] Hirst, A. R., Escuder, B., Miravet, J. F. & Smith, D. K. *Angewandte Chemie-International Edition* **47**(42), 8002–8018 (2008).

[22] Akcora, P. *et al. Nature Materials* **8**(4), 354–U121 April (2009).

[23] Cheng, F., Tao, Z., Liang, J. & Chen, J. *Chemistry of Materials* **20**(3), 667–681 February (2008).

[24] Jun, Y., Seo, J., Oh, S. & Cheon, J. *Coordination Chemistry Reviews* **249**(17-18), 1766–1775 September (2005).

[25] Reimann, S. & Manninen, M. *Reviews of Modern Physics* **74**(4), 1283–1342 October (2002).

[26] Bukowski, T. & Simmons, J. *Critical Reviews In Solid State and Materials Sciences* **27**(3-4), 119–142 (2002).

[27] Penner, R. *Accounts of Chemical Research* **33**(2), 78–86 February (2000).

[28] Ponomarenko, L. A. *et al. Science* **320**(5874), 356–358 April (2008).

[29] Xia, Y. *et al. Advanced Materials* **15**(5), 353–389 March (2003).

[30] Romo-Herrera, J. M., Terrones, M., Terrones, H., Dag, S. & Meunier, V. *Nano Letters* **7**(3), 570–576 March (2007).

[31] Trindade, T., O'Brien, P. & Pickett, N. *Chemistry of Materials* **13**(11), 3843–3858 November (2001).

[32] Jain, P. K., Huang, X., El-Sayed, I. H. & El-Sayed, M. A. *Accounts of Chemical Research* **41**(12), 1578–1586 December (2008).

[33] Gordon, R., Sinton, D., Kavanagh, K. L. & Brolo, A. G. *Accounts of Chemical Research* **41**(8), 1049–1057 August (2008).

[34] White, R. J., Luque, R., Budarin, V. L., Clark, J. H. & Macquarrie, D. J. *Chemical Society Reviews* **38**(2), 481–494 (2009).

[35] Han, X. D. *et al. Nano Letters* **7**(2), 452–457 February (2007).

[36] Sheldon, B. & Curtin, W. *Nature Materials* **3**(8), 505–506 August (2004).

[37] Druzhkov, A. *et al. Journal of Physics-Condensed Matter* **14**(34), 7981–7990 September (2002).

[38] Chen, L.-M., Hong, Z., Li, G. & Yang, Y. *Advanced Materials* **21**(14-15), 1434–1449 April (2009).

[39] Dahl, J., Liu, S. & Carlson, R. *Science* **299**(5603), 96–99 January (2003).

[40] McIntosh, G., Yoon, M., Berber, S. & Tomanek, D. *Physical Review B* **70**(4) July (2004).

[41] Kuykendall, T., Ulrich, P., Aloni, S. & Yang, P. *Nature Materials* **6**(12), 951–956 December (2007).

[42] Bang, J. H. & Kamat, P. V. *Acs Nano* **3**(6), 1467–1476 June (2009).

[43] Oulton, R. F. *et al. Nature* **461**(7264), 629–632 October (2009).

[44] Heisenberg, W. *Physics and Philosophy.* Harper and Row, New York, NY, (1958).

[45] Piner, R., Zhu, J., Xu, F., Hong, S. & Mirkin, C. *Science* **283**(5402), 661–663 January (1999).

[46] Hong, S., Zhu, J. & Mirkin, C. *Science* **286**(5439), 523–525 October (1999).

[47] Feynman, R. *Journal of Microelectromechanical Systems* **2**(1), 4 – 14 March (1993).

[48] von Neumann, J. & Burks, A. *Theory of Self-Reproducing Automata.* University of Illinois Press, Urbana, IL, (1966).

[49] Bartels, L., Meyer, G. & Rieder, K. *Physical Review Letters* **79**(4), 697–700 July (1997).

[50] Eigler, D. & Schweizer, E. *Nature* **344**(6266), 524–526 April (1990).

[51] Bezryadin, A., Dekker, C. & Schmid, G. *Applied Physics Letters* **71**(9), 1273–1275 September (1997).

[52] Hill, T. *Nano Letters* **1**(5), 273–275 May (2001).

[53] Frogley, M., Ravich, D. & Wagner, H. *Composites Science and Technology* **63**(11), 1647–1654 August (2003).

[54] Sarvestani, A. & Picu, C. *Polymer* **45**(22), 7779–7790 October (2004).

[55] Paramsothy, M., Hassan, S. F., Srikanth, N. & Gupta, M. *Materials Science and Engineering A-Structural Materials Properties Microstructure and Processing* **527**(1-2), 162–168 December (2009).

[56] Wetzel, B., Haupert, F. & Zhang, M. *Composites Science and Technology* **63**(14), 2055–2067 November (2003).

[57] Kashiwagi, T. *et al.* *Nature Materials* **4**(12), 928–933 December (2005).

[58] Lee, H., Chou, K. & Huang, K. *Nanotechnology* **16**(10), 2436–2441 October (2005).

[59] Qu, L., Xia, S., Bian, C., Sun, J. & Han, J. *Biosensors & Bioelectronics* **24**(12), 3419–3424 August (2009).

[60] Svenson, S. & Tomalia, D. *Advanced Drug Delivery Reviews* **57**(15), 2106–2129 December (2005).

[61] Gaucher, G. *et al. Journal of Controlled Release* **109**(1-3), 169–188 December (2005).

[62] Delamarche, E., Juncker, D. & Schmid, H. *Advanced Materials* **17**(24), 2911–2933 December (2005).

[63] Tang, Z., Wang, Y., Podsiadlo, P. & Kotov, N. A. *Advanced Materials* **18**(24), 3203–3224 December (2006).

[64] Liao, H., Nehl, C. L. & Hafner, J. H. *Nanomedicine* **1**(2), 201–208 August (2006).

[65] Schmidt, H. *Applied Organometallic Chemistry* **15**(5), 331–343 May (2001).

[66] Haertling, G. *Journal of the American Ceramic Society* **82**(4), 797–818 April (1999).

[67] Turner, R., Fuierer, P., Newnham, R. & Shrout, T. *Applied Acoustics* **41**(4), 299–324 (1994).

[68] Paik, D., Park, S., Shrout, T. & Hackenberger, W. *Journal of Materials Science* **34**(3), 469–473 February (1999).

[69] Bove, T., Wolny, W., Ringgaard, E. & Pedersen, A. *Journal of the European Ceramic Society* **21**(10-11), 1469–1472 (2001).

[70] Jaffe, B., Cook, W. & Jaffe, H. *Piezoelectric Ceramics*. Academic Press, New York, (1971).

[71] Lee, B. W. & Lee, E. J. *Journal of Electroceramics* **17**(2-4), 597–602 December (2006).

[72] Chon, U., Jang, H., Kim, M. & Chang, C. *Physical Review Letters* **89**(8) August (2002).

[73] Yao, Y. *et al.* *Journal of Applied Physics* **95**(6), 3126–3130 March (2004).

[74] Li, H., Feng, C. & Yao, W. *Materials Letters* **58**(7-8), 1194–1198 March (2004).

[75] Chon, U., Shim, J. & Jang, H. *Journal of Applied Physics* **93**(8), 4769–4775 April (2003).

[76] Soga, M., Noguchi, Y., Miyayama, M., Okino, H. & Yamamoto, T. *Applied Physics Letters* **84**(1), 100–102 January (2004).

[77] Kwok, K., Chan, H. & Choy, C. *Ieee Transactions On Ultrasonics Ferroelectrics and Frequency Control* **44**(4), 733–742 July (1997).

[78] Lee, H. & Kimura, T. *Journal of the American Ceramic Society* **81**(12), 3228–3236 December (1998).

[79] Venet, M. *et al.* *Journal of the European Ceramic Society* **25**(12), 2443–2446 (2005).

[80] Rabe, U. *et al.* *Journal of Physics D-Applied Physics* **35**(20), 2621–2635 October (2002).

[81] Sinko, K., Fel, K., Rohonczy, J. & Husing, N. *Smart Materials & Structures* **10**(5), 1078–1084 October (2001).

[82] Li, L., Shen, Y. & Gao, F. *Smart Materials & Structures* **10**(2), 421–426 April (2001).

[83] Hauptmann, P., Lucklum, R., Puttmer, A. & Henning, B. *Sensors and Actuators A-Physical* **67**(1-3), 32–48 May (1998).

[84] Devasia, S., Eleftheriou, E. & Moheimani, S. O. R. *Ieee Transactions On Control Systems Technology* **15**(5), 802–823 September (2007).

[85] Turik, A., Topolov, V. & Aleshin, V. *Journal of Physics D-Applied Physics* **33**(6), 738–743 March (2000).

[86] Uchino, K. *Acta Materialia* **46**(11), 3745–3753 July (1998).

[87] Noheda, B. *et al.* *Applied Physics Letters* **74**(14), 2059–2061 April (1999).

[88] Park, S. & Shrout, T. *Journal of Applied Physics* **82**(4), 1804–1811 August (1997).

[89] Ye, Z., Noheda, B., Dong, M., Cox, D. & Shirane, G. *Physical Review B* **64**(18) November (2001).

[90] La-Orauttapong, D. *et al.* *Physical Review B* **65**(14) April (2002).

[91] Corker, D., Glazer, A., Whatmore, R., Stallard, A. & Fauth, F. *Journal of Physics-Condensed Matter* **10**(28), 6251–6269 July (1998).

[92] Paik, D., Park, S., Wada, S., Liu, S. & Shrout, T. *Journal of Applied Physics* **85**(2), 1080–1083 January (1999).

[93] Fu, H. & Cohen, R. *Nature* **403**(6767), 281–283 January (2000).

[94] Bell, A. *Journal of Applied Physics* **89**(7), 3907–3914 April (2001).

[95] Damjanovic, D., Brem, F. & Setter, N. *Applied Physics Letters* **80**(4), 652–654 January (2002).

[96] Wu, Z. & Krakauer, H. *Physical Review B* **68**(1) July (2003).

[97] Huang, N. *et al.* *Physical Review Letters* **91**(6) August (2003).

[98] Li, S. *et al.* *Physics Letters a* **212**(6), 341–346 April (1996).

[99] Nagarajan, V. *et al.* *Applied Physics Letters* **81**(22), 4215–4217 November (2002).

[100] Pertsev, N., Zembilgotov, A. & Tagantsev, A. *Physical Review Letters* **80**(9), 1988–1991 March (1998).

[101] Sun, H., Tian, W., Pan, X., Haeni, J. & Schlom, D. *Applied Physics Letters* **84**(17), 3298–3300 April (2004).

[102] Chu, M. *et al.* *Nature Materials* **3**(2), 87–90 February (2004).

[103] Waser, R. & Rudiger, A. *Nature Materials* **3**(2), 81–82 February (2004).

[104] Szot, K. & Speier, W. *Physical Review B* **60**(8), 5909–5926 August (1999).

[105] Szot, K., Speier, W., Carius, R., Zastrow, U. & Beyer, W. *Physical Review Letters* **88**(7) February (2002).

[106] Alexe, M., Harnagea, C., Hesse, D. & Gosele, U. *Applied Physics Letters* **79**(2), 242–244 July (2001).

[107] Buhlmann, S., Dwir, B., Baborowski, J. & Muralt, P. *Applied Physics Letters* **80**(17), 3195–3197 April (2002).

[108] Ma, W. & Hesse, D. *Applied Physics Letters* **84**(15), 2871–2873 April (2004).

[109] Roelofs, A. *et al. Applied Physics Letters* **77**(21), 3444–3446 November (2000).

[110] Dawber, M., Jung, D. & Scott, J. *Applied Physics Letters* **82**(3), 436–438 January (2003).

[111] Jung, D. *et al. Applied Physics Letters* **81**(13), 2436–2438 September (2002).

[112] Peter, F. *et al. Applied Physics Letters* **85**(14), 2896–2898 October (2004).

[113] Tiedke, S. *et al. Applied Physics Letters* **79**(22), 3678–3680 November (2001).

[114] Glinchuk, M., Eliseev, E. & Morozovska, A. *Physical Review B* **78**(13) October (2008).

[115] Aluigi, A. *et al. Journal of Applied Polymer Science* **104**(2), 863–870 April (2007).

[116] Dietzel, Y. *et al. Surface & Coatings Technology* **135**(1), 75–81 December (2000).

[117] Dierickx, W., Gabriels, D. & Cornelis, W. *Geotextiles and Geomembranes* **19**(1), 59–73 January (2001).

[118] Vinogradov, I. & Lunk, A. *Surface & Coatings Technology* **200**(1-4), 660–663 October (2005).

[119] Carvelli, V., Corazza, C. & Poggi, C. *Computational Materials Science* **42**(4), 679–691 June (2008).

[120] Mannsbart, G. & Resl, S. *Geotextiles and Geomembranes* **12**(5), 441–450 (1993).

[121] Muthukumaran, A. E. & Ilamparuthi, K. *Geotextiles and Geomembranes* **24**(4), 210–219 August (2006).

[122] Iryo, T. & Rowe, R. K. *Geosynthetics International* **11**(5), 377–389 October (2004).

[123] Vaitkus, A., Laurinavicius, A. & Cygas, D. *Baltic Journal of Road and Bridge Engineering* **1**(1), 29–37 (2006).

[124] Barrett, M., Malina, J. & Charbeneau, R. *Water Environment Research* **70**(3), 283–290 May-Jun (1998).

[125] Moo-Young, H., Gaffney, D. & Mo, X. *Geotextiles and Geomembranes* **20**(5), 289–303 October (2002).

[126] Park, K. & Fleming, I. *Geotextiles and Geomembranes* **24**(1), 64–71 February (2006).

[127] Ahmed, Z., White, T. & Kuczek, T. *Journal of Irrigation and Drainage Engineering-Asce* **123**(3), 194–201 May-Jun (1997).

[128] Miura, N. & Chai, J. *Geosynthetics International* **7**(2), 119–135 (2000).

[129] Smets, T., Poesen, J., Fullen, M. A. & Booth, C. A. *Soil Use and Management* **23**(3), 306–316 September (2007).

[130] Rickson, R. *Earth Surface Processes and Landforms* **31**(5), 550–560 April (2006).

[131] Vishnudas, S., Savenije, H. H. G., Van der Zaagt, P., Anil, K. R. & Balan, K. *Hydrology and Earth System Sciences* **10**(4), 565–574 (2006).

[132] Iryo, T. & Rowe, R. *Geotextiles and Geomembranes* **21**(6), 381–404 December (2003).

[133] Tatlisoz, N., Edil, T. & Benson, C. *Journal of Geotechnical and Geoenvironmental Engineering* **124**(11), 1109–1119 November (1998).

[134] Bergado, D., Long, P. & Murthy, B. *Geotextiles and Geomembranes* **20**(6), 343–365 December (2002).

[135] Haeri, S., Noorzad, R. & Oskoorouchi, A. *Geotextiles and Geomembranes* **18**(6), 385–402 December (2000).

[136] Madhav, M., Gurung, N. & Iwao, Y. *Geosynthetics International* **5**(4), 399–424 (1998).

[137] Vaitkus, A., Cygas, D., Laurinavicius, A. & Juzenas, A. A. *Baltic Journal of Road and Bridge Engineering* **2**(1), 45–50 (2007).

[138] Yu, N. *Composites Part B-Engineering* **30**(7), 709–712 (1999).

[139] Moulson, J. & Herbert, J. *Electroceramics*. Chapmann and Hall, (1990).

[140] Shannon, R. D. *Acta Crystallographica* **A32**, 751–767 (1976).

[141] Goel, S., Chiang, M. & Buhro, W. *Inorganic Chemistry* **29**(23), 4640–4646 November (1990).

[142] Parr, J. *Polyhedron* **16**(4), 551–566 (1997).

[143] Kokozay, V. & Sienkiewicz, A. *Polyhedron* **14**(12), 1547–1551 June (1995).

[144] Skopenko, V., Kokozay, V., Polyakov, V. & Sienkiewicz, A. *Polyhedron* **13**(1), 15–18 January (1994).

[145] Findeis, B. *et al. Journal of the Chemical Society-Dalton Transactions* **1**(1), 125–132 January (1996).

[146] Kakaliou, L. *et al. Inorganic Chemistry* **38**(26), 5964–5977 December (1999).

[147] Otero, A. *et al. Inorganic Chemistry* **46**(5), 1760–1770 March (2007).

[148] Fan, M., Zhang, H. & Lattman, M. *Inorganic Chemistry* **45**(16), 6490–6496 August (2006).

[149] Baumann, R., Davis, W. & Schrock, R. *Journal of the American Chemical Society* **119**(16), 3830–3831 April (1997).

[150] Baumann, R., Stumpf, R., Davis, W., Liang, L. & Schrock, R. *Journal of the American Chemical Society* **121**(34), 7822–7836 September (1999).

[151] Akagi, F., Matsuo, T. & Kawaguchi, H. *Journal of the American Chemical Society* **127**(34), 11936–11937 August (2005).

[152] Sanchez, C. & Livage, J. *New Journal of Chemistry* **14**(6-7), 513–521 Jun-Jul (1990).

[153] Blachard, J., Barbouxdoeuff, S., Maquet, J. & Sanchez, C. *New Journal of Chemistry* **19**(8-9), 929–941 Aug-Sep (1995).

[154] Yi, G. & Sayer, M. *Journal of Sol-Gel Science and Technology* **6**(1), 65–74 (1996).

[155] Yi, G. & Sayer, M. *Journal of Sol-Gel Science and Technology* **6**(1), 75–82 (1996).

[156] Sanchez, C. & Livage, J. *New Journal of Chemistry* **14**(6-7), 513–521 Jun-Jul (1990).

[157] Banerjee, A. & Bose, S. *Chemistry of Materials* **16**(26), 5610–5615 December (2004).

[158] Harada, S. & Dunn, S. *Journal of Electroceramics* **20**(2), 65–71 April (2008).

[159] Guiffard, B. & Troccaz, M. *Materials Research Bulletin* **33**(12), 1759–1768 December (1998).

[160] Wu, A., Vilarinho, P., Salvado, I. & Baptista, J. *Journal of the American Ceramic Society* **83**(6), 1379–1385 June (2000).

[161] Cushing, B., Kolesnichenko, V. & O'Connor, C. *Chemical Reviews* **104**(9), 3893–3946 September (2004).

[162] Burda, C., Chen, X., Narayanan, R. & El-Sayed, M. *Chemical Reviews* **105**(4), 1025–1102 April (2005).

[163] Garnweitner, G., Hentschel, J., Antonietti, M. & Niederberger, M. *Chemistry of Materials* **17**(18), 4594–4599 September (2005).

[164] Piticescu, R. M., Vilarnho, P., Popescu, L. M. & Piticescu, R. R. *Journal of the European Ceramic Society* **26**(14), 2945–2949 (2006).

[165] Traianidis, M., Courtois, C., Leriche, A. & Thierry, B. *Journal of the European Ceramic Society* **19**(6-7), 1023–1026 (1999).

[166] Camargo, E., Frantti, J. & Kakihana, M. *Journal of Materials Chemistry* **11**(7), 1875–1879 (2001).

[167] Chang, Y., Chang, Y., Chen, I., Chen, G. & Chai, Y. *Journal of Crystal Growth* **243**(2), 319–326 August (2002).

[168] Linardos, S., Zhang, Q. & Alcock, J. *Journal of the European Ceramic Society* **26**(1-2), 117–123 (2006).

[169] Uekawa, N., Kajiwara, J., Kakegawa, K. & Sasaki, Y. *Journal of Colloid and Interface Science* **250**(2), 285–290 June (2002).

[170] Binder, J., Wedemeyer, H. & Reuter, H. *Advanced Materials* **9**(13), 1049–& November (1997).

[171] Das, R., Pati, R. & Pramanik, P. *Materials Letters* **45**(6), 350–355 October (2000).

[172] Depero, L., Bonzi, P., Musci, M. & Casale, C. *Journal of Solid State Chemistry* **111**(2), 247–252 August (1994).

[173] Li, W., Gao, L. & Guo, J. *Nanostructured Materials* **10**(6), 1043–1049 August (1998).

[174] Das, R., Pathak, A. & Pramanik, P. *Journal of the American Ceramic Society* **81**(12), 3357–3360 December (1998).

[175] Ebelmen, M. *Annales des Chimie et des Physique* **16**, 129 (1846).

[176] Geffcken, W. & Berger, E. German Patent 736,411, May (1939).

[177] Lakeman, C., Xu, Z. & Payne, D. *Journal of Materials Research* **10**(8), 2042–2051 August (1995).

[178] Livage, J., Bouhedja, L. & Bonhomme, C. *Journal of Sol-Gel Science and Technology* **13**(1-3), 65–70 (1998).

[179] Sayer, M. & Sreenivas, K. *Science* **247**(4946), 1056–1060 March (1990).

[180] Li, J. & Yao, X. *Journal of Wuhan University of Technology* **20**(4) December (2005).

[181] Yang, W. *Ceramics International* **27**, 373–384 (2001).

[182] Zhang, M., Salvado, M. & PM, V. *Journal of the American Ceramic Society* **86**(5), 775–781 (2003).

[183] Zhou, Q., Chan, H. & CL, C. *Journal of Materials Processing Technology* **63**, 281–285 (1997).

[184] Pechini, M. U.S. Patent 3,330,697, July (1967).

[185] Fang, T., Wu, M. & Tsai, J. *Journal of the American Ceramic Society* **85**(12), 2984–2988 December (2002).

[186] Li, X., Agarwal, V., Liu, M. & Rees, W. *Journal of Materials Research* **15**(11), 2393–2399 November (2000).

[187] Zhou, Z., Deng, Y., Jiang, Y., Wan, H. & Ng, S. *Dalton Transactions* (13), 2636–2638 July (2003).

[188] Hodgson, S., Shen, X. & Sale, F. *Journal of Materials Science* **35**(21), 5275–5282 November (2000).

[189] Zhang, L. & Xue, D. *Journal of Materials Science Letters* **21**(24), 1931–1933 December (2002).

[190] Hui, Z. & Michele, P. *Journal of Materials Chemistry* **12**(12), 3787–3791 (2002).

[191] Lamas, D., Lascalea, G. & de Reca, N. *Journal of the European Ceramic Society* **18**(9), 1217–1221 (1998).

[192] Calzolai, G. *et al. Nuclear Instruments & Methods In Physics Research Section B-Beam Interactions With Materials and Atoms* **249**, 928–931 August (2006).

[193] Maxwell, J., Teesdale, W. & Campbell, J. *Nuclear Instruments & Methods In Physics Research Section B-Beam Interactions With Materials and Atoms* **95**(3), 407–421 March (1995).

[194] Provencher, S. *Computer Physics Communications* **27**(3), 229–242 September (1982).

[195] Rudiger, A. *et al. Applied Physics A-Materials Science & Processing* **80**(6), 1247–1255 March (2005).

[196] Roelofs, A., Schneller, T., Szot, K. & Waser, R. *Nanotechnology* **14**(2), 250–253 February (2003).

[197] Glinchuk, M. & Farhi, R. *Journal of Physics-Condensed Matter* **8**(37), 6985–6996 September (1996).

[198] Jiang, B., Peng, J., Bursill, L. & Zhong, W. *Journal of Applied Physics* **87**(7), 3462–3467 April (2000).

[199] Zhong, W., Wang, Y., Zhang, P. & Qu, B. *Physical Review B* **50**(2), 698–703 July (1994).

[200] Warren, S. C. *et al. Science* **320**(5884), 1748–1752 June (2008).

[201] Li, X.-G., Li, J. & Huang, M.-R. *Chemistry-A European Journal* **15**(26), 6446–6455 (2009).

[202] Park, J.-H., Akedo, J. & Nakada, M. *Japanese Journal of Applied Physics Part 1-Regular Papers Brief Communications & Review Papers* **45**(9B), 7512–7515 September (2006).

[203] Varin, R. A., Czujko, T., Chiu, C., Pulz, R. & Wronski, Z. S. *Journal of Alloys and Compounds* **483**(1-2), 252–255 August (2009).

[204] Rao, C., Kulkarni, G., Thomas, P. & Edwards, P. *Chemical Society Reviews* **29**(1), 27–35 January (2000).

[205] JoseYacaman, M., Rendon, L., Arenas, J. & Puche, M. *Science* **273**(5272), 223–225 July (1996).

[206] Neralla, S., Kumar, D., Yarmolenko, S. & Sankar, J. *Composites Part B-Engineering* **35**(2), 157–162 (2004).

[207] Gadow, R., Kern, F. & Killinger, A. *International Journal of Materials & Product Technology* **35**(3-4), 334–345 (2009).

[208] Dogan, A., Poosanaas, P., Abothu, I., Komarneni, S. & Uchino, K. *Journal of the Ceramic Society of Japan* **109**(6), 493–499 June (2001).

[209] Takacs, L. *Materials Letters* **13**(2-3), 119–124 March (1992).

[210] Tajima, K., Hwang, H., Sando, M. & Niihara, K. *Journal of the European Ceramic Society* **19**(6-7), 1179–1182 (1999).

[211] Wang, J., Zhang, Y., Yang, M., Chen, L. & Ding, B. *Rare Metal Materials and Engineering* **34**(11), 1790–1793 November (2005).

[212] Wilson, A., Wright, J., Murphy, J., Stroud, M. & Thorpe, S. *Sensors and Actuators B-Chemical* **19**(1-3), 506–510 April (1994).

[213] Fleischer, M. *Measurement Science & Technology* **19**(4) April (2008).

[214] Banerjee, S. & Chakravorty, D. *Journal of Applied Physics* **85**(7), 3623–3625 April (1999).

[215] Andrei, G., Dima, D. & Andrei, L. *Journal of Optoelectronics and Advanced Materials* **8**(2), 726–730 April (2006).

[216] Kickelbick, G. *Progress in Polymer Science* **28**, 83 – 114 (2002).

[217] LeBaron, P., Wang, Z. & Pinnavaia, T. *Applied Clay Science* **15**(1-2), 11–29 September (1999).

[218] Liu, J. *et al. Science* **280**(5367), 1253–1256 May (1998).

[219] Iijima, S. *Nature* **354**(6348), 56–58 November (1991).

[220] Tahir, M. N. *et al. Angewandte Chemie-International Edition* **45**(29), 4803–4809 (2006).

[221] Mammeri, F., Le Bourhis, E., Rozes, L. & Sanchez, C. *Journal of Materials Chemistry* **15**(35-36), 3787–3811 (2005).

[222] Maity, A. & Biswas, M. *Journal of Industrial and Engineering Chemistry* **12**(3), 311–351 May (2006).

[223] Takeichi, T. & Guo, Y. *Journal of Applied Polymer Science* **90**(14), 4075–4083 December (2003).

[224] Yang, B., Xu, H., Wang, J., Gang, S. & Li, C. *Journal of Applied Polymer Science* **106**(1), 320–326 October (2007).

[225] Gubinyi, Z., Batur, C., Sayir, A. & Dynys, F. *Journal of Electroceramics* **20**(2), 95–105 April (2008).

[226] Hua, Z. *et al. Materials Chemistry and Physics* **107**(2-3), 541–546 February (2008).

[227] Bezzi, F. *et al. Journal of the European Ceramic Society* **25**(14), 3323–3334 September (2005).

[228] Seol, K., Takeuchi, K. & Ohki, Y. *Applied Physics Letters* **85**(12), 2325–2327 September (2004).

[229] De Cicco, G., Morten, B., Dalmonego, D. & Prudenziati, M. *Sensors and Actuators A-Physical* **76**(1-3), 409–415 August (1999).

[230] Wolny, W. *Journal of the European Ceramic Society* **25**(12), 1971–1976 (2005).

[231] Frantti, J. *Journal of Physical Chemistry B* **112**(21), 6521–6535 May (2008).